A novel fluorophotometer for measuring concentration and diffusion of autofluorescent ophthalmic medication in the human eye

BUTTENSCHON, KIM-KRISTIN

A novel fluorophotometer for measuring concentration and diffusion of autofluorescent ophthalmic medication in the human eye

Kim-Kristin Buttenschön

Supervisors: Prof. J.M. Girkin and Prof. G.D. Love

Submitted in conformity with the requirements
for the degree of Doctor of Philosophy
Department of Physics
University of Durham

Abstract

As society is aging, the frequency of age-related diseases is increasing. An area of age-related diseases that requires special attention is that of ocular diseases as they eventually cause blindness and therefore have a huge impact on the quality of life of the patient. Understanding the underlying cause of the disease and being able to treat it effectively is thus becoming increasingly important. To evaluate the effectiveness of a treatment, the behaviour of the medication in the body needs to be known or estimated. Monitoring the diffusion of medication is commonly referred to as pharmacokinetics, and the pharmacokinetics of ophthalmic medication are currently assessed by sacrificing animal eyes at given points in time after the application of the drug. This procedure does not allow for a high enough temporal resolution and incorporates a number of disadvantages such as the fact that the eyes are non-human and that the behaviour of the drug has to be extrapolated from the data obtained from different eyes. An instrument that can measure the pharmacokinetics of ophthalmic medication in a non-invasive manner will therefore increase the knowledge about the behaviour of the compound of interest considerably.

This thesis presents a novel ocular fluorophotometer which can measure the diffusion of inherently ophthalmic drugs with high temporal and axial resolution (0.6 s and 124 μm, respectively) and a sensitivity of 2 nM in terms of Fluorescein concentration. The design process of the instrument and its performance in terms of resolution and noise are discussed. Thorough consideration of the eye safety of the instrument is presented. The instrument is calibrated for both a fluorescence standard (Fluorescein sodium salt) and an ophthalmic drug for treating open angle glaucoma (Brimonidine) and it is shown that the concentration of a sample with high signal to noise ratio can be accurately recovered with an error below 20%. It is however found that for samples with less good signal to noise ratios the accuracy decreases significantly. The repeatability of the measurements is also assessed and found to be slightly worse than the accuracy with an error of below 23% within one week. The calibration in *in vitro* porcine eyes is also discussed and suggestions made for its improvement. Further measurements of diffusing fluorescent compounds are then presented and discussed. It is found that the diffusion can be monitored with high temporal resolution and that the concentration after complete diffusion is measured correctly. Finally, measurements of *in vivo* eyes of human volunteers are presented and discussed. The instrument is shown to be of a similar standard to a commercially available instrument, and it is believed that the instrument presented here has the potential to become the new gold standard ocular fluorophotometer.

Acknowledgements

Firstly, I want to thank my supervisor John Girkin, Dan Daly from Lein AD and Madhu Cherukury from Allergan for their invaluable support over the years of my PhD. I am very grateful to John for offering me the opportunity to work in his group on this interesting and challenging project, and for encouraging me that there are no stupid questions. Working with you is extraordinarily inspiring!

I would like to acknowledge funding from the Engineering and Physical Sciences Research Council and I am thankful to Lein Applied Diagnostics Ltd. and Allergan Inc. for giving me the opportunity to work closely with industrial partners through their CASE studentship.

I am also thanking all my colleagues who helped me with my work at the university, and who were courageous enough to volunteer to have their eyes measured! Particular thanks to Graham, for all the interesting discussions and for letting me use the equipment from his lab, and for listening to endless tales of woe. Thanks to Chris for helping me to find out where all that astigmatism was coming from! A big thank you also to the gamelan-people - playing the gamelan kept me sane during the course of my PhD and I would thus like to thank you all for giving me a good time. Folke, thank you for helping me with endless maths questions.

Without Prof. Dr. Sowada I would have never made it here, so thank you very much for igniting the spark in me with your inspiring lectures and labs.

My special thanks go to Rob and Meg for giving me a home away from home, and for being there for me when I needed you. Finally, I would like to thank my family and friends for all their support, encouragement and friendship. Thank you Birger and Rob for the proof-reading and sanity-check.

Declaration

The work presented in this thesis is based on research carried out at the Centre for Advanced Instrumentation, Department of Physics at the University of Durham, England. No part of this thesis has previously been submitted for a degree or any other qualification at the University of Durham or any other university. The research reported in this thesis is the sole work of the author unless indicated otherwise in the text. The opthalmic drug used for the presented research has been supplied by Allergan Inc., California, USA. The instrument discussed in this thesis is based on a prototype developed by Lein Applied Diagnostics Ltd., Reading, UK. The author was granted a CASE studentship by Lein Applied Diagnostics Ltd. in collaboration with Allergan Inc. Work that involved human volunteers was carried out in accordance with the Declaration of Helsinki and the experimental protocol was approved by the departmental ethics committee.

Copyright Notice

Contents

List of Figures

Publications

- Buttenschön K.K., Girkin J.M., Daly D., Tracking ophthalmic drugs in the eye using confocal fluorescence microscopy, *Proceedings of SPIE* Vol. 8214, 821403 (2012)
- Buttenschoön K.K., Girkin J.M., Daly J.D., Development of a low-cost confocal instrument to measure the axial dimensions of components in the anterior section of the eye, *Clinical Optometry* 2010(2): 67-72, 2010
- Buttenschön K.K., Girkin J.M., Wilson C.G, et al., Measurement of the tear film and anterior chamber by confocal microscopy, *Proceedings of SPIE* Vol. 7550, 755028 (2010)

Chapter 1

Introduction

"Oculus animi index", the eyes are a mirror of the soul, an old Latin proverb says. What is meant is that the eyes and face reflect our inner thoughts, but this proverb can also be translated into a modern medical context. Our eyes are refined optical instruments which we use to assess our surroundings and find our way in the world. They can, however, also be used by researchers and ophthalmologists to observe and quantify processes that are going on in our bodies. The aqueous humour, which fills the anterior chamber of the eye and is thus the first compound that is observed when looking into the eye, is derived from the body's blood supply and thus frequently contains metabolites and medication also found elsewhere in the body. Therefore, the eye can be a window to the compounds present both in the eye and in the bloodstream - a window to the well-being of the body.

The society we live in today is without a doubt an aging one, leading to an increase in frequency of age-related diseases. One of the areas that requires special attention is that of ocular diseases, since ocular diseases such as glaucoma and age-related macular degeneration have a huge impact on the quality of life. They eventually cause blindness, thus restricting the freedom and independent living capabilities of the patient. Therefore, understanding the causes of these diseases and having

the ability to treat them effectively is becoming increasingly important.

To be able to evaluate the effectiveness and efficiency of a drug and design an appropriate treatment for a patient, the behaviour of the medication in the body needs to be known or at least estimated. The temporal distribution of the concentration of the drug throughout the body thus has to be evaluated and understood before treatment. The monitoring of the processes a medication undergoes in a body is classified as pharmacokinetics, or in other words as "what the body does to the drug" [1]. Pharmacokinetics is the mathematical basis for assessing the processes that the drug undergoes after administration and the time course over which these processes take place. The processes a drug undergoes in the body are absorption, distribution, metabolism and excretion, generally shortened as ADME, and knowledge of these processes and the rates at which they occur can be used to define the drug concentration within the region of interest.

Currently, pharmacokinetic modelling is used to define the processes of ADME and thus estimate the concentration at the region of interest. The behaviour of the drug in the body is however dependent on many factors such as the general health of the patient and the combination with other medical compounds present in the blood, so that the estimation of the actual pharmacokinetics in a patient relies on drug and metabolite concentrations measured in plasma, blood or urine samples at specific time points after administration [2][3]. For ocular pharmacokinetics, the relevant tissues cannot be sampled in humans and the evaluation of opthalmic drugs before they are released onto the market therefore has to be performed using animal models [4]. The radioactively labelled compound is administered and the animals are sacrificed and dissected at different time points throughout the trial to measure the concentration of the drug at the point of interest.

Although the drug diffusion through cornea, sclera and other tissues in the eye has been thoroughly studied [5][6], not much is known about the diffusion and distribution of ophthalmic drugs in the aqueous humour which makes topical treatment at the point of interest very difficult. As described above, the pharmacokinetics of opthalmic drugs are currently evaluated using test animals, but this, apart from being a complicated surgical procedure, is a high cost and material factor since many eyes have to be sacrificed to get a better understanding of the temporal diffusion be-

haviour of the drug. Furthermore, the eyes that these tests are performed on are generally healthy and also not human which makes it hard to predict the behaviour of the drug in the real world application. Most importantly though, this does not enable the researcher to get a clear picture of the actual diffusion properties of the drug or its behaviour in different eyes since there are comparatively big time gaps between the sacrifice of eyes and the number of eyes that can be used is limited.

Therefore, a system that can monitor the diffusion of ophthalmic medication non-invasively over long periods of time in near real time will increase the knowledge about the specific behaviour of the compound of interest considerably and thus enable researchers to design medications for a more effective and efficient treatment.

This dissertation presents an instrument which aims to solve this problem. The instrument, hereafter also referred to as the F410, is capable of monitoring the diffusion of inherently fluorescent ophthalmic drugs with a quantum yield as low as 0.43%[1] continuously over any given time span with a temporal resolution of 0.6s and an axial resolution of 124 µm. A data point is recorded every 20 µm throughout the depth of the anterior chamber to the back of the lens. Since this particular prototype was designed to be able to measure the pharmacokinetics of Alphagan-P (Brimonidine), an α_2 adrenergic agonist used for treating open-angle glaucoma produced by Allergan Inc. which has an absorption maximum in the UV wavelength region, the wavelength used for exciting the fluorescence in the anterior chamber of the eye is 402 nm. The excitation source can however easily be changed to adapt the instrument for other applications.

The instrument operates in a physically non-invasive manner since the medication is purely measured using light and thus reduces the number of animal eyes that have to be sacrificed to zero. It furthermore enables the researcher to monitor the diffusion of the medication in several eyes at once. Several other instruments have been developed which would be suitable for tracking fluorescent drugs in the anterior chamber of the eye, the accepted gold standard instrument being the Fluorotron Master™ (Coherent Radiation Inc., California, USA), but although they have been

[1] As measured following the guide published by Jovin-Horiba [7]

used to measure auto-fluorescence and fluorescent dyes in the anterior chamber of the eye, as far as the author is aware none of them have been used to actively track the position and concentration of fluorescing ophthalmic medication over a given length of time. They furthermore take a comparatively long time to acquire a set of data (approximately 20 s for a single anterior chamber scan with the Fluorotron Master^{TM}), and they do not have the necessary resolution and depth discrimination to monitor the diffusion properties of the drug accurately enough to gain any new understanding.

The F410, on the other hand, has the advantage that no sectioned or three-dimensional images are being acquired, but a one-dimensional depth scan through the anterior chamber of the eye is obtained. This not only makes the scanning process much faster but also reduces the disk space needed to save the data. It furthermore allows for on-the-fly data analysis after each scan, assuring that a specified number of well aligned scans is taken and that no data that is too noisy or otherwise unusable is saved to disk. This helps with the usability of the system since the operator does not have to go through the scans and use personal judgment to find the ones that meet all the criteria of a well aligned scan. It also makes sure that the correct, statistically significant number of scans is being taken at the first instance, so no re-measurement of patients needs to occur. Since the F410 consists of the combination of a confocal reflection microscope and a confocal fluorescence microscope, both resolution and depth discrimination are improved compared to similar instruments.

In addition to these advantages the instrument is fairly small, transportable and can be mounted on an ophthalmic stage for ease of measurement and patient comfort. The F410 is cost-effective and thus affordable even for small institutions.

Since the instrument measures the ocular dimensions in addition to the fluorescence from within the eye, it can also be used to simultaneously monitor corneal and tear film thicknesses with a small change of pinhole size for better axial resolution. This will help to create better understanding of the effects of dry eye syndrome and its treatments on the tear film and cornea, again enabling a more tailored approach to individual treatment. With a few modifications the instrument

can also be used to monitor the diffusion of medication in the posterior chamber of the eye, thus creating access to better understanding diseases that affect the retina such as age-related macular degeneration, which is currently the second largest cause of blindness in the developed world [8]. However, the applications the F410 is suitable for are not limited to the eye but can for example be extended to measuring the diffusion properties of skin.

The author therefore believes that this novel, non-invasive instrument will play a leading role in better understanding the diffusion properties of inherently fluorescent ophthalmic medication and reducing the number of animal sacrifices necessary for this area of research.

1.1 Synopsis

This dissertation deals with the measurement of the diffusion of inherently fluorescent medication in the anterior chamber of the eye. In the second chapter, a short summary of the human eye and its function is given, alongside with a discussion of common diseases that affect the anterior section of the eye. A literature review on existing instruments for measuring fluorescence in the eye is presented and the limitations of the available instruments discussed.

In chapter three, the basic theory behind confocal microscopy and the principle of fluorescence is summarised. The concept of the point-spread function and axial resolution is introduced both for conventional reflection systems and fluorescent systems, which is important in the evaluation of an instrument's performance. The Beer-Lambert law of absorption is introduced which influences the intensity of the measured fluorescence and thus plays an important role for the instrument presented in this thesis. In the last section of this chapter fluorescence decay curves are modelled for Fluorescein to show how the intensity is dependent on the measurement depth.

Chapter four describes the fluorescence properties of the drug to be measured, Brimonidine. The design of the instrument for measuring fluorescence in the anterior chamber of the eye is presented and its performance in terms of axial resolution and measurement noise discussed in depth. The

safety of the instrument for extended viewing by human eyes is evaluated thoroughly.

Chapter five deals with the calibration of the instrument. The calibration routine is first explained using a model and then shown to work in cuvettes. Both Fluorescein and Brimonidine calibrations are presented at laser powers that are beyond the eye safe limit and within the exposure limit safe for the eye with the current configuration of the instrument. It is shown that the instrument can recover the concentration from the measured fluorescence intensity and both the accuracy and the repeatability of the obtained measurement is assessed. The calibration of the instrument for *in vitro* porcine eyes is also presented and evaluated in this chapter.

Further experiments are presented in chapter six. The central corneal thickness and tear film thickness was measured after the application of eye drops for treating dry eye syndrome, and it was found that the thickness increased temporarily after the application of the eye drops. The measurements were taken with a commercially available instrument and a prototype of the instrument presented in this thesis. Measurements of drops of Fluorescein and Brimonidine diffusing in cuvettes are presented and it is shown that the diffusion can be monitored in near real time. The concentrations can be recovered from the measurements accurately for Fluorescein but the results show that the fluorescence properties of Brimonidine need further investigation before the concentration can be recovered from the measurement. Measurements of the diffusion of both Brimonidine and Fluorescein in *in vitro* porcine eyes are also presented and discussed. It is shown that a better way of calibrating the instrument to *in vitro* eyes has to be found. Lastly, this chapter presents a study of the autofluorescence of the human cornea and lens measured both over one day and one week in healthy volunteers. It is found that the corneal autofluorescence seems to decrease over the course of a day which contradicts findings made in the literature.

Chapter seven concludes with a summary of the findings presented in this thesis, and chapter eight gives suggestions for improvements and future work. These include basic measures to improve the signal to noise ratio and to increase the eye safe laser power to achieve better sensitivity of the instrument.

Chapter 2

Background

2.1 Structure and diseases of the human eye

2.1.1 The Eye - A Brief Summary

The human eye is a very complex and not yet fully understood system which consists of several components (fig. 2.1). The main components that will be shortly introduced in this section are the tear film, the cornea, the aqueous humour, the iris, the lens, the vitreous humour and the retina.

The tear film is the outermost component of the eye and crucial for nourishing and lubricating the cornea as well as maintaining the general health of the eye surface and preventing infections. It is made up of three layers, the mucous, the aqueous and the lipid layer. The mucous layer produced in the conjunctival goblet cells located above the tarsal portion is a hydrophilic layer coating the cornea, allowing for an even distribution of the tear film. The second layer is mostly made up out of water (hence the name aqueous layer) and is produced in the lacrimal glands. It moistures and provides the cornea with oxygen and nutrients such as salt, electrolytes and vitamins. The outermost lipid layer is produced by the meibomian (tarsal) glands and provides a hydrophobic

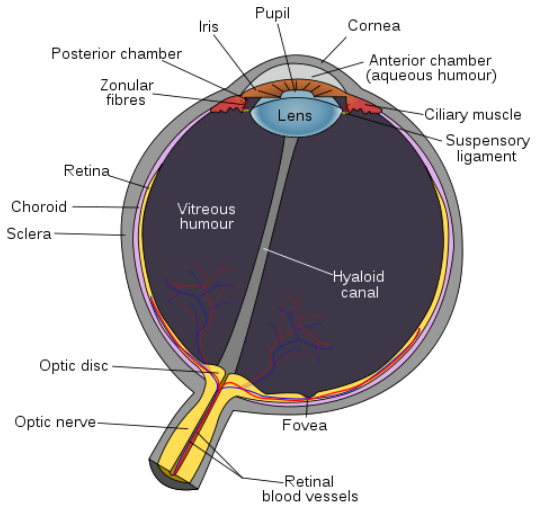

Figure 2.1: Schematic diagram of a horizontal section through a right eye [9].

barrier that prevents tears from spilling onto the cheek and also retards evaporation. A schematic diagram of the lacrimal apparatus is shown in figure 2.2.

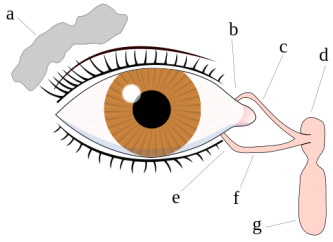

Figure 2.2: A schematic digram of the human lacrimal apparatus showing the production and drainage components with a) lacrimal gland, b) superior lacrimal punctum, c) superior lacrimal canal, d) lacrimal sac, e) inferior lacrimal punctum, f) inferior lacrimal canal, g) nasolacrimal canal and h) tarsal portion [10].

The cornea is the clear outer component of the eye in front of the iris and the lens which accounts for the major part of the eye's optical power (about two thirds [11]). It merges into the sclera, the white outer coat of the eye. Both tissues are mainly made out of collagen fibres with a homoge-

neous structure, protecting the inner parts of the eye. The collagen fibres in the cornea, however, are much more organised than the ones in the sclera, giving the main reason why the cornea in contrast to the sclera is transparent [12]. The limbus (not shown in the diagram) is the merging point of cornea and sclera; special structures for draining aqueous humour from the anterior chamber of the eye are located here.

The aqueous humour is produced by the ciliary processes located in the ciliary body behind the iris, and flows into the posterior chamber of the eye between the iris and the lens. It then passes through the pupil into the anterior chamber, where it is drained through the trabecular meshwork located in the limbus into Schlemm's canal and thus out of the eye into the bloodstream (fig. 2.3). The mechanisms of aqueous humour formation are not yet completely understood, but it has been shown that part of it is produced by filtration of blood plasma [13]. The role of the aqueous humour is to supply nutrients to the intraocular components such as the cornea and lens and to transport waste material away. It also creates an intra-ocular pressure to mechanically support the anterior structures of the eye and ensure normal optical function.

The main blood supply of the eye is located in the uveal tract which consists of the iris, the ciliary body and the choroid. The iris is the aperture stop for the optical system eye, being opaque due to deposition of melanin pigment and blood vessels. Muscles in the iris control the size of the pupil. The ciliary body is not only responsible for producing aqueous humour but also controls lens accommodation via the ciliary muscles. The choroid layer covers the complete posterior segment, supplying the retinal photoreceptors with blood.

Behind the iris lies the lens, which together with the iris forms the separation between the anterior and the posterior chamber of the eye. The crystalline lens is the second refractive component in the eye in addition to the cornea, accounting for roughly one third of the eye's optical power. Its focal length is variable (in contrast to the fixed focus of the cornea) and is controlled by the ciliary muscles. By changing the shape of the lens, the eye can view objects over a large range of focal distances. The crystalline lens sits within a lens capsule which forms its outermost layer [15]. The lens itself can then be divided into two regions, the nucleus and the cortex [16]. It consists

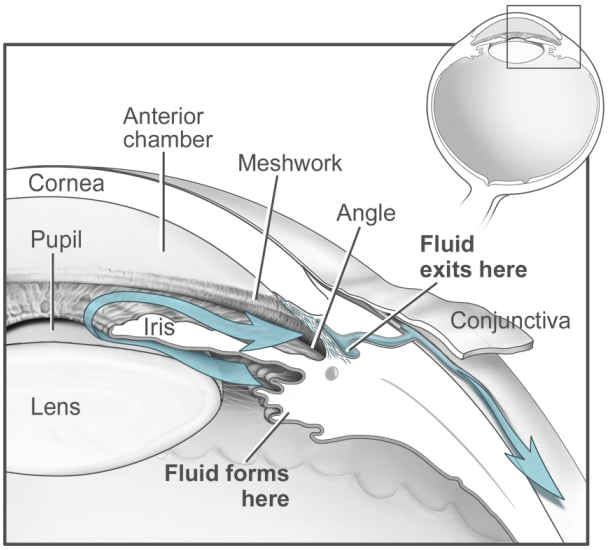

Figure 2.3: Diagram showing the flow of the aqueous humour. The aqueous is produced by the ciliary processes in the ciliary body and released into the posterior chamber. It then flows through the pupil into the anterior chamber where it is drained through the trabecular mashwork and Schlemm's canal into the bloodstream. Courtesy: National Eye Institute, National Institutes of Health (NEI/NIH) [14].

of concentric layers of protein filled fibre cells which stretch from the anterior epithelium to the posterior surface of the lens [12][15].

The vitreous humour, which fills the posterior chamber of the eye, accounts for about 80% of the interior volume of the eye [11]. It consists of water, hyaluronic acid and collagen fibres [17]. Due to the collagen fibres in relation with the hyaluronic acid, the vitreous has a gel-like structure which mechanically supports surrounding structures such as the retina. In contrast to the aqueous humour, the vitreous humour is not replenished. The physiological function of the vitreous is unclear, but there is evidence that it regulates the growth and shape of the eye during development [18]. It might also serve as a shock absorber for the retina.

The retina, finally, is the innermost layer of the eye. It is constructed out of different types of cells of which the most important ones are the ganglion cells, which are the nerve cells that transport

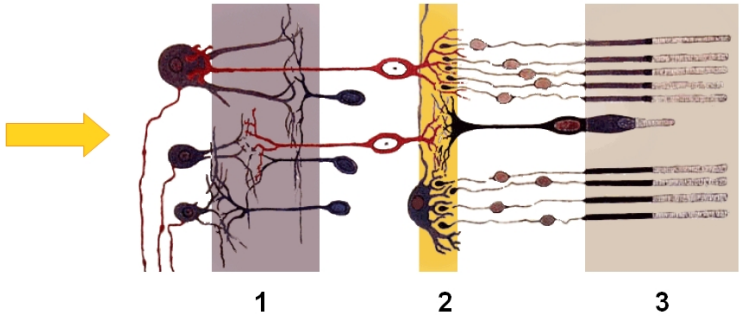

Figure 2.4: A schematic cross section of the human retina [19]. The yellow arrow indicates the direction of the incoming light. 1: Ganglion cells, 2: Interneurons, 3: Photoreceptors.

the visual signal to the brain, and the photoreceptors. The ganglion cells and photoreceptors are connected by a network of interneurons that transform the chemical change induced by the photoreceptors into a neuronal signal. Counterintuitively, the ganglion cells lie closest to the lens of the eye with the interneurons behind them. The light therefore has to pass through the layers of nerve cells before it reaches the retina. The blood supply of the retina is provided by the choroid which lies below the photoreceptors and is not transparent. The photoreceptors can be divided into two groups, the rod cells and the cone cells, where the rod cells are responsible for low-light black and white vision and are most dense in the peripheral area of the cornea whereas the cone cells are responsible for daylight colour vision. They are most dense in the fovea, the spot of the retina with the highest photoreceptor density that controls sharp central vision. A schematic section through the retina is shown in figure 2.4.

The average dimension of the anterior-posterior axis is 24.2 mm [20], but this number varies from person to person and more so in diseased eyes. The thickness of the tear film is approximately 3 μm [21][22]. Other sources state the tear film to be approximately 10 μm [23]. The mean thickness of the cornea is 0.52 mm [24], the depth of the anterior chamber is about 3.5 mm in an adult eye [11]. The lens has a thickness of approximately 4 mm and the depth of the vitreous chamber is about 16.6 mm (both measured in Prof. Girkin's eye).

2.1.2 Dry Eye Syndrome

Keratoconjunctivitis sicca (KCS), also called 'dry eye syndrome' (DES) is a condition caused by the eye not producing enough tears or the tears evaporating too quickly. If the tear film is changed in any way such as the lacrimal glands not producing enough of the aqueous substance (aqueous tear-deficient dry eye) or the meibomian glands being infected and thus not able to produce the lipid layer which slows evaporation (evaporative dry eye), the cornea cannot be nourished by only the tear film any longer. To compensate for this deficiency, the cornea is nourished via the blood vessels in the conjunctiva and in the eye lids, leading to swollen lids and red eyes. In addition to the eyes becoming dry and tired, this malfunction of the tear film can also lead to inflammation of the cornea which can result in ulcers or scars on the cornea and some loss of vision.

The condition can be caused by a general fault in the tear producing apparatus, but it is also advanced by the intake of drugs which alter the composition of the tear film over a longer period of time such as antihistamines, β-blockers, neuroleptics, oestrogen, reserpine, antidepressants and others [25][26], but other sources claim that some of these medications do not have any influence on KCS [27]. Other contributing circumstances include age as the most common cause, skin disease around the region of the eye, infrequent blinking when working at the computer, long-term contact lens wear, immune system disorders, hot, dry or windy climate, air-conditioning and passive as well as active smoking. Women are roughly 1.5 times more likely to suffer from KCS than men [27], and the prevalence of the disease seems to be higher in Asian populations [28].

Dry eye syndrome rarely leads to total loss of vision, but it has a huge impact on the quality of life of the patient. It makes it more difficult to perform daily tasks such as reading, driving or using a computer. Symptoms include a stinging, burning, sandy feeling in the eye, a feeling that the pressure in the eye is elevated, pain and redness of the eye, heavy eyelids, episodes of blurred vision, extensive tear flow, a stringy discharge from the eye and eye fatigue [25][26].

There are various approaches to treating KCS depending on the cause of the illness. Normally, the condition is caused by external factors such as an underlying disease, taking medication, wearing

contact lenses or working in a dry environment or in front of a computer. In most of these cases KCS can be cured by removing the causing factor. Unfortunately, this is not always possible. Several other options exist for these more severe conditions, including giving of 'artificial tears' to moisten the eye when the condition is mild. In more severe cases, lubricating ointments to be used at night are given, or punctal plugs are inserted into the punctus of the eye to block tear drainage. If these plugs are effective, the punctus can be cauterised. If the cornea is inflamed, cyclosporine is the only drug available [25] to treat the symptoms. It increases tear production and reduces corneal damage.

2.1.3 Glaucoma

'Glaucoma' denominates a group of diseases which can damage the optic nerve at the point where it leaves the eye, including atrophy of the optic nerve, loss of retinal ganglion cells and cupping of the nerve head [29]. It is the largest cause of blindness in the developed world [8]. Figure 2.5 shows how this disease affects the vision in comparison to the vision of a healthy person.

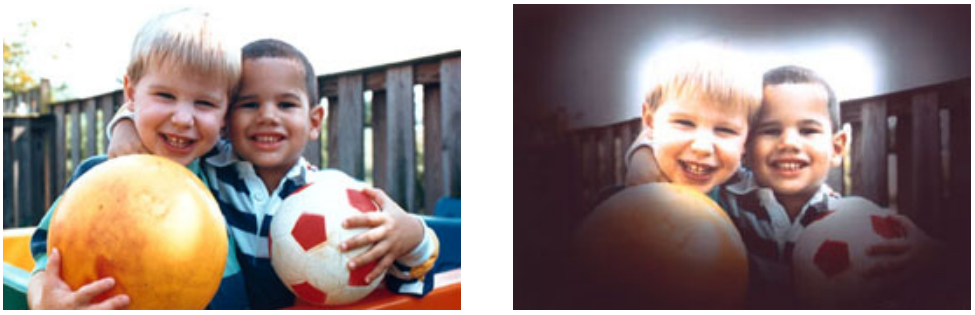

(a) Normal vision **(b)** Vision with glaucoma

Figure 2.5: Demonstration on how the vision of a glaucoma patient deteriorates. a) Two playing children seen as by a normal person. b) The same picture seen as by a person suffering from glaucoma. Courtesy: National Eye Institute, National Institutes of Health (NEI/NIH) [14].

Elevated intra-ocular pressure (IOP) is one of the main risk factors for developing glaucoma, but it is no longer considered to be the only trigger. Glaucoma may also be caused by a mixture of

several factors such as high IOP[1] and weakness of the optic nerve, or even when no elevated IOP is present. Advanced age, ethnic origin, genetic predisposition, severe myopia and thinness of the cornea are now also known to be risk factors [29][14][30].

The pressure in the eye is controlled by the production and drainage of aqueous humour. Normally, there is an equilibrium between the production and drainage of aqueous humour, but when the aqueous cannot leave the eye due to blockage or if too much fluid is produced, the pressure rises, leading to a high risk of developing glaucoma.

Glaucoma is divided into four main groups, with open-angle (chronic) glaucoma being the most common form. In chronic glaucoma, the aqueous humour reaches the drainage channels (thus the name open-angle: The angle in which iris and limbus meet is accessible) but is not transported out of the eye due to the slow blockage of the channels over many years. This leads to a slow buildup of the intra-ocular pressure leading to impaired vision due to damage of the optic nerves. Acute (closed-angle) glaucoma, in contrast, develops when there is a sudden and complete blocking of the aqueous flow in the eye. This is caused by the iris pushing forward against the trabecular meshwork, hindering the aqueous humour from exiting the eye. This form of glaucoma may go along with the development of severe pain and causes permanent damage to the optical nerves if not immediately treated, but it is also much less common in western countries. The two other forms of glaucoma are seldom: Secondary glaucoma develops when the IOP rises due to another eye condition, and congenital glaucoma is a rare but serious form of glaucoma in babies caused by malformations in the eye [14][30].

Although elevated intra-ocular pressure is only one of the major risk factors of glaucoma, the treatment currently available still only concentrates on lowering the IOP by using various pharmaceuticals, laser trabeculoplasty and trabeculectomy. The two latter options are not desirable because of the disturbance they cause to the system eye, trabeculectomy even more so since it involves creating a new hole for the fluid to exit the eye. Both methods work well on some patients,

[1] Normal intra-ocular pressure is defined to be in the range of 8 to 21 mm Hg. A pressure that is higher than 21 mm Hg is classified as being ocular hypertensive [11].

but not all, and the effects may wear off over time, creating the need for further treatment.

Depending on the severity of the rise in IOP the treatment is usually started using eye drops which lower the IOP by reducing the production of aqueous humour or opening up the drainage channels. A wide range of pharmaceuticals is available, many of them containing β-blockers which are normally used to treat patients with heart problems. They lower pulse frequency and blood pressure and can have other side effects which are highly undesirable. A second problem consists in that only about 5% of the eyedrops stay in the eye [31]. The rest are washed out or even worse enter the bloodstream which can lead to side-effects.

Due to these problems, researchers are currently working on developing an implant to replace the eye drops, releasing medication over a longer period of time directly into the vitreous chamber of the eye. This will increase the efficiency of the drug and also reduce the side effects because the medication dosage can be decreased. Unfortunately, not much is known about drug movement in the eye. The overall aim of this PhD therefore is to measure drug movements and concentrations in the anterior chamber of the eye.

2.2 Current techniques for measuring the diffusion of medication or fluorescent compounds in the anterior chamber

There are, of course, available techniques for measuring the pharmacokinetic properties of non-fluorescent and fluorescent medication in the anterior chamber of the eye. The most common technique for evaluating the pharmacokinetics of any ocular drug is to administer the drug to test animals and sacrifice their eyes at specific points in time after the administration of the drug to measure the concentration in the relevant ocular tissues [4]. As already mentioned in the introduction to this dissertation, this process does not provide high enough temporal resolution to evaluate the complete behaviour of the respective medication. Furthermore, many eyes have to be sacrificed to obtain one measurement curve, which makes the whole procedure extraordinarily

complicated and expensive, apart from the fact that many animals have to die for the sake of research. Another complication is that different reactions to the drug between animals can neither be excluded nor quantified so that it is not possible to evaluate their influence on the measurement.

A similar, if less destructive, method is applied to quantify the behaviour of the drug *in vivo* in a single individual. After the drug has been administered, one or more relevant levels are measured at specific time points by extracting concentrations from for example blood, urine or plasma [2][3]. From these concentrations, an estimate of the concentration at the site of interest can be made using mathematic modelling [3]. However, as with the animal experiments, these measurements do not provide good enough temporal resolution for the complete understanding of the behaviour of the medication. Furthermore this method creates the added disadvantage that the concentration of interest cannot be measured at the actual relevant position but has to be estimated from concentrations measured elsewhere.

A non-invasive method that can accurately measure the concentration within the eye with high temporal and spatial resolution is therefore needed to address these issues. This will enable a much better understanding of the temporal behaviour of the drug as well as reducing the cost of the drug-trials since less or no animals have to be sacrificed to evaluate the ocular pharmacokinetics of the respective medication.

However, an ophthalmic compound can only be detected non-invasively if it has some unique optical property such as e.g. fluorescence, polarisation or coherence of scattered or reflected light that varies with concentration, or if it can be measured indirectly through measuring the optical properties of another compound. An example of the latter would be to measure fluorescein concentrations and clearance times to determine the influence of a specific opthalmic drug on the aqueous humour flow or the behaviour of the tear film [32][33]. It would however be most desirable to measure the concentration of the medication itself rather than just being able to quantify its influence on other parameters.

Since the task of this dissertation was to build an instrument that can measure the ophthalmic drug

known as Brimonidine, which is a very weakly inherently fluorescent compound, non-invasively, this review of currently available measurement methods will concentrate on the detection of fluorescence from within the anterior chamber of the eye.

Instruments that measure the fluorescence from any part within the eye are generally referred to as ocular fluorophotometers. Of these, quite a few different models are available which will be discussed in this section.

Although the idea of quantitatively measuring the concentration of Fluorescein in the anterior chamber of the eye has been around since the late 19^{th} century [34], and some instruments were built in the first half of the 20^{th} century that were able to subjectively quantify the concentration of Fluorescein in the eye [35][36], the first objective ocular fluorophotometer was not built until 1954 when Langham and Wybar modified a slit lamp to research the origin and the circulation of the aqueous humour [37]. Their fluorophotometer was able to measure relative changes in concentration which were related to an absolute value that was obtained from the aqueous humour which was extracted immediately after the last measurement with the fluorophotometer. Maurice improved Langham's instrument by addressing issues such as uncertainty of the target area (eye-instrument alignment), internal scattering that was reaching the photodetector and poor sensitivity due to the light source which did not have high enough intensity in the blue wavelengths [38]. Maurice's instrument was then further improved by Waltmann and Kaufman in 1970 [39] who used fibre optics to stabilise the target area and modified the optical set up such that only an adapter was needed to turn a commercially available slit-lamp into a fluorophotometer. Aoshima et al. shortly afterwards demonstrated a fluorophotometer that had a much higher sensitivity than aforementioned devices due to the use of a single photon counter as the detector [40]. This fluorophotometer was not used for ocular measurements, but the improvements made could be implemented into any existing ocular fluorophotometer just as easily. In 1977, Smith et al. [41] made another improvement by replacing the mercury arc lamps used in the fluorophotometers before for a tungsten-halogen lamp which is a much more stable light source. They furthermore improved the signal to noise ratio by using an optical chopper and lock-in amplifier to reject any

signal that came not from the sample, such as dark noise from the photo-multiplier.

Minor improvements were made by Jones et al. in both 1979 and 1982 [42][43], but no further break-through was achieved until 1985 when McLaren and Brubaker were the first to apply scanning of the beam along the optical axis in the anterior chamber to take measurements in rapid succession [44]. This technique had been used for vitreous fluorophotometry [45], but had not been applied to the anterior chamber beforehand. Very shortly afterwards, Coherent Radiation Inc. invented the Fluorotron Master^{TM} which addressed many of the issues of other fluorophotometers by providing optimised aptertures, filters, light sources etc [46][47]. Since this instrument was mainly developed for vitreous fluorophotometry, the main improvement was that by using a novel optical design no contact lens was needed to measure the fluorescence in the posterior chamber of the eye, which all previous vitreous fluorophotometers did not achieve. Since this instrument also provided improved axial resolution and was reviewed to be superior to other commercially available instruments [48], it became the standard fluorophotometer used in ocular research and has been used widely since then (e.g. [49][50][51][52][53]). It has been accepted as the "gold standard" ever since [54].

The instruments discussed above have been used to measure either the auto-fluorescence of the cornea and lens, or to measure certain properties of the cornea, aqueous humour and blood-ocular barriers and the influence of medication on them. They have, however, very rarely been applied to measure the actual medication itself. In fact, the author of this thesis could not find any proof in the literature that compounds other than highly fluorescent dyes and markers have been used to assess the pharmacokinetics of specific drugs. This means that either an indirect method is used or the molecular structure of the drug has to be altered, leading to unpredictable errors in the measurement.

In addition, even though the Fluorotron Master^{TM} has been accepted as the gold standard fluorophotometer, its axial resolution is not sufficient to resolve individual layers such as the tear film from the cornea. The axial resolution in a confocal microscope is normally measured by scanning a highly reflective surface such as a mirror through the focus of the beam and measuring the full

width at half maximum of the returned point spread function as described in chapter 3. The resolution in a fluorophotometer, however, is measured in a slightly different way due to historical reasons. The website of the Fluorotron Master^{TM} [55] states the axial resolution ("Depth of resolution") as 2 mm at 3% peak signal. According to Zeimer [45] and Munnerlyn [46], this value relates to the half width at the point of the point-spread function where the signal has fallen to 3% of the peak signal. This slightly unusual definition of the axial resolution has been derived on the grounds that in fluorophotometry signals strongly varying in fluorescence are encountered very close to each other, for example the fluorescence from the retina or the crystalline lens (very high signal) in comparison to the fluorescence from the vitreous humour (very low signal). It is therefore most important to know how much of the high signal is "tailing" into the low signal next to it and at what distance the low signal can be read accurately without falsification by the neighbouring peak.

Due to the optical design of the Fluorotron Master^{TM}, where the measurement volume and thus the axial resolution is defined by the steepness of the angle with which the excitation and the emission beam intercept and the width of the excitation and detection slits, it is not likely that a better axial resolution can be achieved while keeping a high sensitivity. The anterior chamber can only be measured with an axial resolution (as defined above, not the full width at half maximum!) of 0.2 mm when using a special adapter for the instrument since the Fluorotron was originally designed to measure the fluorescence in the posterior chamber of the eye, which is still one of its main applications. A higher axial resolution is however needed to obtain more precise profiles of fluorescence distribution within the anterior chamber and to be able to resolve e.g. the tear film from the cornea [52][56][32][57].

The scientific community will therefore benefit greatly from an instrument that has high axial resolution so that individual layers of components can be resolved. It would also be of use if the compound of interest can be measured directly rather then via indirect methods, although using fluorescence as the quantity of detection this obviously will only work with inherently fluorescent medication or drugs that have been tagged with a fluorescent compound.

Chapter 3

Theory

The measurement principle of the instrument presented in this thesis is based on confocal microscopy in combination with fluorescence detection. This chapter therefore introduces the basic theory behind the confocal principle as well as the definition of axial and lateral resolution of an instrument. The theory of fluorescence is also discussed and the additional theory of the combination of fluorescence with a confocal imaging principle is presented. Furthermore the Beer-Lambert law of absorption is introduced. Since the instrument will first be tested on homogeneous solutions of Fluorescein a simulation of the intensity decay of several modelled concentrations of Fluorescein was additionally carried out to predict the behaviour of the measurement data.

3.1 Confocal fluorescence microscopy

3.1.1 The confocal principle

The use of a confocal imaging system to improve image resolution and contrast and to enable optical sectioning and thus the collection of three-dimensional images was first thought of and

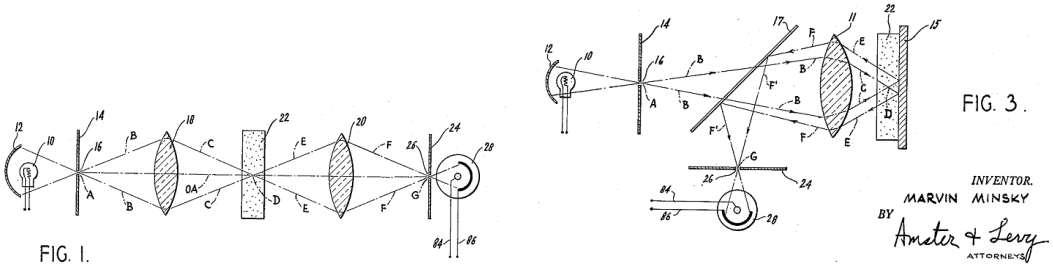

(a) (b)

Figure 3.1: Schematic drawings of Minsky's confocal microscope in a) transmitted and b) reflected light mode [58].

patented by Marvin Minsky in 1957 [58], who is a cognitive scientist in the field of artificial intelligence and wanted to obtain three-dimensional, real-time images of neural networks in brain tissue for his research [59]. Unfortunately, his invention met with little interest. This was probably because the computers that re-constructed the measured intensities from each point into a three-dimensional image were very slow, leading to disproportionately long image acquisition times. Furthermore no high-quality images could be obtained using the method suggested by Minsky since the image was build on a cathode ray tube, leading to poor image quality, and the available light sources were not intense enough to allow for good enough signal to noise ratios.

Minsky's invention was forgotten until 1971, when Davidovits and Egger implemented a laser as light source, thus drastically improving the signal strength [60]. They also added a computer-controlled scanning mechanism to scan the sample through the focus, making image acquisition a lot easier. The confocal microscope was then subject to only minor improvements until White and Amos created the first laser scanned user friendly system in 1985 [61], which increased the image acquisition speed drastically compared to the optically superior sample scanning method used before [62]. After this new addition, the requests to fund the purchase of this equipment increased monumentally [63]. After further development the confocal microscope was finally commercialised in the late 1980s [64]. During the 90s, improvement in optics and electronics as well as computing power lead to a sheer explosion in the number of applications for which confocal laser scanning microscopy was and still is the perfect choice.

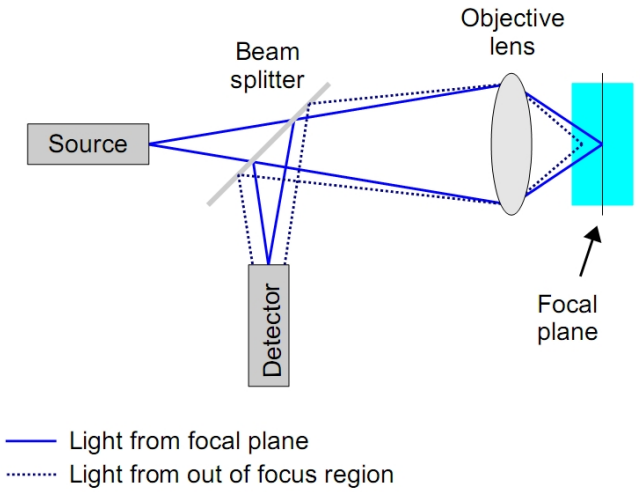

Figure 3.2: Schematic diagram of a wide-field microscope.

Conventional microscopes generally use a technique called wide-field illumination to illuminate the specimen. In this technique, a wide cone of light is focused into the sample, covering a large volume (figure 3.2). Conventional microscopes are generally either configured in transmission or in reflection mode. In transmission mode, the illumination light is transmitted through the sample towards the objective lens, whereas in reflection mode the illumination light is focused into the sample through the objective lens. Most of the light transmitted or reflected by the sample is then collected by the objective lens and can be viewed either directly through an eyepiece or can be projected onto a camera. The collected signal will be a convolution of signals from all layers within the sample that transmit or reflect enough light to be picked up by the detector, significantly reducing contrast and resolution of the acquired image, especially when imaging through thick specimens. This leads to the three-dimensional interpretation of the data becoming very complex since this technique does not offer good enough axial resolution to distinguish between the focal plane and the layers that lie above and below it.

This problem can be circumvented by cutting the sample into thin slices which do not generate much background signal, but this is not always feasible and even less often desired. Researchers

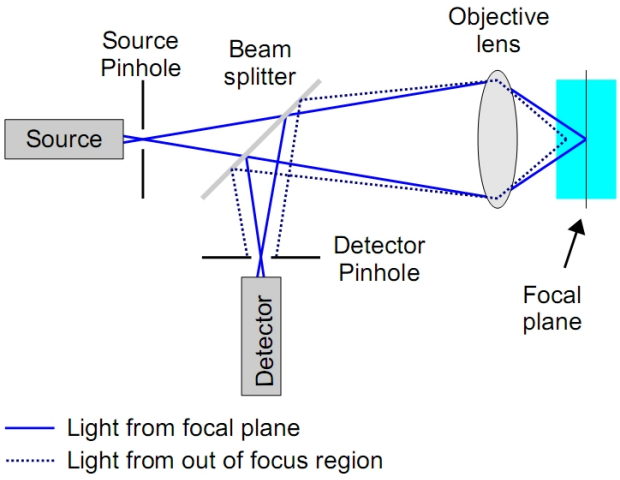

Figure 3.3: Schematic diagram of a typical confocal microscope.

nowadays mainly want to understand the function and behaviour of the specimen they are investigating in relation to its natural surroundings and if possible while being alive. Cutting the specimen into thin slices is - for obvious reasons - quite detrimental to that. A number of algorithms has been developed to aid with the interpretation of three-dimensional images from thicker samples, but they are only a cure for the symptom and not for the problem and require comparatively long calculation times.

In a confocal microscope, on the other hand, a different imaging technique is used that almost eliminates the problem of the image being blurred by signal from layers that are not in focus. This is achieved by using pinholes in optical conjugate planes in front of the illumination light source and the detector. The pinhole in front of the light source creates a diffraction limited point source that is re-imaged into the sample. The collected transmitted or reflected light only travels through the conjugate pinhole in front of the detector if it is coming from the focal plane; unwanted signal from out-of-focus planes is rejected at the pinhole, leading to a much higher signal to noise ratio.

The general principle of a confocal microscope, configured in reflection mode, is shown in figure 3.3. Light from an illumination source, depicted in bright blue in the diagram, is focussed through

a pinhole before passing through a beam splitter onto the back aperture of the objective lens. It is then focussed into the sample by the objective lens, being reflected by features in the sample, similar to a conventional microscope. The reflected light from the focal plane within the sample, also shown in bright blue, is collected by the objective lens and diverted by the beam splitter before being focussed through the detector pinhole onto the detector. Light reflected from out of focus regions, however, is not focussed at the pinhole as shown by the dotted dark blue line. It creates a comparatively large spot at the pinhole plane of which only a small fraction passes through the pinhole and is thus collected by the detector, contributing to the resulting image. Using this principle of optically conjugate pinholes to illuminate the sample and collect the reflected signal results in a much better signal to noise ratio and drastically improves the axial resolution of the system. Two-dimensional images can easily be obtained by scanning the focal spot of the illumination beam across the sample, and three-dimensional image stacks can be computed by altering the position of the objective lens along the optical axis after each two-dimensional scan.

Axial and lateral resolution of a confocal system

The resolution that can be achieved with a confocal microscope is limited by several factors. Even in a perfect imaging system that does not have any optical aberrations, the objective lens will not re-image the (infinitely small) point source as a point into the sample. Diffraction of the light at the boundaries of the lens will spread out the image of the excitation point so that the light is focussed to an intensity distribution within the specimen rather than an infinitely small point. Thus, the imaging properties of a system are characterised by the spread of the image of a point source when focussed by the objective lens. This intensity distribution is called point-spread function (PSF) and takes the form of an Airy diffraction pattern [65]. An example of resolved and unresolved Airy patterns is given in figure 3.4.

Resolution is defined as the distance between two features that are just distinguishable. For an ideal, aberration-free objective lens, both the lateral and the axial resolution are only limited by the wavelength of the illumination light, the numerical aperture (NA) of the lens and diffraction.

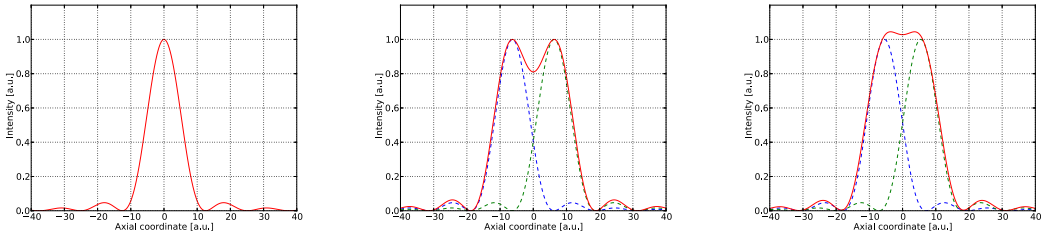

Figure 3.4: The theoretical axial point-spread function of the F410. (a) Intensity distribution of a single point. (b) Two resolved points showing the Rayleigh criterion. (c) Two unresolved points.

The imaging is said to be diffraction-limited in this scenario. The NA is related to the semi-aperture of the lens α and the refractive index n of the sample the beam is focused through by

$$\mathrm{NA} = n \cdot \sin\alpha. \tag{3.1}$$

The Airy diffraction pattern formed by the objective lens can be calculated from diffraction theory using a number of approximations. For a system with cylindrical symmetry it is conventional and convenient to use the dimensionless optical coordinates ν and u instead of real space units [66][67] for the calculation. The lateral coordinate ν is defined by

$$\nu = r \cdot \frac{2\pi}{\lambda_m}\sin\alpha = r \cdot \frac{2\pi}{\lambda}\mathrm{NA}, \tag{3.2}$$

with r being the radial coordinate relative to the optical axis and $\lambda_m = \lambda/n$ being the wavelength of the light in the medium with refractive index n. Similarly, the axial coordinate is defined by

$$u = z \cdot \frac{2\pi n}{n\lambda_m}\sin^2\alpha = z \cdot \frac{2\pi}{n\lambda}\mathrm{NA}^2, \tag{3.3}$$

with z being defined relative to the focal point. The image intensity of a point imaged by a lens can be written as [67]

$$I = |h|^2, \tag{3.4}$$

where h is the amplitude PSF of the lens given by

$$h(u,\nu) = \int_0^1 P(\rho)\, e^{\frac{1}{2}ju\rho^2} J_0(\nu\rho)\rho d\rho. \tag{3.5}$$

This is the Fourier transform of the circular aperture of the objective lens.

Since the parameter u represents the defocus of the lens, it can be set to $u = 0$ when the assumption is made that the lens focusses on the object plane. Following Born and Wolf this yields [66]

$$I(0,\nu) \propto \left| \frac{2J_1(\nu)}{\nu} \right|^2 \tag{3.6}$$

for the intensity of the point across the focal plane, where $J_1(\nu)$ is the first-order Bessel function of the first kind. The intensity distribution along the optical axis can similarly be found by setting $\nu = 0$ [66]:

$$I(u,0) \propto \left(\frac{\sin\frac{u}{4}}{\frac{u}{4}} \right)^2. \tag{3.7}$$

As mentioned above, the lateral and axial distribution of the intensity follows from diffraction at the circular aperture of the objective lens and forms an Airy pattern. Figure 3.4(a) shows that the intensity distribution has several side lobes surrounding the main peak intensity. Two features of equal intensity within the sample are said to be resolved if the maximum of the Airy pattern of the first feature falls into the first minimum of the Airy pattern of the other feature. This definition of resolution was first derived by Lord Rayleigh [68]. If this definition is followed, the lateral resolution is defined as the radius of the Airy disc which stretches laterally from the centre of the maximum of order zero to the centre of the first minimum. The centre of the first minimum is found at $\nu_0 = 1.22\pi$, which when inserted into equation (3.2) leads to

$$r_0 = \frac{0.61\lambda}{\mathrm{NA}}. \tag{3.8}$$

Equally, the first minimum of the axial PSF can be found at $u_0 = 4\pi$, and if substituted into equa-

tion (3.3) yields

$$z_0 = \frac{2n\lambda}{\mathrm{NA}^2}. \tag{3.9}$$

Figure 3.4(b) demonstrates that two points are resolved if their separation is equal or greater than r_0, leading to a drop in intensity of approximately 20% between the two points [66]. This radius of the Airy disc is normally used to define resolution in wide-field microscopy.

In a confocal micrsocope, however, the image results from the illumination of the sample from a point source and the detection of the transmitted or more commonly reflected light through a conjugate point, the detection pinhole. Both the intensity distribution of the illumination point and of the detection point are described by the PSF of the system. The resolution is then determined by the product of the illumination and the detection PSF[66][65]:

$$\mathrm{PSF}_{conf} = \mathrm{PSF}_{ill} \cdot \mathrm{PSF}_{det}, \tag{3.10}$$

or, in terms of intensity distribution,

$$I_{conf} \propto \left| \frac{2J_1(\nu)}{\nu} \right|^4, \tag{3.11}$$

leading to a "sharpening" of the central Airy disc. The Rayleigh criterion for resolution can under these circumstances not be used to define the resolution of the system. The Rayleigh criterion is related to the position of the first minimum of the intensity distribution, and this position does not change when the distribution is squared. Using the Rayleigh criterion would thus lead to an underestimation of the resolution of the system, since resolution is not only a function of the separation of two individual points but also of the contrast between those two points. As stated above, using the Rayleigh criterion of resolution in a conventional microscope leads to an intensity "dip" of approximately 20% between the two maxima. Through the sharpening of the PSF in confocal microscopy, this dip would increase significantly if the Rayleigh criterion was used to determine the resolution, thus leading to a theoretical resolution much bigger than actually available. This problem can be circumvented, and several different approaches to this problem exist.

The first approach as suggested by Webb [65] is to use the dip in intensity between two points in a conventional microscope, i.e. 20%, to find the axial and lateral distance from the centre of the Airy disc at which the two points can be resolved in a confocal microscope. The separations between the maximum intensities of those two points are then

$$r_0 = \frac{0.44\lambda}{\mathrm{NA}} \tag{3.12}$$

for the lateral resolution and

$$z_0 = \frac{1.5n\lambda}{\mathrm{NA}^2} \tag{3.13}$$

for the axial resolution respectively.

An alternative approach suggested by Müller [66] is to use the full-width half-maximum (FWHM), the spread of the intensity distribution at half the maximum intensity, instead of the radius of the Airy disc as used in conventional microscopy to determine the resolution of a confocal microscope, since contrary to the radius of the Airy disc, the FWHM in a confocal microscope differs from that in a conventional microscope. For the conventional case, it is a reasonable approximation to say that the FWHM equals the radius of the Airy disc, i.e. the distance to the first minimum:

$$\mathrm{FWHM} \approx r_0. \tag{3.14}$$

The FWHM of the confocal PSF is then determined by the square of the illumination PSF and thus

$$\mathrm{FWHM}_{conf} = \frac{\mathrm{FWHM}_{ill}}{\sqrt{2}}. \tag{3.15}$$

The factor of $\frac{1}{\sqrt{2}}$ describes the decrease of the width of the FWHM with squaring of the PSF. Both the lateral and the axial resolution are therefore increased by a factor of $\sqrt{2}$ in comparison to conventional microscopy and yield

$$r_0 = \frac{0.61\lambda}{\sqrt{2}\mathrm{NA}} = \frac{0.43\lambda}{\mathrm{NA}} \tag{3.16}$$

and

$$z_0 = \frac{2n\lambda}{\sqrt{2}\mathrm{NA}^2} = \frac{1.41n\lambda}{\mathrm{NA}^2} \tag{3.17}$$

for the lateral and the axial resolution respectively. These values are very similar to those derived by Webb.

The FWHM of the axial PSF is a value that is easy to measure by scanning the focus of the objective lens through a highly reflective sample such as a mirror. It is therefore commonly used to describe the axial resolution of a system. However, it should be noted that the FWHM of the axial PSF does not actually correspond to the axial resolution as defined in equations (3.9) and (3.17) since it does by definition not use the distance to the first minimum as the criterion. To find the distance from the centre of the Airy disc to the position of the lateral half maximum intensity value, ν from equation (3.2) has to be set to $\nu = 1.02\pi$, and to find the axial distance for the point of half maximum intensity, $z = 3.52\pi$. This leads to a relation between the FWHM and the lateral and axial resolution of [65][66]

$$\mathrm{FWHM}_{lat} = 0.84 \cdot r_0 \tag{3.18}$$

and

$$\mathrm{FWHM}_{ax} = 0.88 \cdot z_0. \tag{3.19}$$

From the derivation of the resolution of a confocal microscope it follows that both the lateral and axial resolution decrease with pinhole size. Increasing the size of the detector pinhole thus increases the volume that is sampled from the specimen, and therefore the overall intensity on the detector and the signal to noise ratio. This is an important trade-off that has to be kept in mind when designing a confocal instrument. It is no use having an instrument that is able to distinguish between features that are say 1 μm apart, if this means that virtually no signal reaches the detector and the signal to noise ratio is poor. On the other hand, the pinhole should not be made too big since if it is above a certain size a confocal microscope will have no better axial resolution than a conventional microscope or might even perform worse [67].

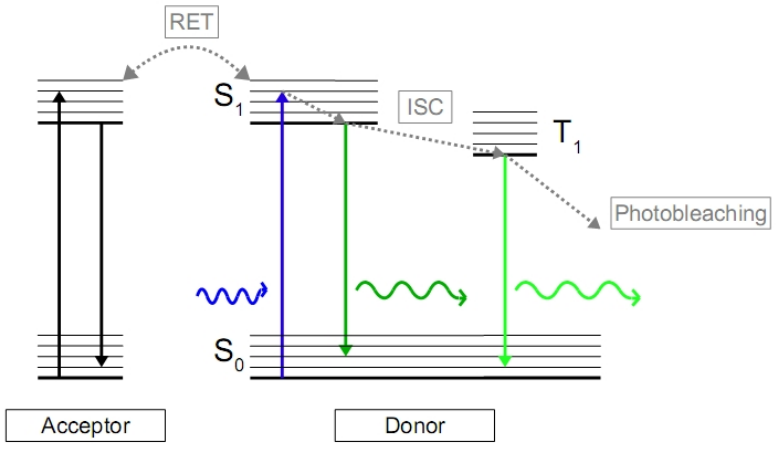

Figure 3.5: A Jablonski diagram, the schematic representation for the process of fluorescence.

3.1.2 Fluorescence microscopy

Theory of fluorescence

The confocal principle described in section 3.1.1 works both in the described normal illumination mode and in fluorescence mode. Fluorescent imaging is however the more widely used method by life scientists since it allows for better distinction of specific features.

The process of fluorescence is best explained using a Jablonski diagram (figure 3.5). When light of the correct wavelength is incident on a fluorescent compound, an electron within one of the molecules of the fluorophore will absorb a photon with a certain probability. The absorption of the photon's energy excites the electron from a low energy ground state (S_0) into a high energy excited state (S_1), which is associated with a change in the molecular orbital of the electron. Within each state, there are several vibrational and rotational energy levels which the electron can be excited to, but they are unstable and after a very short transient time (sub-picoseconds [69]) the electron falls back into the lowest energy level within the excited state. The energy released during this process is absorbed as heat by the surrounding molecules. From the lowest energy level of S_1 the electron falls back into the low-energy ground state S_0, releasing the remaining held energy in form of a

photon of a longer wavelength. The time that passes until all the energy has been released as a longer wavelength photon is called the fluorescence life-time, τ, and is normally in the range of nanoseconds.

The light emitted by the fluorophore is always of lower energy and thus longer wavelength than the excitation light. This is due to the electron losing energy as heat when falling from a higher vibrational level in S_1 back into the lowest energy level of S_1 in the transient process described above. Furthermore, the electron does not always fall back to the lowest energy level in S_0 but might fall into a vibrational energy level. The energy and thus wavelength of the emitted photon depends on which level the electron falls back to. After the electron has re-entered the unexcited ground state, it can go through the process of absorbing and emitting light almost indefinitely until either the intensity of the excitation light has become too weak for the electrons to absorb photons by moving the focus or the fluorescent molecule has photobleached, which is a process that is not yet fully understood and leads to the modification of the fluorophore so that it no longer fluoresces.

It is important to note that light absorption and emission only occurs at specific wavelengths dependent on the fluorophore used. This is due to the fact that the absorption and emission bands are defined by the energy gaps between the different states the electron can exist in, which is highly dependent on the specific molecule used. Furthermore, the fact that the fluorescence occurs at longer wavelengths allows for the detection of fluorescent signals that are weak in comparison to the excitation intensity, especially if an emission filter is used to single out the emission wavelength from the excitation wavelength. An example of the absorption and emission spectrum of the standard fluorophore Fluorescein in an aqueous solution is given in figure 3.6.

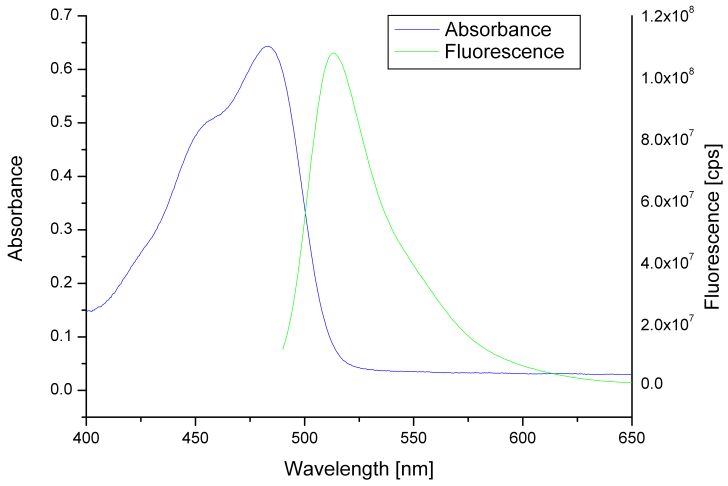

Figure 3.6: Absorption and fluorescence spectrum of Fluorescein.

Quantum yield and fluorescence quenching

The efficiency with which fluorescence is emitted depends on the molecular structure of the fluorophore. This efficiency is known as the quantum yield Q [69] and is expressed by the equation

$$Q = \frac{\text{Number of photons emitted}}{\text{Number of photons absorbed}} \tag{3.20}$$

and has a value from 0 to 1. There are however a number of mechanisms that can lead to non-radiative energy transfer so that the absorbed energy is not emitted as a photon of longer wavelength. An example of this is energy transfer through collision with other molecules, which reduces the number of electrons in the excited state without generating fluorescence. If there is a so called acceptor molecule present that matches the energy bands of the fluorophore, the stored energy can also be transferred to this acceptor molecule by long-range interaction, again without any release of radiation. Furthermore, there is a small possibility that the electron will not be excited into a singlet state but into a so called triplet state T_1, a process called inter-system crossing. Normally, electrons are paired, meaning that they have a spin opposite to each other and a total

spin of zero. There is a quantum mechanical probability though that the electron that gets excited has the same spin as the electron left behind, in which case the total spin equals one. There are three spin combinations that electrons can take to create a total spin of one, and the excited state they are in is thus called a triplet state, in contrast to the singlet state where only one combination of spins is possible to yield a total spin of zero.

For the energy to be released from the triplet to the ground state $T_1 \rightarrow S_0$, a so called "forbidden" transition needs to take place where the electron has to flip its spin. The probability of this to happen is very low, making the decay rate of this energy transition slow. It can take up to several seconds to complete. This process is therefore denoted phosphorescence rather than fluorescence. From this triplet state, the molecule cannot only return to the ground state S_0 but also bleach in a photochemical reaction. As a last example of processes that can lead to non-radiative energy transfer, re-absorption of the fluorescent light has to be mentioned. This can occur if the emission and absorption spectra of the fluorophore overlap, again reducing the number of emitted photons. All these mechanisms that lead to a reduction in the number of photons emitted by the fluorophore are denoted as quenching [70][71] and can, if they occur, reduce the quantum yield of a system quite significantly [71]. An example of fluorescence quenching in an aqueous Fluorescein solution is shown in figure 3.7. It is clearly visible that above a certain concentration the relationship between the fluorescence intensity and the concentration starts to become non-linear. It is possible to predict the amount of quenching present in a system if several factors are known, however since every compound has specific characteristics finding a model for the quenching of one compound does not automatically lead to a general prediction for other compounds. It would therefore be beyond the scope of this thesis to predict the behaviour of the quenched fluorescence intensity with concentration of Fluorescein. Instead, it is taken care to only use the linear part of the intensity versus concentration curve for calibration as is common practice when using fluorophores that are prone to quenching.

Fluorescence only occurs where enough photons of the correct excitation wavelength are present to excite the molecules into a higher energy state as described above. Since a focal spot is scanned

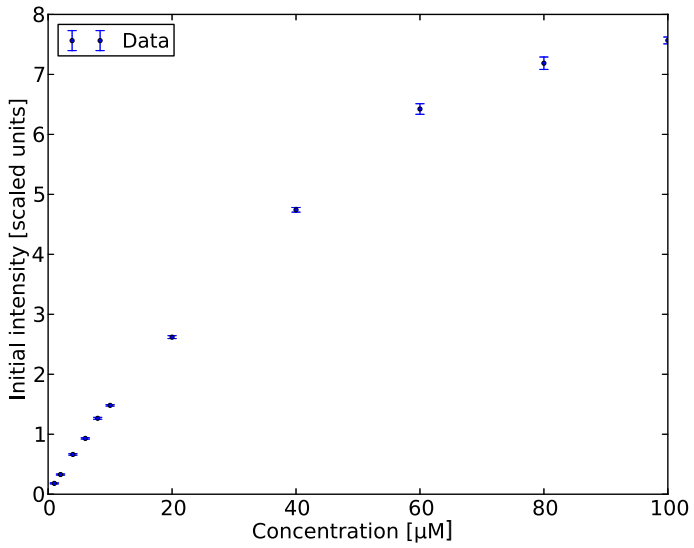

Figure 3.7: Fluorescence intensity of Fluorescein versus concentration. The relationship between intensity and concentrations starts to become non-linear at high concentrations due to self-quenching mechanisms.

across the specimen to create a two-dimensional image, the intensity of the laser is usually chosen such that fluorescence is mainly excited within the focal volume, providing some initial axial sectioning capability. The intensity of the excitation light is usually significantly lower in out of focus planes so that fewer photons are absorbed and less fluorescence occurs. One could therefore argue that imaging in fluorescent mode using a laser excitation source rather than in transmission or reflection mode using wide-field illumination leads to a certain intrinsic confocality of the system. However, the out of focus planes still generate enough fluorescence to be measured by the detector and thus disturb the resulting image significantly, if less so than in a conventional microscope. Therefore the combination of the confocal principle with fluorescent imaging results in the perfect tool for the life scientist that not only provides three-dimensional imaging capability at excellent lateral and axial resolution but also the possibility to distinguish different processes and parts of interest within the specimen with high contrast by using selective fluorophores.

3.1.3 Resolution of a confocal fluorescence system

As in a reflection or transmission confocal microscope, the resolution in a system that images fluorescence rather than reflected or transmitted light is determined by a multiplication of the PSF of the focus in the sample and the PSF created by the pinhole. However, contrary to a non-fluorescent system, these PSFs cannot be considered to be exactly the same due to the shift in wavelength between the excitation and the emission light. It therefore follows that

$$\mathrm{PSF}_{conf} = \mathrm{PSF}_{ex} \cdot \mathrm{PSF}_{em}, \tag{3.21}$$

where the subscripts ex and em denominate the excitation and emission (or detection) PSF, respectively. To correct for this shift in wavelength, the ratio of the excitation and emission wavelength β has to be added to the equation. It can then be shown [66] that the FWHM of the lateral PSF is approximated by

$$\mathrm{FWHM}^{r}_{conf} \approx \frac{\mathrm{FWHM}^{r}_{ex}}{\sqrt{1+\beta^2}} \approx \frac{1}{\sqrt{1+\beta^2}} \cdot \frac{0.61\lambda_{ex}}{\mathrm{NA}}. \tag{3.22}$$

Similarly, the influence of the shift in wavelength on the axial resolution results in

$$\mathrm{FWHM}^{z}_{conf} \approx \frac{1}{\sqrt{1+\beta^2}} \cdot \frac{2n\lambda_{ex}}{\mathrm{NA}^2}. \tag{3.23}$$

Therefore, both the axial and the lateral resolution in a fluorescence confocal microscope is lower than in a reflection confocal microscope.

3.2 Depth-dependent fluorescence intensity decay through absorption

The intensity of the fluorescence excited in a homogenous solution of a fluorophore will change depending on where in the solution the focus of the excitation beam is. This is due to the fact that

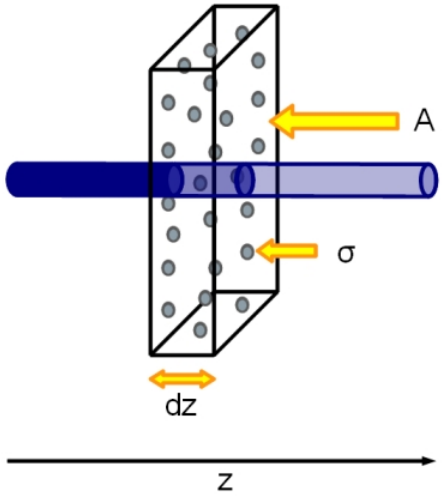

Figure 3.8: A schematic diagram demonstrating the Beer-Lambert law.

the deeper the focus is, the more photons will have been absorbed and scattered in the volume of solution the beam has already passed through, thus leaving less photons available to excite molecules of the fluorophore deeper within the solution. This leads to a decrease of the fluorescent signal which is dependent on the depth of the focus, the concentration of absorbing particles and their absorption properties.

This phenomenon is usually described in terms of either absorbance or transmittance of light through a thickness of solution rather than in terms of loss of fluorescent signal with depth, but the principle behind both are the same:
A solution of thickness l is divided into infinitesimal thin slices perpendicular to an axis z that is parallel to the direction the photons travel in. These slices have an area A and thickness dz along the z-axis. Each of these slices contains a number density of absorbing particles, N, which may be described as having an area of absorption, the absorption cross section σ, so that when hit by a photon within this area the probability of absorption is 1. Otherwise the photon is transmitted through the slice (figure 3.8). It therefore follows that the fraction of photons that are absorbed in this slice is equal to the fraction of the absorption area of the particles in respect to the whole area of the slice, $\sigma N dz$.

If the intensity of the light incident on the slice of solution described above is expressed as I_z, the decrease in intensity as the light passes through the slice can be written as $-dI_z$ and is given by

$$dI_z = -\sigma N I_z dz,$$

where dz denotes the change in thickness of the slice. Note that the change in intensity always has to be negative since fewer photons pass through the slice than are incident on it. The solution of this first order differential equation after separation of variables gives the available intensity at position z:

$$ln(I_z) = -\sigma N z + C.$$

For a real slice of thickness l, the intensity is I_0 at $z = 0$ and I_l at $z = l$. The difference in intensity measured when entering ($z = 0$) and leaving ($z = l$) the solution can then be written as:

$$ln(I_l) - ln(I_0) = (-\sigma N l + C) - (-\sigma N 0 + C) = -\sigma N l,$$

which leads to the equation that describes the fraction of light that is being transmitted by the solution:

$$T = \frac{I_l}{I_0} = e^{-\sigma N l}. \tag{3.24}$$

Therefore, the intensity I_l that is left of an initial intensity I_0 after the beam has passed through a solution with depth l, concentration N and absorption cross section σ is defined by

$$I_l = I_0 e^{-\sigma N l}. \tag{3.25}$$

It is, however, generally considered to be easier to use the base 10 logarithm rather than the natural logarithm. The general convention is thus to write equation (3.25) as

$$I_l = I_0 10^{-\epsilon c l}, \tag{3.26}$$

where c is the concentration in moles per litre and ϵ is the material- and wavelength-specific extinction coefficient. Note here that $\epsilon c \neq \sigma N$, but the base 10 logarithm can easily be converted to the natural logarithm by multiplying $ln(10)$ so that $\sigma N = ln(10)\epsilon c$. Using the base 10 logarithm holds other advantages as well since the molar concentration is more often used than the number density of absorbing particles per unit volume to describe the concentration of a solution, and the extinction coefficient of a specific material is found more often in the literature than its absorption cross section.

The principle of light absorption as a function of the thickness of a slice of material was first described by Bouguer and Lambert. Beer later added that the absorption is also dependent on the concentration of absorbing particles within the thickness of this slice [72], and together these two principles form the Beer-Lambert law which describes that the the absorption of light in percent, A, when travelling through a material of thickness l in cm, is dependent on a material- and wavelength-specific constant, σ in cm^2, and the concentration of absorbing particles, N in molecules per cm^3 [69]:

$$A = ln(\frac{I_l}{I_0}) = \sigma N l. \tag{3.27}$$

Or, alternatively as derived above,

$$A = log(\frac{I_l}{I_0}) = \epsilon c l, \tag{3.28}$$

so that when the absorbance, the path length and the concentration of the sample are known the absorption cross section and/or the extinction coefficient can be calculated.

3.3 Modelling fluorescence decay curves

The Beer-Lambert law predicts the intensity of the light transmitted through a sample from the incident intensity and material specific coefficients. The F410, however, measures the returned fluorescent light from the sample and not the transmitted light, nor is the actual incident intensity measured. Therefore the law is used in a slightly different context where I_0 is the initial intensity

of the fluorescent light at position 0 (no attenuation of the excitation beam), and I_l is consequently the predicted fluorescence intensity at position l in the sample. The law can be modified this way since the intensity of the fluorescent light is linearly dependent on the intensity of the excitation light so that when the excitation light attenuates according to Beer's law, the excited fluorescence will attenuate with the same factor.

The initial fluorescence intensity I_0 is however not only dependent on the intensity of the excitation light but also on the concentration of the fluorophore in the sample. Therefore, the model of attenuation has to be changed slightly to accommodate for the change in initial intensity with concentration c:

$$I_l = I_0(c) \cdot e^{-ln(10)\cdot\epsilon cl} \tag{3.29}$$

Thus, to model the decay of the fluorescence from a fluorophore of known concentration c or N with depth of focus within the solution, both $I_0(c)$ or $I(N)$and ϵ or σ have to be found.

To create a valid model of the behaviour of the fluorescence intensity with fluorophore concentration and depth of excitation beam the properties of Fluorescein Sodium salt (F6377, Sigma-Aldrich), a fluorescent standard very commonly used in ophthalmic research [73], were used. Fluorescein has an absorption maximum at 493.5 nm and an emission maximum at 515 nm, both slightly depending on the buffer solution. However, Fluorescein's quantum yield -and thus its extinction coefficient- is strongly pH dependent with a buffer solution of pH 9.5 giving the highest quantum yield of 0.95 [74][75]. Purified water, on contrary, has a pH of 7.0 and thus reduces the quantum yield significantly to about 0.76 [76], although values as high as 0.92 have also been reported [74]. Furthermore, the literature concentrates on the extinction coefficient and absorption cross section measured at the most used excitation wavelength, 488 nm[70][75][77]. Since both values are wavelength- and pH-dependent, this creates a problem when not working at the usual excitation wavelength or the generally used pH level since very little information can be found in the literature about other wavelengths and pH levels. Therefore the extinction coefficient had to be calculated from the absorbance using the Beer-Lambert law (equation (3.28)).

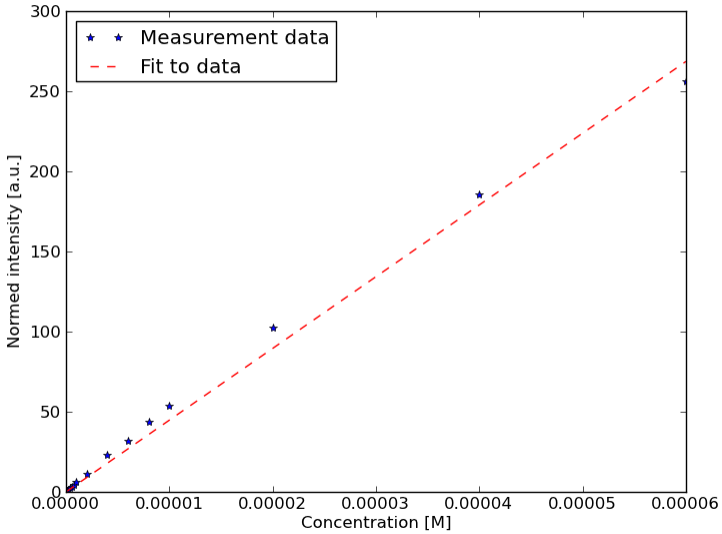

Figure 3.9: Fit to the initial fluorescence intensities at position zero. R^2 = 0.9925

To get a good estimate of the extinction coefficient ϵ the absorbances of Fluorescein solutions at different molar concentrations were measured with a professional spectrophotometer (Shimadzu UV-3600) as described in section 4.1. Since the path length of the cuvette is known, the extinction coefficient for each wavelength contributing to the loss of signal can be calculated. Equation (3.28) was chosen over equation (3.27) since the concentration of the sample solutions was calculated in moles per litre rather than in the number density of absorbing particles per unit volume. The extinction coefficients were calculated both for the excitation wavelength of 402 nm to account for the absorption of the excitation light, and for the maximum emission wavelength as measured by a professional spectrometer (Jobin Yvon Horiba FluoroMax 3) of 510 nm to account for re-absorption of fluorescent light within the solution. The calculated extinction coefficients ϵ_{402} and ϵ_{510} were then combined to form the complete attenuation coefficient, ϵ. The best estimate of the combined extinction coefficient was found by taking the mean of the values for the individual combined

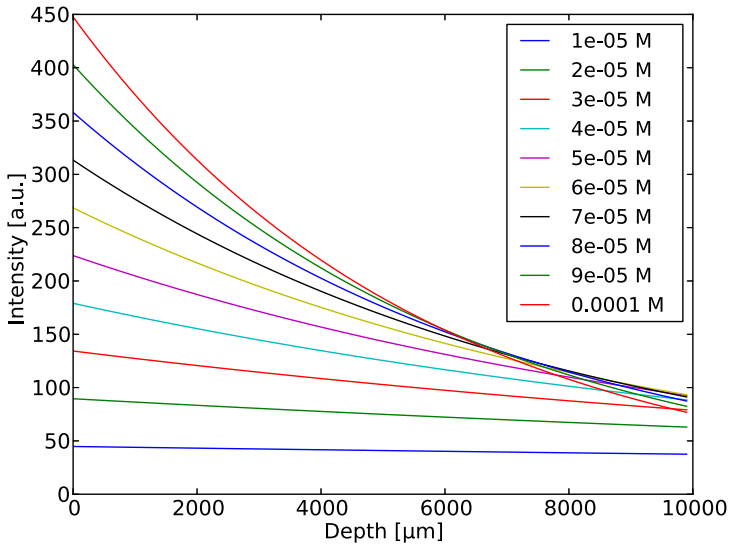

Figure 3.10: Theroretical intensity decay with depth of focus for different Fluorescein concentrations ranging from 10 to 100 µM.

extinction coefficients calculated from the different concentrations:

$$\epsilon = (0.77 \pm 0.04)\mathrm{M}^{-1}\mu\mathrm{m}^{-1},$$

valid only if the concentration is given in moles per litre and the depth in micrometres, otherwise the coefficient has to be accommodated for changes in magnitude. These magnitudes for concentration and depth were chosen since the concentrations measured by the F410 span a range from low nanomoles to high micromoles per litre and thus will be easiest to read in scientific notation, and the position of the scanning stage that holds the final lens and thus gives the position of the focus within the sample is recorded in micrometres by the instrument.

$I_0(c)$ can also easily be modeled using the maximum fluorescence intensities measured for different Fluorescein concentrations by a commercial spectrometer; however to make the model closer to the actual measurements taken by the instrument described in this thesis, the fluorescence intensities at position zero of the scanning lens (i.e. no attenuation of the excitation beam) for different

Fluorescein concentrations as measured with the F410 were used. The initial intensities and the linear fit are shown in figure 3.9. For this model the whole data set was used to find the gradient of the fit. This is however only valid when modelling and it has to be kept in mind that for the correct calibration of the instrument the quenched concentrations need to be omitted as explained above. $I_0(c)$ can therefore be determined and was found to be

$$I_0(c) = 4.47 \cdot 10^6 \frac{\mathrm{V}}{\mathrm{M}} \cdot c,$$

again only valid if the concentration is given in moles per litre. Thus, the intensity of the fluorescence I_l coming from any depth l within a solution can be modelled for any chosen concentration c by inserting the determined constants into equation (3.29).

An example of modelled curves ranging from 10 to 100 µM in 10 µM steps is shown in figure 3.10. As expected, it is clearly visible that the decay rate slows down with lower concentrations. Since the decay rate changes linearly with concentration it can be used to calculate the concentration from a given intensity as described in chapter 5.

Chapter 4

Instrumentation

To be able to build an instrument that is capable of measuring the compound of interest, in this case the glaucoma medication Brimonidine, the fluorescence properties of that compound need to be known. Measurements to determine the quantum yield of Brimonidine were therefore carried out. Since it was found that Brimonidine does not have a very high quantum yield it became clear that the instrument would have to be extremely sensitive to be able to measure the concentrations of interest to Allergan Inc. An instrument with a confocal set-up was therefore chosen to ensure high sensitivity and a good axial sectioning capability. The instrument presented in this chapter is based on a prototype optical glucose meter supplied by Lein AD which was redesigned and then consequently built by the author of this thesis to be able to simultaneously measure reflection and fluorescence and incorporate the minimal number of lenses to reduce the background fluorescence in the system. The performance of this novel instrument in terms of axial resolution and signal to noise ratio are discussed in this chapter. Since the instrument is to be used on human volunteers, special attention is given to the consideration of the laser safety of the instrument for intentional viewing.

4.1 Measurement of the quantum yield of Brimonidine

For the construction of the instrument it was of importance to know how sensitive it had to be to be able to measure the pharmaceutical compound of interest, in this case the glaucoma-medication Brimonidine. Initial tests performed by the manufacturer showed that Brimonidine is an intrinsic fluorophore. However its fluorescence is very weak and additionally quenched by the Bromine present in the compound. Therefore it was considered useful to quantify the strength of Brimonidine's fluorescence to determine what specifications the instrument had to be built to. The quantification of the fluorescence of a specific compound is generally achieved by measuring the quantum yield, i.e. the efficiency by which absorbed photons are transformed into fluorescence. The quantum yield of any fluorescent compound can be measured using different concentrations of two reference standard fluorophores as well as the compound of interest and a calibrated spectrometer as described in the "Guide to Recording Fluorescence Quantum Yields" published by Jobin Yvon Horiba [7].

4.1.1 Methodology

To find the quantum yield of any fluorescent compound, five concentrations of two reference standard fluorophores and of the sample need to be measured. The concentrations of the solutions are chosen such that the absorbances are identical for each compound, and dependent on the path length of the measurement cuvette. For a path length of 10 mm, no solutions with absorbances greater than 0.1 at any wavelength in the absorption spectrum should be used since non-linearity effects through self-quenching can occur at high concentrations as described in chapter 3. If a longer path length cuvette is to be used for the measurement, the maximum absorbance has to be adjusted accordingly to keep the absorbance at the same value, e.g. 0.2 for a path length of 20 mm. Since a path length of 10 mm was chosen for this experiment, solutions with absorbances as close as possible to 0.02, 0.04, 0.06, 0.08 and 0.10 are then to be created for each of the three compounds. Once the solutions have been made, the absorption spectrum has to be measured to confirm the

value of absorption for each compound and concentration; then, the fluorescence spectrum at a chosen excitation wavelength is recorded. The integrated intensity of each fluorescence measurement is plotted against the absorbance for that sample for each of the compounds. The resulting graph will show a linear relationship between the intensity and the absorbance with an intercept at zero if the measurement has been taken correctly. If this linear relationship is not visible, the measurement has to be repeated. The gradients determined from the linear regression are directly related to the quantum yields of the compounds through equation (4.1) [7]:

$$\Phi_X = \Phi_{ST} \left(\frac{M_X}{M_{ST}} \right) \left(\frac{n_X^2}{n_{ST}^2} \right), \tag{4.1}$$

where the subscripts X and ST denominate the unknown sample and the reference standard respectively, Φ is the quantum yield, M the gradient determined from the graph of integrated fluorescence intensity against absorbance and n the refractive index of the solvent.

As a first step, the two reference standards are cross-calibrated using equation (4.1) by calculating the quantum yield of each sample relative to the other, i.e. using one fluorophore as the test sample (X) and the other as the standard sample (ST). The calculated quantum yield should match the values found in the literature. Since the measurement process to obtain the quantum yield is susceptible to error due to incorrect dilutions of concentrations, the value is generally considered to be a good match if the integrated intensity values have good linearity with an intercept at zero and when the calculated quantum yield is within 10% of the literature value. If the calculated values deviate too much from the actual value, the measurements have to be repeated. Once this process is completed and satisfactory values have been obtained for the reference samples, the quantum yield for the test sample can be determined using the same method. However, for the test sample two values of the quantum yield are calculated, one using the first fluorophore as reference standard and one using the other fluorophore as reference standard. The average of these two values then represents the quantum yield of the test sample. This process is necessary to further reduce the error in the measurement.

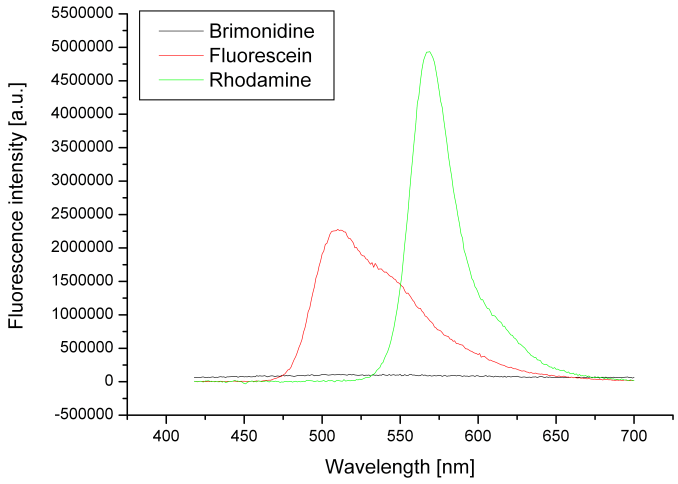

Figure 4.1: Fluorescence spectra of Fluorescein (red, 3 µM), Rhodamine B (green, 7 µM) and Brimonidine (black, 26 mM). Excitation wavelength was 402 nm.

4.1.2 Measurement results

For the purpose of measuring the quantum yield of Brimonidine, Fluorescein and Rhodamine B were chosen as reference fluorophores, firstly because they are well accepted reference standards for such measurements [77][78] and secondly because they were readily available within the research group. In a first attempt to measure the quantum yield, the protocol mentioned above was followed strictly. An example of the fluorescence spectra obtained is shown in figure 4.1 for the lowest concentrations of Fluorescein (3 µM) and Rhodamine B (7 µM) as well as the highest concentration of Brimonidine (26 mM). This graph shows that Brimonidine fluoresces very little even at very high concentrations, in fact so little that the signal to noise ratio of the measurements was very poor. This was due to the fact that the integration time on the spectrometer was set to only one second for the reference standard measurements and had to be kept constant for all measurements to obtain comparable results.

The area of the fluorescence spectrum for each concentration and compound was then calculated

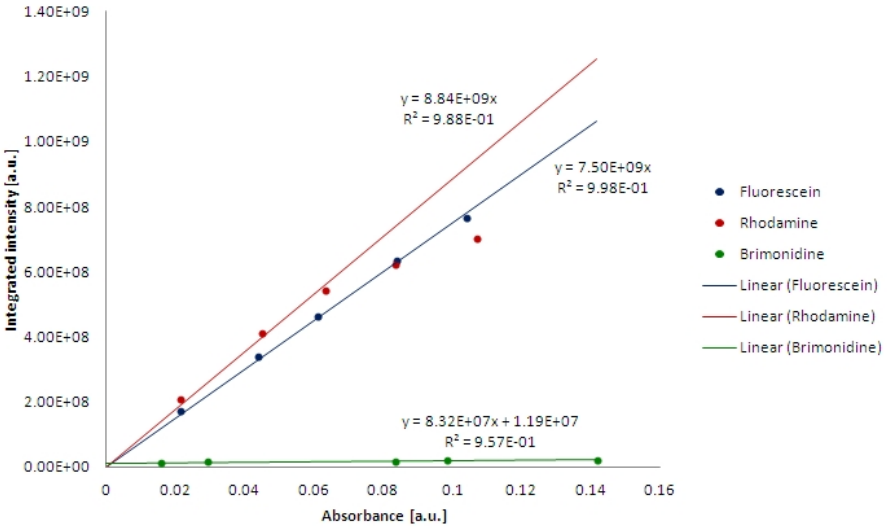

Figure 4.2: Fluorescence intensity shown versus absorbance for the three measured compounds. The intensity of Rhodamine is non-linear with the absorbance due to fluorescence quenching.

using Origin 7. The results of the measurements are shown in figure 4.2. The value of the quantum yield of Brimonidine can be calculated using the gradients displayed on the graph for the respective compound and the known values of the quantum yield for Fluorescein (about 0.76 in pure water [76]) and Rhodamine B (approximately 0.68 in 94% ethanol [79]).

However, the graph shows some problems with this measurement. Firstly, the values of Brimonidine, although being linear with absorbance, do not intercept the y-axis at zero. This does obviously not alter the gradient of the linear fit, but it shows that this measurement was not very accurate and therefore has to be repeated until a satisfactory relationship is measured that does have an intercept at zero, probably using a longer integration time on the spectrometer to reduce the noise. Secondly, the values obtained for Rhodamine seem to be subject to self-quenching processes. This might be explained by the fact that the absorbances of the chosen concentrations did exceed the maximum value of 0.1 at wavelengths that are longer than the measurement wavelength. The values follow a linear trend for the first three measurement points as shown by the linear regression but then start to become non-linear with absorbance. This measurement therefore also has to be

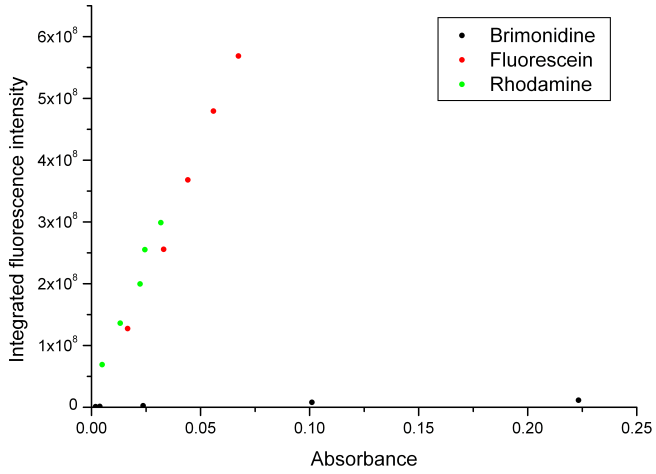

Figure 4.3: Correct measurement of fluorescence intensity with absorbance. No quenching is present.

repeated using lower concentrations of Rhodamine.

To increase the signal to noise ratio, the measurements were subsequently repeated using a longer integration time of 2 s and a physical width of 2 mm on both the excitation and the emission slit, increasing the spectral bandwidth and the intensity of the fluorescent signal recorded by the spectrophotometer. The concentrations used did not follow the protocol presented above but were mixed for convenience rather than identical absorbances across the different compounds. This was assumed a valid approach since this will not change the gradient of the integrated intensity versus absorbance plot. The offset of the Brimonidine data set could not be removed from the measurement. The integrated fluorescence intensity versus absorption curves obtained for the three different compounds used in the measurement are shown in figure 4.3. The offset in the Brimonidine curve is most likely due to the absorption spectrometer being less sensitive than the fluorescence spectrometer (two different machines were used to measure the respective values) and thus not detecting the correct absorbances for the low concentrations of Brimonidine whereas the fluorescence was still detected. Another possible explanation is that scattering from the water

or the Brimonidine molecules themselves hides the absorbance which is very low for those concentrations (in the range of 0.001 - 0.004). It is also possible that fluorescence quenching occurs in all measured concentrations of Brimonidine and the correct intercept is thus not found. To account for this offset, two fits to the curve of Brimonidine were used to calculate its quantum yield: A first fit that was forced through the zero intercept on the y-axis and a second fit that was allowed to intercept the y-axis at the most appropriate point.

The literature value of the quantum yield of Rhodamine B in ethanol varies widely from 0.49 [80] to 0.97 [81], depending on the type of ethanol. Since optics grade ethanol was used for this measurement, the values for 94% ethanol (between 0.68 [79] and 0.97) were assumed to be closest to the true value. The measurement shows that Rhodamine in the ethanol used for this measurement has a slightly higher quantum yield than Fluorescein since the gradient of the integrated intensity versus absorbance curve is steeper (9.6×10^9 in comparison to 8.4×10^9 for Fluorescein). Therefore the mean of the two known values was taken and thus a quantum yield of 0.825 was assumed for Rhodamine B for the calculations. The same problem applies to Fluorescein where values ranging from 0.65 [81] to 0.92 [74] can be found in the literature. The value of 0.92 seems however a bit high considering that the pH of water (pH = 7.0) is below the pH that yields the highest quantum yield (pH > 9.0). This value was therefore disregarded and the mean of 0.65 and 0.76 was taken and the quantum yield of Fluorescein in water thus considered to be 0.705.

The quantum yields calculated for Fluorescein and Rhodamine B from the measurement curves were 0.68 and 0.85 respectively, which is within the 10% error band as specified in the measurement protocol and actually very close to the assumed value. This shows that the measurement parameters were valid. Brimonidine's quantum yield was then calculated using the values extracted from the literature and was found to be 0.0035 for the fit with the non-zero intercept and 0.0047 for the forced zero intercept fit. The average of these two measurements is 0.0041. It was therefore assumed that Brimonidine has a quantum yield of approximately 0.41%.

In comparison, the quantum yield of Fluorescein in water is approximately 0.7 as calculated above. This shows that Brimonidine fluoresces approximately 171 times less than Fluorescein, meaning

that the instrument has to be built to be very sensitive to be able to measure concentrations smaller than 1 μM of Brimonidine which is the goal of this project. In animal eyes, concentrations of Brimonidine as small as 80 nM have been measured using radioactive labelling [82]. It would therefore be excellent if the F410 could achieve the same sensitivity, and in fact in discussions with Allergan the desired lowest measurable value was set to be 10 ng ml^{-1} which is equal to 33 nM. However, if a concentration of smaller than 500 nM can be measured that would be a great achievement.

The calculation of the quantum yield of Brimonidine is not only useful to help determine the physical sensitivity the instrument needs to have (i.e. to help decide which set up and which photo-detectors need to be used to achieve the goal set above), but also to be able to relate the measurements taken with Brimonidine to a reference standard which was chosen to be Fluorescein dissolved in purified water. This is particularly important for other researchers who might be interested in using the instrument built during this project for other compounds since they will be able to relate the measurements presented in this thesis to their own compound using the relation between Brimonidine's and Fluorescein's quantum yield, as long as the quantum yield of the compound they want to investigate is known or can be measured. This means that if they know that a 100 nM solution of a compound with a quantum yield of 0.0041 can be measured using this instrument, they will be able to calculate what concentration of their compound will be measurable using the same set-up.

4.2 The F410

4.2.1 Specifications

The research project discussed in this thesis is a collaboration between Durham University and two industrial partners, Allergan Inc. and Lein AD Ltd. The instrument built during the course of this PhD or an improved version thereof is to be used in real life applications either on animal

models or in clinical trials to measure the diffusion of Brimonidine, a drug for treating open angle glaucoma, in the anterior chamber of the eye. Specifications to which the instrument has to adhere to thus had to be agreed upon. These specifications define the parameters and performance aim of the instrument such as laser and electrical safety and accuracy and resolution of the measurement. The final set of specifications was drafted after the best design of the instrument was determined and can be seen in appendix A. The performance of the instrument in relation to these specifications will be discussed both in the next section, in chapter 5 and in chapter 6.

4.2.2 Experimental set-up

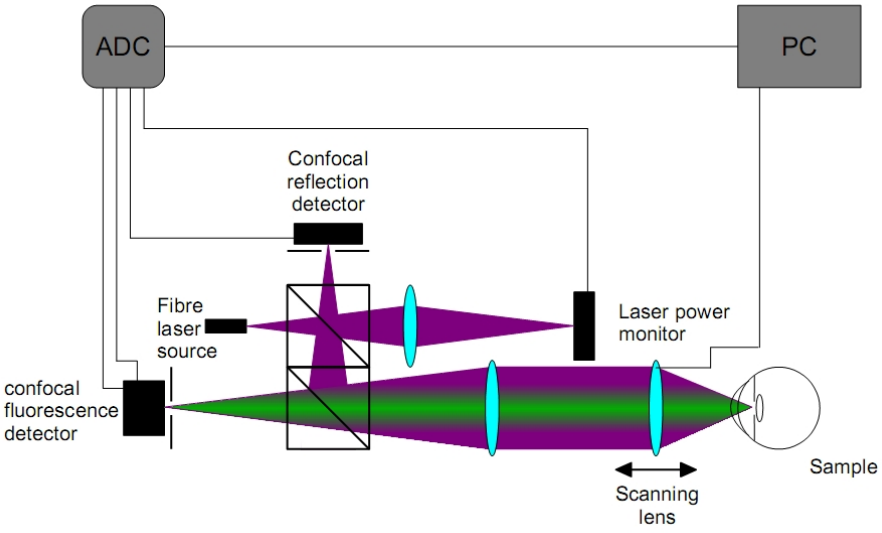

Figure 4.4: Schematic diagram of the F410. After the beam leaves the laser part of it is transmitted through a beam splitter onto a laser power monitor. The other part is reflected by the beam splitter and reflected by a dichroic mirror before being collimated by a lens. It is then focused by a scanning lens, which scans the focus of the beam along the optical axis of the instrument through the sample. The returned fluorescent light is transmitted by the dichroic mirror onto the fluorescence detector while any reflected light is reflected off the dichroic mirror onto the reflection detector.

The F410 is a combination of a confocal reflection microscope and a confocal fluorescence microscope. It does however not create a magnified fluorescence or reflection image of the sample.

Instead, it generates a depth profile of the signal strength along the optical axis of the eye. Unlike a microscope, where either only the fluorescence or only the reflection from the sample can be recorded, the F410 measures both signals simultaneously, thus adding spatial information to the fluorescence signal. This enables the researcher to not only know how much fluorescence is emitted, and consequently determine the concentration in the sample, but also where in the sample the fluorescence occurred. This provides crucial information when monitoring the diffusion properties of the compound of interest.

The major part of the instrument was built using the Thorlabs 32 mm cage-mount system to make the set-up small and more rigid than a conventional bench-top set-up. This decreases the chance of accidental misalignment of optics with respect to each other since they are interconnected and forced into alignment by the cage structure.

A schematic diagram of the F410 is shown in figure 4.4, and a correct optical representation in figure 4.5. A photograph of the optical set up is shown in figure 4.6.The pigtail laser diode (Thorlabs, λ = 402 nm, 10 mW) is coupled into the instrument using a cage mount adapter. Part of the beam then passes through a 8:92 (reflection:transmission) cube mounted pellicle membrane beam splitter (Thorlabs) and is focused by a plano-convex lens (f = 50 mm, Thorlabs) onto a photo detector (Thorlabs, 350-1100 nm, λ_{max} = 970 nm) for the purpose of external monitoring of the laser intensity. The other part of the beam is reflected off the beam splitter onto a dichroic mirror (Thorlabs, 50% transmission/reflection at 425 nm, reflection band 380-410 nm, transmission band 440-700 nm) which reflects the blue light towards a collimating lens (achromatic doublet, Thorlabs, f = 200 mm). The collimated beam is focussed by a doublet meniscus lens combination (CVI Melles Griot, f = 47.11 mm) that is mounted on a motorised stage (SMAC Europe Ltd.) which scans the focus along the optical axis of the instrument through the sample. Light that is reflected off the sample passes back through the scanning lens, is diverted by the dichroic mirror towards the first beam splitter and is subsequently focused through a pinhole ($\varnothing$= 100 µm) mounted in an xyz translation stage onto the reflection detector (Thorlabs, 350-1100 nm, λ_{max} = 970 nm). Any fluorescent light emitted from the sample has a longer wavelength and passes through the dichroic mirror.

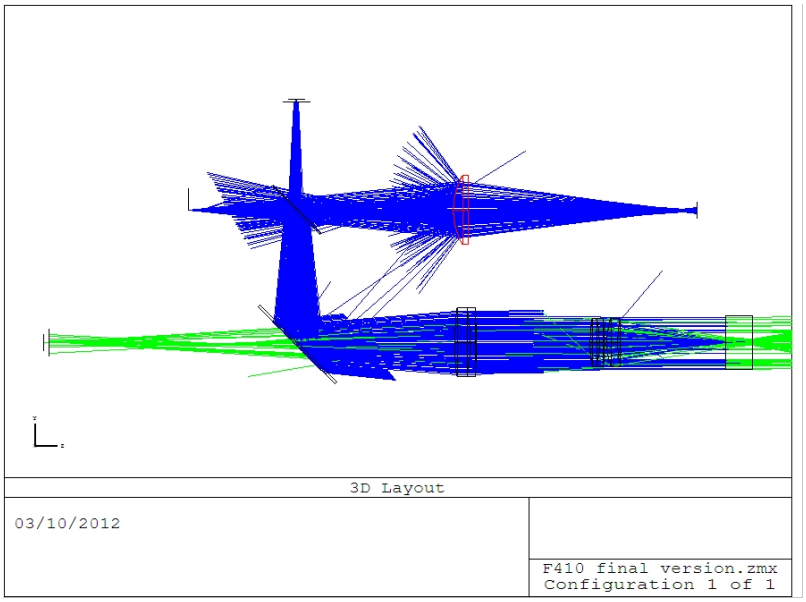

Figure 4.5: A schematic diagram of the instrument as simulated in Zemax.

It is then focussed through an additional longpass emission filter (Thorlabs, cut-on wavelength 450 nm) to remove any residual excitation light and a second pinhole ($\varnothing = 50\,\mu m$), also mounted in an xyz translation stage, onto the fluorescence photo-multiplier tube (PMT) detector (Hamamatsu photonics part number H9306-04, multialkali cathode type, peak sensitivity 530 nm, dark current 0.1 mV at a control voltage of 1 V). The data is recorded using an analogue to digital converter (ADC) (Measurement Computing). The position of the scanning stage, the laser intensity, the control voltage of the photo-multiplier, the reflection and the fluorescence signal are recorded simultaneously. To couple the data sampling to the position of the scanning stage, a conversion is triggered every 20 µm that the stage has moved by using the pulsed signal from the internal optical encoder of the scanning stage as described below. This way, the speed of the stage which is influenced by acceleration and deceleration at the beginning and end of travel does not corrupt the data. If not for this arrangement it would be impossible to determine the position within the sample at which the measurements were taken.

The instrument is currently run by the electronics supplied by the manufacturers of the various

components. These will in a future version be combined into purpose-built in-house electronics to reduce the number of cables and move the electronics to the inside of the instrument's casing. Plans for the new electronics have been submitted, but unfortunately they were not finished by the time this thesis was submitted which is why no improvement can be reported here. The home built electronics will include power supplies for all components and control electronics for the photo-detectors and the photo-multiplier tube. The laser is driven by a generic blue laser diode driving printed circuit board (Thorlabs) and the scanning stage is controlled using the controller supplied by the manufacturer. Only three cables will connect the final version of the F410 to the outside world - a cable for supplying power, a USB cable for communication with the ADC and a RS232 cable that is used to communicate with the controller of the scanning stage. The instrument will be able to be either run off the European standard voltage or off the voltage supplied in the United States of America. This feature was added since the instrument is ultimately to be used in trials at Allergan Inc., California. The reference voltage of the PMT will be settable in four discrete steps of 0.25, 0.50, 0.75 and 1.00 V to change the overall gain of the instrument. This ensures good resolution over a large range of concentrations. Currently, the reference voltage can be set to any value between 0 and 1V.

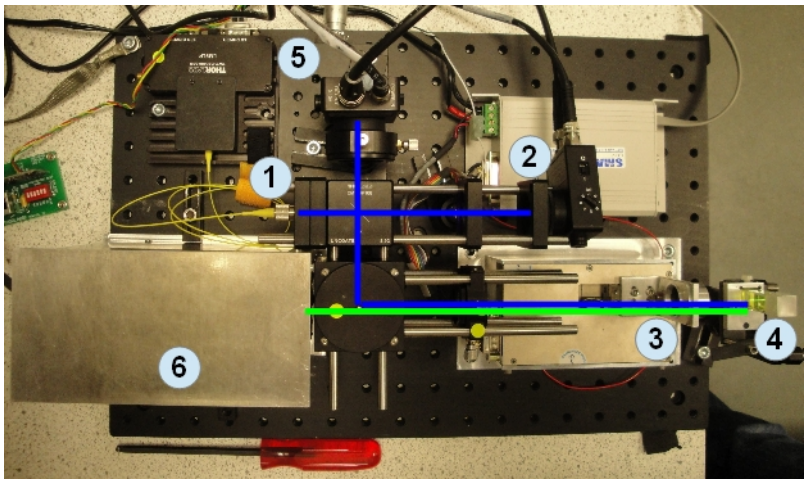

Figure 4.6: A photograph of the F410 showing the laser source (1), the laser safety monitor (2), the scanning stage (3), the sample (4), the reflection detector (5) and the fluorescence detector (6).

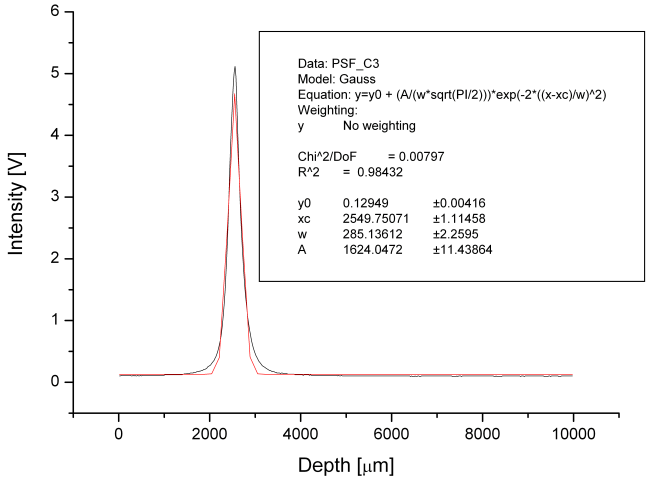

Figure 4.7: Axial point-spread function of the reflection arm of the F410. The full-width half-maximum of the response is 285 μm.

4.2.3 Lateral and Axial resolution

The pinholes chosen for the confocal reflection and confocal fluorescence detection may seem quite big. However, as discussed in chapter 3, a trade off has to be made between pinhole size and signal strength and thus signal to noise ratio. Since the photo diode used for the detection of the reflection from the sample is not enhanced for UV detection and thus has low yield for short wavelengths a comparatively big pinhole had to be used in this arm of the instrument to improve the intensity of the detected light. The fact that this decreases the axial resolution is not a problem in this case since the reflection is only used as a landmark feature to determine the start of the sample and not for specific thickness measurements. The FWHM in this arm as measured by scanning the focus of the beam through a mirror is 285 μm. The measurement and a gaussian fit is shown in figure 4.7. Theoretically, as determined by using equation (3.17), the axial resolution in a confocal microscope with the properties of the F410 (a wavelength of 402 nm and a numerical aperture of 0.187) is as good as 16 μm. The corresponding FWHM equals 14.08 μm as calculated from equation (3.19). The reason why no comparable value is achieved with the F410 lies partly in the fact that

the pinhole diameter is above the optimal size as discussed in [67], and partly in the fact that the beam is quite aberrated and the focus thus slightly blurred. The aberrations have been minimised as much as possible by replacing the original dichroic mirror with a thicker version but residual aberrations remain which decrease the axial and lateral resolution. The lateral resolution has not been determined since it was less important to this project and is a lot harder to measure in the current system. It would have required an external lateral scanning target to have been built as the instrument only scans in the axial direction. This target would then have to have been moved exactly perpendicular to the axially scanning beam, and the resulting axial measurements would then have to have been analysed to remove the possibility of axial defocus from affecting the lateral measurement. This procedure would have lead to large measurement errors and the lateral resolution was thus not determined. The theoretical lateral resolution of the instrument as calculated from equation (3.16) is 0.9 μm with an associated FWHM of 0.756 μm.

The axial resolution of the fluorescence detection arm was determined in the same way as the axial resolution of the reflection arm. The emission filter was removed for this measurement to allow for a residual amount of excitation light reflected by the mirror to pass through the dichroic mirror onto the PMT. The obtained PSF is shown in figure 4.8. Due to the fact that the pinhole in the fluorescence arm is only half the diameter of the pinhole in the reflection arm, the axial FWHM is increased to 124 μm. The axial resolution in this arm of the instrument was originally even further improved by using a smaller pinhole of 25 μm diameter, however to increase the intensity of the collected fluorescence signal for the measurements of Brimonidine which has a very low intensity as discussed in section 4.1 it was decided to increase the pinhole size. As described in chapter 3 the actual axial resolution in a fluorescence confocal microscope is dependent on the excitation and the emission wavelength of the system as the excitation and the emission PSFs cannot be assumed to be the same. The emission detected by the F410 is not a single wavelength band but all wavelengths longer than 470 nm to the cut-off of the PMT. Both Fluorescein and Brimonidine are not excited at their ideal wavelength - Fluorescein's absorption maximum is at 493.5 nm and Brimonidine's absorption maximum is in the UV-A band - but for the purpose of the calculation of

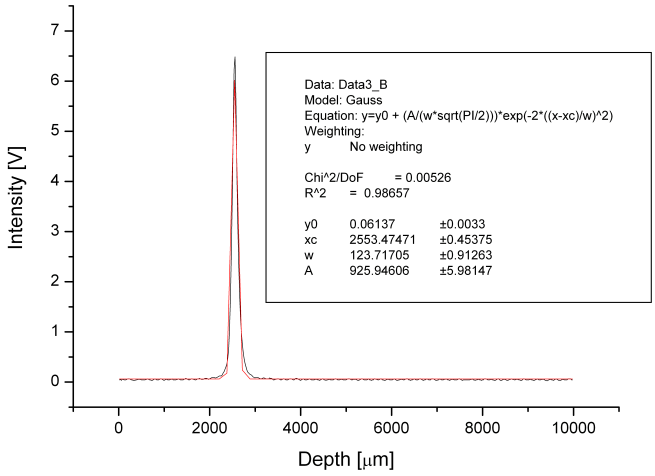

Figure 4.8: Axial resolution of the fluorescent arm of the instrument. The full-width half-maximum of the point-spread function is 124 μm.

the theoretical axial resolution the maximum emission wavelength (510 nm) of Fluorescein when excited with a wavelength of 402 nm was used. The theoretical axial FWHM thus increases from 14.08 μm to 18 μm and the lateral FWHM from 0.756 μm to 1 μm.

As discussed in chapter 3, the FWHM describes the width of the PSF at the 50% signal level. However, to be able to compare the F410 with other fluorophotometers, the axial resolution has to be expressed as the half width of the PSF at the point where the signal has fallen to 3%. This resolution was therefore determined for the fluorescence arm and found to be 280 μm, which is slightly worse than the resolution of the Fluorotron Master^{TM} when using its anterior chamber adapter, but an order of magnitude better than the Fluorotron's resolution without the adapter.

4.2.4 Noise

Since the fluorescence intensity of Brimonidine is very low as described in section 4.1, the signal coming from the PMT has to be amplified and filtered in order to increase the signal to noise ra-

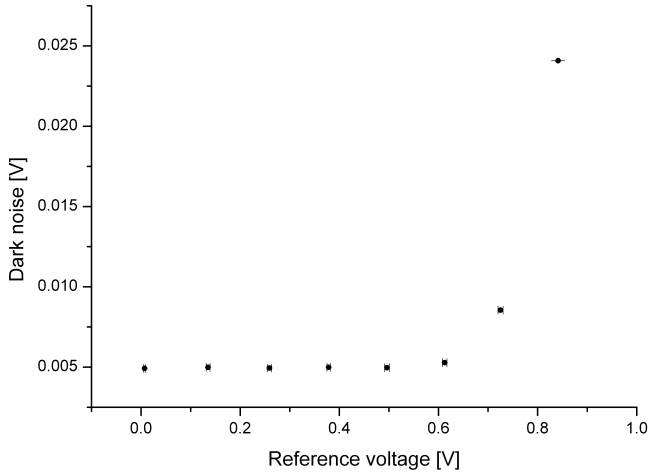

Figure 4.9: The relationship between the reference voltage of the photomultiplier and the dark noise produced by the detector.

tio and make the measurements of Brimonidine samples more reliable. The PMT itself provides some amplification through the variable reference voltage that changes the internal gain, however this method of amplification does not provide enough gain to make lower concentrations of Brimonidine visible. Increasing the reference voltage on the PMT furthermore increases the dark noise of the detector which is caused by the flow of thermal electrons from the photocathode and the dynodes. The dark noise increases exponentially with the reference voltage as shown in figure 4.9. Other probable sources of noise are unwanted background signal (e.g. from room lights or fluorescence within the optics) that is registered by the PMT, especially at higher gains, and statistical variations in the number of photons hitting the detector from the emitted fluorescence in the sample during the integration, also called photon or shot noise. To determine the main contributor of additional noise, measurements were taken with the laser switched on but no sample in place, and with samples of Fluorescein of different concentrations. It was found that very little background signal is registered by the PMT when no sample is present, provided that either the instrument is in a black box or the room lights are switched off (figure 4.10). The main contributer of noise to the measurements is the variation in the number of photons hitting the detector. This particular type

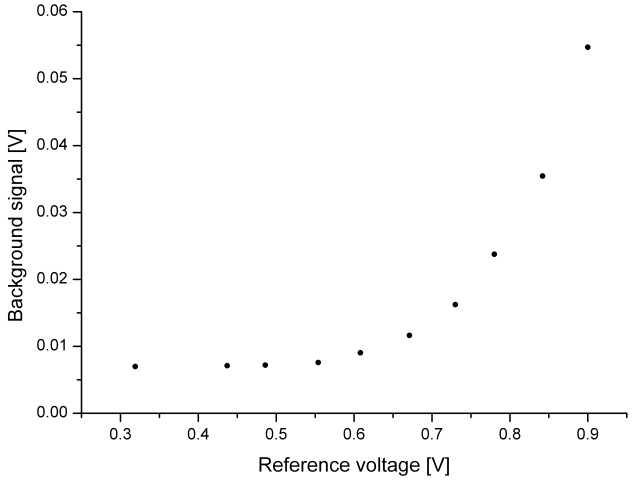

Figure 4.10: The unwanted signal intensity shows an exponential relationship with increasing PMT reference voltage.

of noise is governed by Poisson statistics, which describe the occurrence of independent random events. The shot noise is thus equivalent to the square root of the amplitude of the detected signal. The fluctuation is greatest if high concentrations are measured at high reference voltages as shown in figure 4.11. The shot noise created by a 100 µM solution of Fluorescein at a reference voltage of approximately 700 mV for example is ≈0.21 V, compared to a background signal of ≈0.012 V and a dark noise of ≈0.008 V, showing that random fluctuations in photon arrival are the main contributer of noise to the measurement. Therefore, some electronic filtering had to be introduced into the set up to reduce the noise in the measurement before amplification. This was achieved by connecting the PMT output to an active low pass filter with a corner frequency of 88 Hz and an amplification of 1800 V/V. The corner frequency has to be chosen carefully since a trade-off between noise rejection and rejection of actual measurement data has to be found. Theoretically, the signal can change with a very high frequency if it is assumed that for each "step" of the scanning stage the signal changes from 0 to 100%. The length of a step will have to be defined as the stage scans continuously and thus the returned signal changes continuously. If a step of the stage is defined as 1 µm and the stage is run at the maximum possible speed (40 mm s^{-1}), the highest

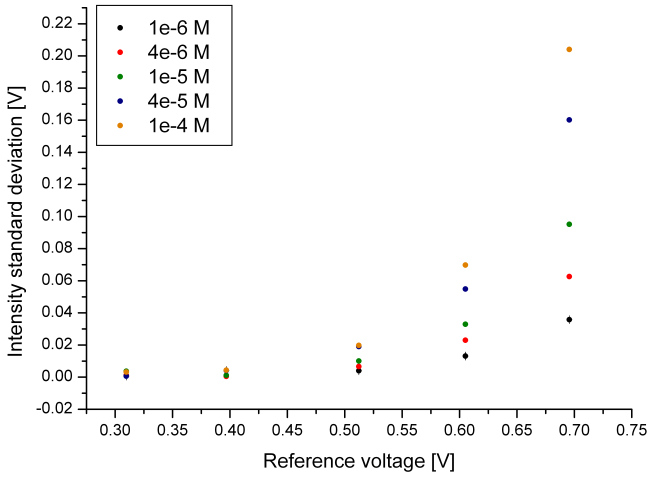

Figure 4.11: The dependency of the fluctuation of the photon count with PMT reference voltage and concentration of the sample.

frequency the signal could change with is 40kHz. To confirm if this frequent change can occur in a real measurement situation, calculations of the diffusion speed of a drop of Fluorescein in water were made.

Fluorescein has a diffusion coefficient of $(4.25 \pm 0.01) \times 10^{-6}\text{cm}^2\text{s}^{-1}$ at 25 degrees centigrade [83]. Although the temperature in the research laboratory is usually lower at about 20 degrees centigrade, the value for 25 degrees centigrade was used because no value for lower temperatures could be found in the literature. To calculate how much Fluorescein will have diffused over a specific distance within a given time the one-dimensional diffusion equation (Fick's second law) has to be used. The diffusion equation states that the concentration change dC with time t is dependent on the diffusion coefficient D (which in turn is dependent on the mass of the compound), the initial concentration C at position zero and the distance x from position zero:

$$\frac{dC}{dt} = D\frac{d^2C}{dx^2}. \tag{4.2}$$

According to the literature [84], the solution to this equation is given by

$$c(x,t) = \frac{M}{\sqrt{4\pi Dt}} \exp\left(-\frac{x^2}{4Dt}\right), \tag{4.3}$$

with c being the concentration at position x and time after the release t, M being the total mass of the substance released per unit cross-sectional area, and D being the diffusion coefficient. This solution is a fundamental solution that only applies for specific boundary conditions which state that no initial concentration is to be present except from a localised release that takes the form of a Dirac function (i.e. an infinitely tall and infinitely narrow peak) which in the case considered here would be the initial drop of Fluorescein, and that the substance will take an infinite time to reach the infinitely far away end of the mathematical domain. Therefore this solution provides the means to calculate the spreading of an instantaneous localised release of a substance in an initially substance free medium.

For the release of a drop of Fluorescein in an infinitely wide volume of water the mass of the released Fluorescein has to be calculated first. Therefore, some assumptions have to be made. First of all it was assumed that a concentration of 1 M was released, and secondly that 1 µl of this concentration would be released over a 1 µm diameter area. Thus the total mass per unit area of released Fluorescein would be 4.2×10^6g cm^{-2}. Since the step width was defined as 1 µm for the consideration of the theoretically maximum possible frequency of change above, the same value was used for the consideration of the actual diffusion speed. To scan 1 µm, the scanning lens needs 0.025 ms when operating at a speed of 40 mm s^{-1}. Thus, using the solution to the diffusion equation given in equation (4.3), the amount of Fluorescein that would have spread this distance within the given time frame would be 7 g cm^{-2}. This is a reduction in concentration of more than 99% compared to the position before. This shows that Fluorescein diffuses very slowly and thus the maximum signal change of 40 kHz is theoretically possible in a real measurement situation.

However, any frequency higher than 1000 Hz will not be measurable by the system. This is due to the fact that the sampling speed of the ADC is 2 kHz and thus according to the Nyquist criterion no

frequencies above 1 kHz can be resolved. This upper frequency limit defines how steep a concentration gradient the F410 is capable of measuring if no low pass filter is applied. Therefore, either no filter or a low pass filter with a corner frequency of 1 kHz and a steep cut-off should be applied to make sure that none of the possible signal change is lost. This however creates a problem due to the sensitivity of the system to any stray light entering the outer case which will fluctuate at a frequency of 50 Hz and multiples thereof. It would thus be desirable to filter out any frequencies at and above 100 Hz to remove as much of the influence of noise created by mains voltage and external light as possible (a corner frequency of below 50 Hz is not feasible). It was therefore decided that using a low-pass filter with a corner frequency below 100 Hz would be necessary to increase the signal to noise ratio, even if this also means rejecting any signal change above 100 Hz. It was furthermore experimentally confirmed that a filter with such a low corner frequency would not influence the signal for the calibration measurements which rely on a fast response of the data acquisition system. Therefore, while waiting for the home build electronics to be designed and made, a simple single-stage active low pass filter with a corner frequency of 88 Hz and a gain of 1800V/V was used to increase the signal to noise ratio. The more refined electronic control system will incorporate a 5 stage Chebychev low pass filter with an amplification of 1000 V/V, a pass band frequency of 75 Hz and a stop band frequency of 95 Hz. Additional amplification of 1000 V/V is added in a separate stage before the filter so that the total amplification of the filtering system will be 2000 V/V.

4.2.5 Control software

The F410 is controlled via purpose-written software (see appendix B). All software was programmed using Python. The software includes the calibration of the instrument and the measurement routine as well as the data analysis and display. It was written for functionality rather than practicality and has not been combined into a single control programme yet. It is currently split into four master programmes and several smaller routines. The four master programmes control the calibration, the data acquisition, the analysis of the data and the display of the data in

various ways. Even though it would obviously be better if the software was combined into one single programme with a graphical user interface the available software can still be used easily by a trained person. A short description of the different software parts is provided below.

1. Calibration

   The calibration software is currently split in several sub-programmes. In the first programme, parent2.py, the data sets are first shifted for every concentration such that the reflection peaks are in the same place. In the next step the signal is averaged over the complete data set. The averaged signal is then scaled to a gain of one in the PMT to make sure that the measurements are comparable even when originally taken at different gains. After this step, the unnecessary part of the array is truncated (i.e. any data before the inside of the cuvette or eye) to ensure a good fit to the data. The fitting is slightly different for Brimonine than for Fluorescein. As described in chapter 5, the data for Fluorescein follows an exponential decay due to high absorbance, whereas the data for Brimonidine follows a linear trend. Therefore, a selection for Fluorescein or Brimonidine calibration has to be made in the software and the appropriate fitting functions are then used for the data. The obtained fitting parameters are subsequently saved into a text file. A second programme, a-of-c.py, associated with the calibration is used to read the fitting parameters from the file and create a linear fit to the fitting parameters. This second fit is the important one since using the obtained parameters in the data analysis software allows for concentrations with unknown parameters to be determined.

2. Data acquisition

   The data acquisition (AD converter control v12.py) is controlled via the ADC and the scanning position of the motorised stage. The ADC is armed by the programme before the stage is started. The position of the stage is controlled by an optical encoder which returns a TTL pulse every 0.5 µm. This signal is picked off and divided using a counter so that a pulse is given to the trigger of the ADC every 20 µm the stage has moved. The ADC trigger re-arms automatically after each measurement point collection. The number of collected measure-

ment points is checked by reading the status of the ADC which returns the index of the last data point of the data array. Once the set number of samples has been collected for one scan (i.e. one movement of the stage from starting to stopping position or from stopping to starting position), the triggering loop is stopped and the collected values are converted from internal units to voltage. If the recorded scan was a backward scan starting movement at the position defined as stop and moving to the position defined as start, the obtained data array is flipped to resemble a forward scan. The array that was collected from a single scan is then appended to an array that holds the data for all scans from that measurement session. After the data of one scan has been appended to the measurement array the trigger of the ADC is re-armed by the software and the cycle repeated until the defined number of scans has been collected. Once all scans have been appended the measurement array is written to a text file for further analysis. Figure 4.12 shows a simplified flow chart of the data acquisition process.

3. Data analysis

   The data analysis software (recover.py, conc-det.py) calculates the concentration of the substance in the sample from the obtained fluorescence intensity file. For this, the signal is first scaled to gain one of the PMT and the background signal subtracted. In the next step, the calibration parameters for the specific substance (i.e. either Brimonidine or Fluorescein) are loaded from the calibration file. Using the calibration parameters, the concentration is recovered as described in chapter 5 by following a five-step procedure where in the first step the concentration is determined from the current intensity, in the second step the decay rate for that concentration is found, in the third step the expected intensity at the next position is calculated using the determined decay rate, in the fourth step the expected intensity is compared to the actual intensity at the next position and in the fifth step the intensity at the next position is corrected by the difference determined in step four (unless the change is smaller than a certain error band). This process is repeated until the end of the data array has been reached. In the case of Brimonidine, no decay rate is used to calculate the intensity at the next position since the decay caused by Brimonidine is so small that it vanishes in the

noise as described in section 5.1.3. The array with the determined concentration values is then returned to the data analysis programme and saved as a text file as well as a graphical representation.

4. Data display

   This very simple programme (DAV5.2.py) loads the fluorescence intensity data or the concentration data from the measurement file and saves a graphical representation for each single scan. A second programme is available which saves a three-dimensional representation of the data so that diffusion patterns are more easily visible to the untrained person.

4.3 Laser safety

Since the F410 is the prototype of an ophthalmic instrument that will be used on human volunteers, the consideration of the safety for the human eye regarding to exposure to the laser beam of the instrument is of great importance. Several points have to be considered which will be discussed in this section.

In general, the thermal and photochemical hazards for the eye caused by the laser beam have to be investigated. This includes the hazard to the retina and the hazards to the cornea and lens which are particularly sensitive to blue and UV light. According to the British Standard [85], the retinal hazard region ranges from a wavelength of 400 nm to 1400 nm. This includes retinal thermal hazard from 400 to 1400 nm, with the risk being quite low at the shorter wavelengths, and blue-light photochemical hazard from 400 to 550 nm. Light below 400 nm is filtered out by the human cornea and lens, and thus causes a hazard to those regions rather than the retina (photokeratitis in the cornea and cataract in the lens). However, the transition between UV and blue light is much less defined in nature than in science - some people might respond with the same effects to light of slightly longer wavelength as others do to UV. Therefore, it is important to not only follow the suggestions of the standard as given by the laser wavelength but to also take into account the damage the light might do to cornea and lens, especially since the beam is focused into a small

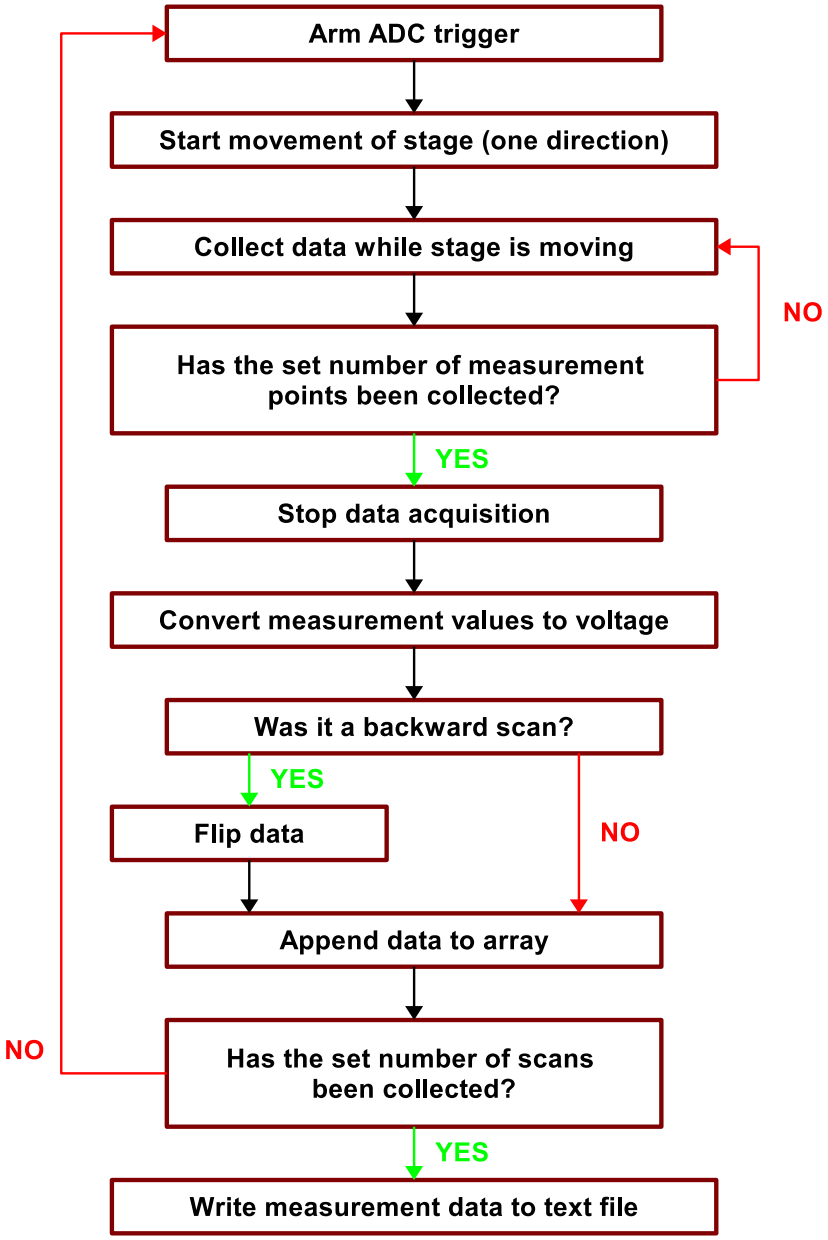

Figure 4.12: Simple flow chart of the data acquisition process.

spot and has a high irradiance (power density) in the focus.

4.3.1 The British standard for the safety of laser products

The British standard for the safety of laser products describes and defines the characteristics of the different laser classes (1, 1M, 2, 2M, 3R, 3B, 4). The classes are defined by how much power or energy is emitted from the laser at a point that is accessible to humans (this power or energy is also called accessible emission). A laser or a laser system can be classified by measuring the output power as described in section 9 of BS-EN60825-1 and then comparing the obtained value with the values given for the respective laser classes. Conversely, from the values given in the standard, a laser system can be forced into a specific class by applying neutral density filters or other appropriate beam attenuation.

Two values relevant to the safety of the eye can be extracted from the standard; the maximum permissible exposure (MPE) and the accessible emission limit (AEL). The MPE describes the maximum limit above which damage of the eye might occur. It includes correction factors to not only prevent damage to the retina but also to the cornea and lens, which are especially susceptible to damage from UV, blue and infrared light. Therefore, no further precautions have to be taken to consider damage to the cornea and lens when operating at short wavelengths when the conditions the standard applies to are given. The values given in the standard have been determined using experimental data from studies and are rather conservative to ensure that they can be used safely; the actual damage threshold lies up to fives times above the given limit. Furthermore, the MPE is only a guideline value, so common sense has to be applied if values slightly higher than the MPE are encountered (e.g. if the MPE is exceeded by only very little a system might still be considered eye safe). The second value, the AEL, is the limit of emission that is allowed to be accessible to humans for a particular laser class.

The British standard assumes either collimated or divergent light viewed at a distance of 100 mm from the apparent source (e.g. the exit of a fibre) so that an almost diffraction limited spot of the

size of 10 to 25 µm is formed on the retina. With decreasing distance to the apparent source the image size on the retina increases because the eye cannot accommodate for such a close source, and thus a higher radiation level than the AEL may be taken by the eye without causing damage to the retina. In the case of the F410, the beam will only focus on the back of the retina if the eye is far enough away from the exit aperture, however the pupil (even if dilated) will block out most of the highly divergent light and thus decrease the irradiance drastically (see figure 4.18). If the eye is close to the scanning lens (i.e. within the measurement range), the focus will not reach the retina due to the design of the illumination system. This is quite a big deviation from the standard which will be discussed below.

The BS-EN60825-1 has not been derived for intentional viewing of the beam, and although medical applications of lasers (for surgery) are mentioned very briefly, no guidelines for intentional intra-beam viewing with typical illumination arrangements for ophthalmic instruments (such as e.g. Maxwellian illumination, fig. 4.13) are given. Safety factors for cornea and lens are incorporated into the standard, however they only apply to collimated and divergent beams. The AEL and the MPE include these safety considerations, but they are only valid if the beam is focusing on the retina leading to comparatively low irradiances in the cornea and the lens. Therefore, the standard cannot apply for an instrument such as the F410 where high irradiances occur in the cornea and the lens, but not on the retina.

Nonetheless, the British standard can be used to assess the safe limit of retinal irradiance for a Class 1 (and thus inherently eye-safe) laser system. For this purpose, the AEL and the MPE for a Class 1 system have to be calculated. To calculate the appropriate values, it has to be assumed that the beam is collimated when hitting the cornea and thus will focus on the retina. The second assumption that is inherent in the standard is that if the diameter of the beam is smaller than the limiting aperture which is set to the size of the dilated pupil (7 mm), the diameter of the beam is set to the size of the limiting aperture. This is done to account for the smallest possible spot size on the retina, meaning that the measured power has to be averaged over a 7 mm diameter aperture. The AEL for a Class 1 or Class 1M collimated laser at a wavelength of 400 to 450 nm and a viewing

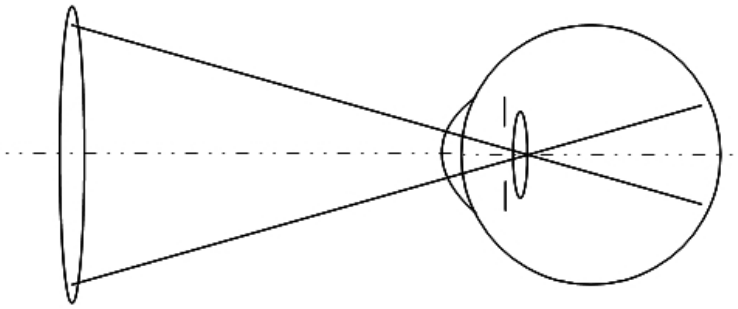

Figure 4.13: A schematic diagram showing Maxwellian illumination of the eye.

time of 10 to 100 s can then be taken from table 4 [85]:

$$3.9 \times 10^{-3}\,\mathrm{J}. \tag{4.4}$$

Depending on the viewing time, the corresponding emission limit ranges from 390 μW for 10 seconds and 39 μW for 100s. The MPE can be taken from table A.1:

$$100\,\mathrm{Jm}^{-2}, \tag{4.5}$$

again with the viewing time being the deciding factor since at 10 s the MPE would equal $10\,\mathrm{Wm}^{-2}$ whereas at 100 s it equals $1\,\mathrm{Wm}^{-2}$.

Both these values are to be measured at the access point (i.e. the cornea). The AEL is derived from the MPE and thus yields an irradiance of $1.01\,\mathrm{Wm}^{-2}$ at the cornea when averaged over the 7 mm diameter pupil for an exposure time of 100 s. Both values only apply at the cornea and not at the retina. The standard specifies this by stating that the equations for the MPE give the "maximum permissible exposure [...] at the cornea". If the AEL derived for an exposure duration of 100 s (39 μW) is used to calculate the safe retinal exposure limit, assuming that the light entering the eye is subsequently focused down to a 180 μm diameter spot on the retina (corresponding to a viewing

angle of 11 mrad as defined in the standard for longer viewing periods), the result is

$$E_{AEL,R} = 1532.6\,\mathrm{Wm}^{-2}.$$

This is the MPE at the retina and the relevant number for the instrument presented in this thesis since every plane within the eye (cornea, lens, retina) needs to be considered separately to evaluate the safety due to the unconventional illumination geometry and the scanning of the lens. The retinal MPE from the standard can then be compared to the actual values encountered in the F410.

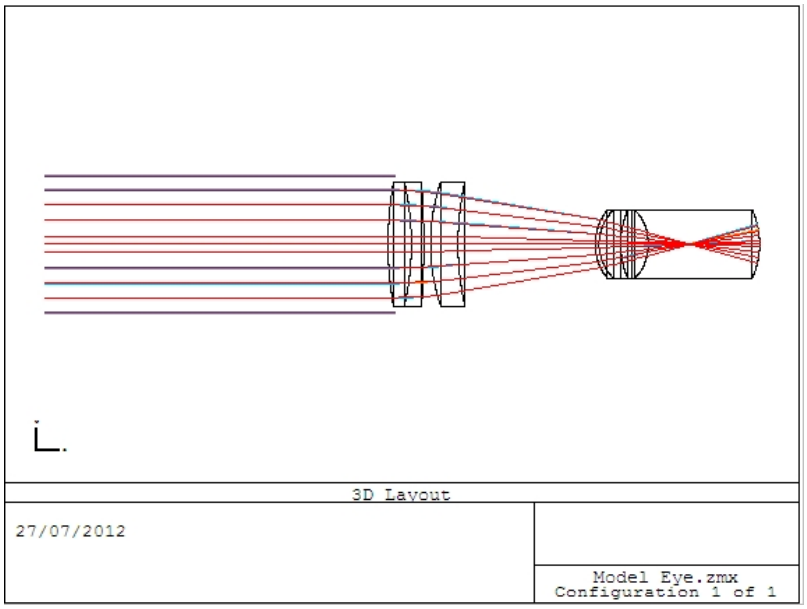

Figure 4.14: Snapshot of the Zemax model that was used to determine the spot sizes on the retina as the focus of the measurement beam scans through the eye.

4.3.2 Simulation of the illumination pattern of the F410

To evaluate the safety parameters of the system at hand it is important to calculate the irradiance at the relevant surfaces of the eye for different positions of the focus. This enables the comparison

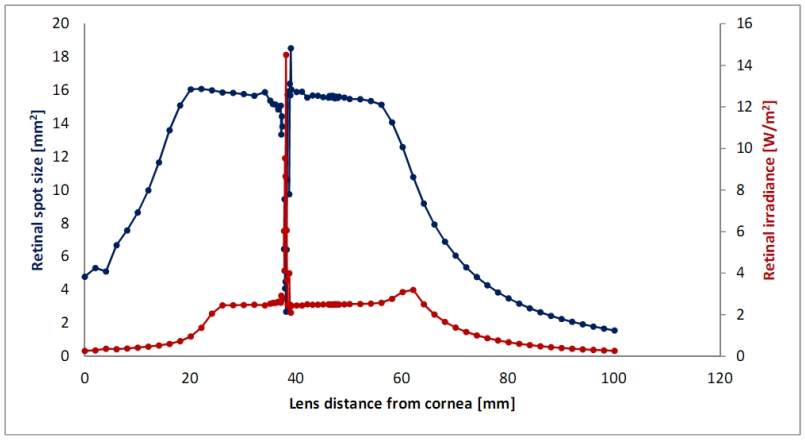

Figure 4.15: Simulation of the spot size and the irradiance as produced by the F410 on the retina as the focus scans through the eye.

of predicted irradiance values with the limits set by the standard and other relevant sources. To help with the evaluation of the measurement system, a model of the scanning lens and the eye was created in Zemax (Radiant Zemax LLC, Version 2011). The scanning lens is a combination of a doublet and a meniscus lens, both supplied by CVI Melles Griot and glued into a home made holder using UV cure glue. The lenses are sold together for a fixed focal length and can thus be imported into Zemax from the CVI lens catalogue in that exact same combination. The eye used for the Zemax simulation was the Liou & Brennan 1997 eye model as supplied by the Zemax knowledgebase article "How to Model the Human Eye in Zemax" which is considered the best currently available model for the living eye since it takes into account the different curvatures of the anterior and posterior surfaces of the lens and also provides a different refractive index for the lens core which other models omit [86]. The scanning lens was then moved in respect to the position of the eye from a distance of 0 mm from the cornea to a distance of 100 mm in steps of 5 mm and the RMS spot size on the retina simulated using Zemax's spot diagram. Figure 4.14 shows a diagram of the simulation optics.

A distance of 0 mm to the cornea will never occur in a real measurement situation, but for the purpose of the model it was included. The data obtained from this model confirms the assumption made above that the beam will never focus on the retina unless the scanning lens is quite a distance

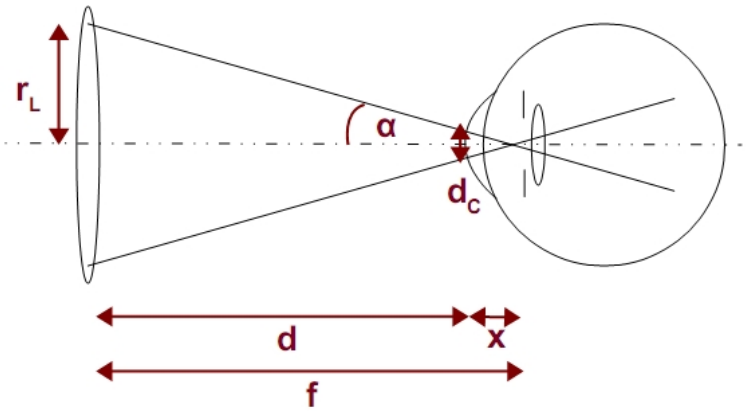

Figure 4.16: The scanning lens positioned such that the focus is in the anterior chamber of the eye. With r_L being the radius of the scanning lens, α being the convergence angle, d being the distance of the lens from the eye, f being the focal length of the lens, x being the depth of the focus in the anterior chamber and d_C being the diameter of the beam on the cornea.

away from the eye. The retinal spot size and irradiance is shown in figure 4.15.

The retinal spot size starts to decrease once the scanning lens is more than approximately 60 mm away from the eye. At this point, due to the focal length of 47 mm and the resulting high divergence of the beam, the pupil starts clipping parts of the beam and thus reduces the possible irradiance on the retina as shown in the graph. According to the model, the highest retinal irradiance is encountered at a distance of approximately 39 mm from the eye; however this is most likely not the case since it is a well known fact that the simple ray tracing mode in Zemax is not capable of accurately modelling the system when the focus of the beam happens to be exactly on the surface of an optical object. The spike in irradiance in figure 4.15 can therefore be disregarded as an artefact of the modelling, as it follows from logical consideration of the beam path that the spot size and thus the irradiance on the retina at this distance of the scanning lens from the eye will be similar to the spot sizes encountered adjacent to this position. However, for the reason of added security, three times the irradiance predicted by Zemax was used to evaluate the hazards to the retina. The factor of three was considered to be a reasonable safety margin.

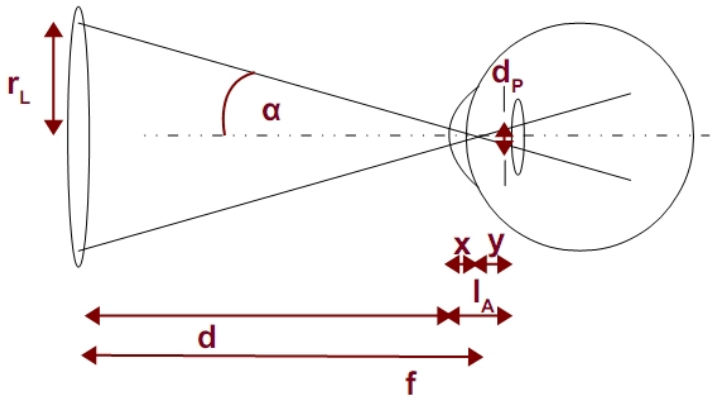

Figure 4.17: The focus inside the anterior chamber of the eye. With r_L being the radius of the scanning lens, α being the convergence angle, d being the distance of the lens from the eye, f being the focal length of the lens, l_A being the depth of the anterior chamber, x being the depth of the focus in the eye, y being the distance of the focus from the pupil plane and r_P being the radius of the beam at the pupil plane.

The irradiance on the retina can be calculated by dividing the incident power by the retinal spot size. The incident power was assumed to be 39 µW which is the AEL for a Class 1 laser for a viewing period of 100 seconds as defined by the British standard. To calculate the correct irradiance, the beam diameter at the pupil plane needs to be taken into account. The retinal spot size as given by Zemax was calculated using a 7 mm diameter pupil as defined in the standard for the smallest spot size on the retina. Even though the pupil will constrict in the measurement conditions presented by the F410 and the spot size on the retina will thus be smaller than predicted by the Zemax model, a smaller percentage of the absolute power of the beam will be let through the pupil and thus the irradiance on the retina will be smaller than when measured with a 7 mm diameter pupil. Therefore it was considered appropriate to use a 7 mm diameter pupil as the limiting aperture for the simulation. In any situation where the beam diameter at the pupil plane is larger than the limiting aperture the irradiance on the retina therefore has to be corrected by the factor that the beam is overfilling the pupil with. This can theoretically be done by dividing the incident power by the clipping factor and then calculating the irradiance for the non-clipped area to account for the decrease in irradiance. However, for the retina the non-clipped area is not known due to the

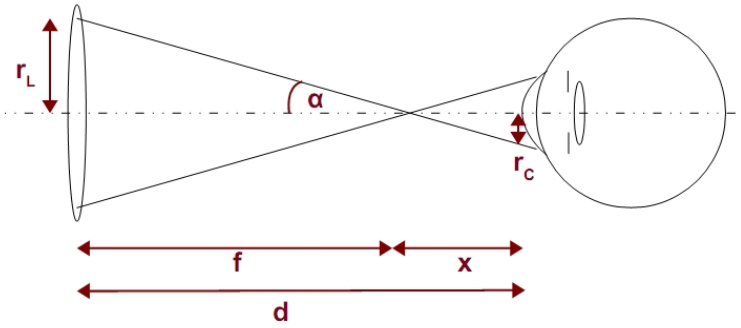

Figure 4.18: The focus outside the eye. With r_L being the radius of the scanning lens, α being the convergence angle, d being the distance of the lens from the eye, f being the focal length of the lens, x being the distance of the focus from the eye and r_C being the radius of the beam on the cornea.

fact that a 7 mm diameter pupil was used in the Zemax model and thus only the clipped spot sizes are known. Therefore, the retinal irradiance in cases where the beam is overfilling the pupil has to be calculated from the clipped irradiance directly after the pupil.

To calculate the irradiance at cornea and lens (or in this case directly after the 7 mm limiting pupil), simple geometric approximation was used. Two general lens positions were considered, one with the focus inside the eye (figures 4.16 and 4.17) and one with the focus outside the eye (figures 4.18 and 4.19). Using the diagram provided in figure 4.16, the spot size and thus the irradiance on the cornea can be calculated for positions of the scanning lens where the focus is inside the eye (0 to 48 mm distance of the lens from the cornea). The spot size is calculated using the law of proportionality:

$$r_C = \frac{r_L}{f} \times (f - d)\,. \tag{4.6}$$

The same principle is used for calculating the spot size at the pupil plane for positions where the focus is inside the eye as depicted in figure 4.17:

$$r_P = \frac{r_L}{f} \times (l_A - (f - d))\,. \tag{4.7}$$

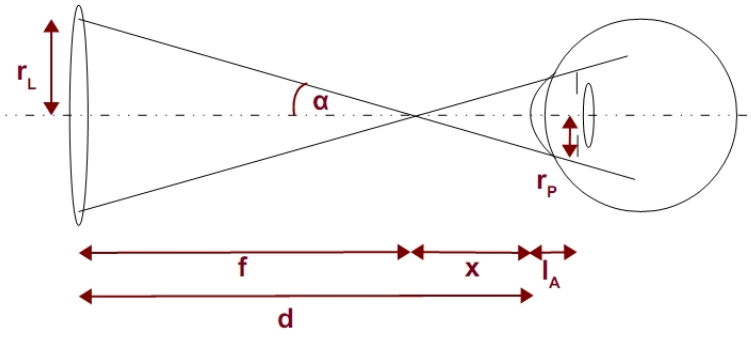

Figure 4.19: The focus outside the eye. With r_L being the radius of the scanning lens, α being the convergence angle, d being the distance of the lens from the eye, f being the focal length of the lens, x being the distance of the focus from the eye, l_A being the depth of the anterior chamber and r_P being the radius of the beam at the pupil plane.

For positions where the focus is outside the eye, the spot size at the cornea is calculated by

$$r_C = \frac{r_L}{f} \times (d - f) \tag{4.8}$$

as derived from figure 4.18, and the spot size at the pupil plane can be calculated by

$$r_P = \frac{r_L}{f} \times ((d - f) + l_A)\,, \tag{4.9}$$

as shown in figure 4.19. The values for the pupil plane are for the full beam size and have to be corrected by dividing them by the factor by which the beam is larger than the pupil size. For any beam sizes that are smaller than 1 mm in diameter the beam size has been set to 1 mm according to the paper discussed in the next section. The spot sizes and respective irradiances for the cornea and the lens (i.e. directly after the pupil) are shown in figures 4.20 and 4.21. The highest irradiance that can theoretically be encountered in the cornea and the lens occurs when the focus is incident on the respective surface. The lateral radius of the focus can be calculated from equation 3.8 which describes the spread of the focus and thus the image in a conventional microscope. The size of the focal spot in the F410 would therefore theoretically be as small as $(1.3\,\mu\text{m})^2$, thus giving a possible

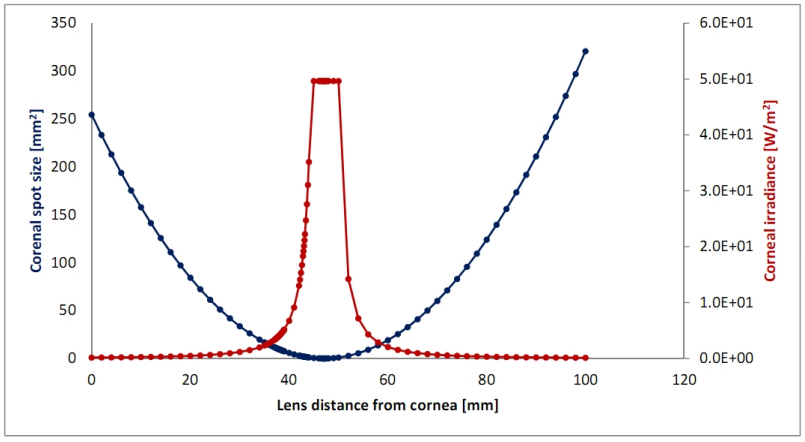

Figure 4.20: Model of the spot size and irradiance produced by the F410 as the beam scans through the cornea. The irradiance shows a flat cut-off at approximately $50\,\mathrm{Wm}^{-2}$ due to the fact that the power was averaged over a 1 mm aperture rather than the theoretical spot size.

irradiance of $7.22 \times 10^6\,\mathrm{Wm}^{-2}$. However, due to aberrations and misalignment in the system it is safe to say that this irradiance will never be reached. Furthermore the power of the beam will be spread over a much greater area than the theoretical focal spot size by small eye movements. Thus the averaging over a 1 mm aperture for small beams as described in section 4.3.3 was used for the calculations. Using this averaging, the highest possible irradiance encountered in the focus and thus in the cornea and the lens is $49.7\,\mathrm{Wm}^{-2}$ as shown by the hat-shaped irradiance cutoff in figures 4.20 and 4.21.

4.3.3 Guidelines for ocular safety with the use of ophthalmic instruments

As discussed above the BS-EN60825-1 does not explicitly state any limits for the irradiance of cornea and lens. Limits are inherent in the values given by the standard but since the standard does not consider the focusing of the light in any part of the eye other than the retina, it is not applicable to the F410. Therefore, another source to define those limits had to be found. Even though it incorporates a section on ophthalmic instruments that recommends an adjusted MPE for the retina, the Amercian standard does not cite any limits for the cornea and lens neither. There

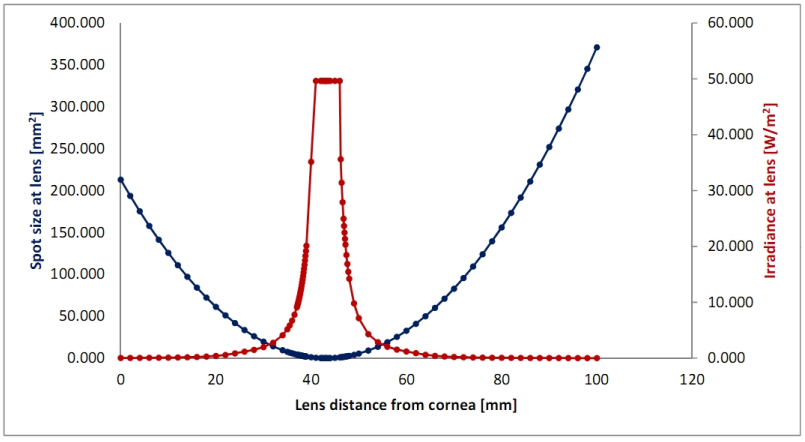

Figure 4.21: Model of the spot size and the irradiance produced by the F410 in the lens. The flat cut off in the irradiance is due to the averaging of the beam power over a 1 mm aperture.

is, however, a task group of the International Commission on Non-Ionizing Radiation Protection (ICNIRP) around Dr. David Sliney who has been looking at damage to the eye from ophthalmic instruments. This group has published at least two relevant papers [87][88] which describe the hazards and limits for the cornea and the lens and are considered guidelines for the American standard. Since the British standard does not apply to the F410, but best practice has to be followed for health and safety reasons, these two papers were considered valid references. The first paper, "Adjustments of guidelines for exposure of the eye to optical radiation from ocular instruments: statement from a task group of the International Commission on Non-Ionizing Radiation Protection (ICNIRP)" [87], is the more relevant one in this case since it does not only adjust the retinal MPEs but discusses the implications for lens and cornea. This paper, which was also recommended to the author of this thesis to evaluate the limits for the F410 by personnel of the British Health and Safety Agency, includes several tables which state the exposure limits for cornea, lens and retina for photochemical and thermal hazards. According to both the British standard and the papers, a wavelength of 402 nm falls in the visible range and does not create any hazard to the cornea, however for the evaluation of the system a long UV-A operating wavelength was assumed. For the lens, a thermal hazard applies for wavelengths of 360 to 450 nm, and for the retina the blue light hazard applies for similar wavelengths. Table 1 states the "exposure guidance and

Ocular surface	Exposure guideline	Aperture	Maximal exposure duration
Cornea	$3\,\mathrm{mJ\,cm^{-2}}$	1 mm	0.6 s
Lens	$1\,\mathrm{J\,cm^{-2}}$	1 mm	201 s
Retina	$2.2\,\mathrm{J\,cm^{-2}}$	1 mm	1517 s

Table 4.1: Exposure guidelines and damage thresholds at relevant ocular planes.

hazard thresholds at each relevant ocular plane". Assuming a wavelength of 400 nm and a maximum irradiance of $49.7\,\mathrm{Wm^{-2}}$, the maximal exposure duration for cornea, lens and retina can be calculated (table 4.1). The calculations show that the guideline limit for the cornea is below the actual exposure occurring in the F410. According to the paper, the cornea should be exposed for only 0.6 s within one day; the exposure duration by the F410 is longer. After careful consideration it was chosen to ignore this safety guideline. The first reason for this decision is that the F410 does not actually operate in the UV but rather in the very short blue wavelength range and thus the cornea should not be affected at all according to both the British standard and the ICNIRP paper. The second reason is that the most dangerous wavelength for the cornea is in the short UV at 270 nm which is a reasonable distance away from a wavelength of 402 nm. Considering these two facts it was decided that the probability for damage to the cornea in healthy individuals is low.

The averaging aperture for the calculations of the actual irradiance is given as 1 mm due to small eye movements which will spread the power over such an area in a very short time, even when the actual focus is smaller than 1 mm diameter. This averaging aperture takes into account head restriction and eye stabilisation. However, the paper states in section 3C ("Applying Infrared Limits to Protect the Cornea and Lens") that the area over which the energy should be averaged in the lens needs further investigation and that it is possible that the aperture should be smaller than 1 mm diameter. It is mentioned several times that 1 mm is the maximum applicable aperture. This aperture was derived from mathematical models of heat dissipation and corneal injuries from infrared lasers. In the case of the F410 a head- and chin-rest is used to help the subject position their eye. However, the head is not restrained and the eye not stabilised and can move freely. It is therefore believed that an averaging aperture of 1 mm is applicable. The British Standard con-

firms that it is rare to get a spot size as small as 135μm in diameter when the exposure duration is 100 s (Annex C). However, the BS-EN60825 applies correction factors for eye movements for long exposure durations so that the numbers from the paper and the standard are not directly comparable.

If the maximal exposure duration that will actually occur in any point of the eye is known, the maximum permittable exposure can be calculated reversely from the equations given in table 4.1. The probing beam exiting the F410 is scanning through the patient's eye on the optical axis with a speed of 40 mm s^{-1}, over a scanning distance of 10 mm. Since the averaging aperture is 1 mm and the convergence angle of the beam is 0.189 mrad, the length of the beam that has the highest irradiance of 49.7 Wm^{-2} is 5.22 mm. Therefore, the focal volume spends approximately 0.13 s per scan within any part of the eye. If it was assumed that one measurement session included 100 scans, and that 10 measurements were taken every day, this would mean that the focus spends a total of 130 s in any part of the eye in one day. This is an exaggeration of the number of scans that will occur in a real life situation; however for the reason of safety margins this was the assumed total exposure duration. If an exposure duration of 130 s is assumed, the maximum permissible exposure for lens and retina can be calculated by dividing the exposure guideline by the exposure duration. Multiplying the smallest resulting irradiance by a 1 mm aperture then gives the total permissible power that may enter the eye, which in this case would be 60 μW.

The second paper, "Maximum permissible exposures for ocular safety (ANSI 2000), with emphasis on ophthalmic devices" [88], contains a guideline on how to use the section of the ANSI 2000 standard that is devoted to ophthalmic instruments. However, similar to the British standard, this section only evaluates the irradiance on the retina. The paper provides guidance on how to use the standard and worked examples for several common ophthalmic instruments. It explains how the assumptions made in the original standard for the viewing of collimated and extended beams, i.e. free head and eye movement, natural constriction of the pupil and natural aversion reflexes of the eye such as lid-closure, were removed from the relevant equations. The paper introduces a corrected MPE for the pupil plane (MPΦ) which is derived from the corneal MPE given in the

standard by removing the response of the pupil to bright light to account for artificially dilated pupils which might occur in an ophthalmic measurement situation. Following the corrected equations from the paper, the thermal and photochemical limits for the power entering the natural or dilated pupil are (from table 3 [88]):

$$\mathrm{MP}\Phi_{th} = 6.93 \times 10^{-4}\, C_T\, C_E\, P^{-1}\, t^{-0.25} = 9.6\,\mathrm{mW} \tag{4.10}$$

$$\mathrm{MP}\Phi_{ph} = 5.56 \times 10^{-6}\, C_B\, \alpha^2\, t^{-1} = 1.99\,\mathrm{mW}, \tag{4.11}$$

with $\mathrm{MP}\Phi_{th}$ being the thermal maximum permissible exposure and $\mathrm{MP}\Phi_{ph}$ being the photochemical limit. The constants C_T, C_E, P and C_B are taken from table 2 for $\alpha = 189\,\mathrm{mrad}$, $\lambda = 402\,\mathrm{nm}$ and $t = 100\,\mathrm{s}$. Since the $\mathrm{MP}\Phi_{ph}$ yields the lower number this value has to be used as the safety limit. The maximum permissible irradiance on the retina is also given in table 3 and can be calculated from

$$\mathrm{MPE}_{r,th} = 2.04\, C_T\, P^{-1}\, t^{-0.25} = 1186\,\mathrm{Wm}^{-2} \tag{4.12}$$

$$\mathrm{MPE}_{r,ph} = 2.45\, C_B\, t^{-1} = 245\,\mathrm{Wm}^{-2}. \tag{4.13}$$

Again, the more restrictive value has to be used as the upper limit. It is furthermore recommended in section 9 ("Additional safety issues") that if repetitive testing of volunteers is to take place in the same session, the photochemical limit divided by the number of exposures over a 24 hour period should not be exceeded. In addition to this it is also explained that due to the nature of the original Standard which assumes that the beam is overfilling the pupil, protection for light damage in the anterior segment of the eye is included for the visible spectrum. For wavelengths between 380 and 1400 nm a spectrally unweighted limit was introduced that recommends a maximum permissible corneal irradiance of $4.0 \times 10^4\,\mathrm{Wm}^{-2}$ for exposure durations above 10 s.

4.4 Discussion and conclusion

In the first section of this chapter it has been shown that Brimonidine, the compound of interest for Allergan Inc., fluoresces very little with a quantum yield of approximately 0.41%. As a comparison, Fluorescein which is a well known fluorescence standard fluoresces about 170 times more. The instrument was therefore conceptualised to detect very low fluorescence intensities by using a photo-multiplier tube detector with a peak sensitivity at 530 nm which is very close to the emission maximum of Brimonidine (around 535 nm). To increase the signal to noise ratio, electrical filtering and amplification was added to the set up using an active low pass filter. Unfortunately, since the home-build electronics were not provided in time to test them before the submission of this thesis, no comment can be made about the performance of the instrument when using professional electronics. The expectation is that the performance will increase drastically due to the fact that much less noise will be induced in the signal itself (shorter and better screened cables) and in the post-processing of the signal, leading to a better signal to noise ratio. Furthermore the instrument did not have a light-tight outer casing for most of the measurements presented in this thesis because the casing was made to fit the instrument once the home-build electronics had been added. This also is believed to have lead to an increase in the measurement noise since unwanted background signal from without the instrument could reach the detector. The photo-multiplier is mounted in a separate light-shielding casing but measurements of noise levels showed that this was not sufficient to block out all of the background light. Therefore some problems with noise remain even though measures have been taken to reduce the noise as much as possible.

The analysis of the axial resolution shows that the instrument can be improved in this region since the reflection arm and fluorescence arm FWHMs are rather big with 285 µm and 124 µm respectively. However, having near theoretical resolution is not as crucial in the F410 as it would be in for example a confocal microscope. Currently, the concentration of the drug can only be measured very crudely by extracting the relevant tissues and analysing the counts from the radioactively labelled medication. No fine depth discrimination is possible with this method and gradients across the aqueous humour will not be detected at all since the whole aqueous is extracted and measured.

Therefore the depth discrimination offered by the F410, even if not perfect, is a huge improvement compared to the currently used method. The lateral resolution of the instrument is of little importance for the current version since only a one-dimensional scan along the optical axis of the eye is performed. The lateral resolution thus only plays a role when assessing the volume of light that is being collected but not in terms of distinction between neighbouring features. The specification for the F410 states an axial resolution of 100 µm as measured by the FWHM to be acceptable. The resolution measured in the fluorescence arm is slightly above this value and thus needs improving in a final version of the instrument if Allergan are interested in developing it further. However for the purpose of the proof of concept this resolution is good enough and shows that the gradient of the concentration of both Brimonidine and the reference standard Fluorescein can be measured accurately. When expressed as the half width of the PSF at the 3% signal level, the axial resolution of the F410 is currently slightly worse than that of the gold-standard instrument, the Fluorotron Master^{TM}. This is only true for the version of the instrument that is adapted for anterior chamber measurements, however, and the axial resolution of the F410 is one order of magnitude better than the unmodified version of the Fluorotron.

For the consideration of the laser safety of the instrument, the different limits for cornea, lens and retina as they can be taken from the BS-EN60825-1, the ANSI 2000 and the ICNIRP guidelines were presented. First of all the retinal safety was considered since this is the value obtained from the standards. According to the British standard, the retinal exposure limit applying to the conditions encountered in the F410 is 1532.6 Wm^{-2}. The Zemax simulation of the spot size and irradiance on the retina shows that the maximum irradiance that is ever encountered on the retina when using the F410 is 14 Wm^{-2}. Unfortunately, this value is not to be trusted due to ray tracing difficulties in Zemax and the maximum irradiance is likely to be lower and thus more eye safe. For additional security reasons however it was decided to use the value obtained from the simulation. The maximum permissible exposures for the retina given in the ANSI 2000 ophthalmic instrument section and the ICNIRP paper are below the value given in the British standard. This is due to the fact that in these documents the natural aversion reactions like pupil contraction and lid closure have

been removed from the calculation, whereas both the British standard and the original ANSI standard rely on those reactions to make their calculations valid. According to both these documents, which are more applicable to the measurement situation at hand than the British standard, the maximum permissible irradiance on the retina ranges from 220 Wm^{-2} to 245 Wm^{-2}. This value is drastically reduced compared to the value given by the British standard. However, even for the reduced value the F410 is below the limit by an order of magnitude and can thus be said to be very safe for the retina for prolonged viewing periods.

For the cornea and lens the situation is more difficult. According to all the sources cited above, a wavelength of 402 nm falls within the visible region and should thus not cause any photochemical damage to either the cornea or the lens. However, in nature no clear dividing line can be drawn between UV light and blue light, and for the lens thermal damage can still occur for the used wavelength. Since the used wavelength is at the limit to wavelengths defined as being UV, it was considered sensible to evaluate the harm that might be caused by UV light of long wavelengths (UV-A). The ICNIRP guidelines and the ANSI ophthalmic paper contradict each other in the safety guidelines for the cornea. The ICNIRP guideline states a limit of 0.3 Wm^{-2} for a viewing period of 100 s, whereas the ANSI 2000 states a limit of 4×10^4 Wm^{-2} for viewing times above 10 s. This discrepancy can possibly be explained by the fact that the corneal limit from the ICNIRP paper applies to the whole UV range of wavelengths, including those that peak in the damage curve, while the ANSI 2000 only considers wavelengths above 380 nm which are less harmful for the cornea. It was thus considered safe to use the value obtained from the ANSI. The theoretical irradiance encountered in the focal spot of the F410 (i.e. 7.22×10^6 Wm^{-2}) would exceed this limit by two orders of magnitude. However due to aberrations in the beam the real focal spot will be larger than the theoretically possible spot size. Additionally, the irradiance will be spread over a larger area by involuntary eye movements, even if the head of the volunteer is stabilised in a head rest. For those reasons an averaging aperture of 1 mm diameter as defined in the ICNIRP guidelines was first used for the calculation of the irradiance in the focal area which yields 49.7 Wm^{-2}. However since this is the maximum aperture that should be used for the calculation and the ICNIRP states

that the area should probably be smaller, the area was later assumed to be only 50 µm in diameter. For this case, the irradiance in the focal spot of the F410 would be approximately $2 \times 10^4 \mathrm{Wm}^{-2}$ which is at half the safe limit given by the ANSI 2000. Therefore, the instrument can also be said to be safe for the cornea for long viewing periods, although the safety margin is probably reduced compared to the retinal safety margin.

For the lens the limit for thermal injury applies. This is set to $100\,\mathrm{Wm}^{-2}$ for exposure times of 100s. This limit applies to a 24-hour period, meaning that the additive exposure should not exceed the given value. Since the focus of the F410 is scanning through the eye, it was still considered to be safe for the total duration that the focal volume spends in any part of the eye within one day. However, this only applies if the power is averaged over a 1 mm diameter aperture, not if it was averaged over a smaller aperture. It therefore is disputable if the F410 is safe for the lens for extended viewing periods. However since no power above the AEL of 39 µW is used during any measurement of volunteers and since the actual exposure time is much shorter than assumed for the calculations, the instrument was still considered safe for the lens as it falls into laser Class 1 and the limits given in the ANSI 2000.

Concluding it can thus be said that the safety for the eye has been evaluated thoroughly and that even though the irradiance occurring in the focal spot of the F410 may be close to some of the exposure limits (which are very conservative experimental limits and by no means a division between safe and unsafe) the instrument falls within all known limits for cornea, lens and retina and is therefore completely safe for extended periods of intentional intra-beam viewing.

Chapter 5

Calibration

The F410 has to be calibrated such that the concentration of a natural fluorophore or other fluorescent compound can be determined from the fluorescence intensity at a specific position within the eye. To be able to do this the relationship between the intensity of the fluorescence, the concentration of the fluorophore and the measurement depth has to be found. In the real-world application, the fluorescent compound will not be distributed equally throughout the eye due to chemical processes such as e.g. binding of the compound to certain molecules within the eye or aqueous flow within the anterior chamber which create situations of inhomogeneous distribution. For the calibration, however, well defined homogeneous solutions are needed. The concentration of the compound at any position within the solution needs to be known to guarantee a reliable calibration of the instrument. Therefore the whole system was first modelled to predict the behaviour of several concentrations of Fluorescein in a cuvette where a homogeneous solution is guaranteed. Measurements were then carried out in the cuvette to demonstrate the validity of the model and to have a standard means of calibrating the instrument using Fluorescein which is one of the most commonly used compounds in ophthalmic research [89][90][70][91] and can thus be regarded as a reference standard. Measurements using the pharmaceutical compound Brimonidine were also carried out in a cuvette to get a better understanding of the concentrations that would be suitable

for the calibration of Brimonidine in the eye. As a last step, homogeneous solutions of Fluorescein concentrations were measured in *in vitro* porcine eyes by first removing as much of the aqueous humour as possible using a syringe and then refilling the anterior chamber with a known concentration of Fluorescein. By comparing the measurements obtained for Fluorescein in *in vitro* eyes to the measurements taken in the cuvette the F410 can also be calibrated to the measurement of fluorescent compounds within the eye. Measurements were both taken with the highest available laser power (approximately 0.6 mW) and a lower laser power of 39 µW that is eye safe for the current configuration of the instrument as determined in chapter 4. The higher laser power was included to initially test the system and to show the performance at better signal levels which might be reached in the future if the improvements suggested in chapter 8 are implemented into the system.

5.1 Calibration in the cuvette

A set of curves as shown in figure 3.10 can be used to find all the parameters needed to calibrate the instrument. For the most important step, i.e. for determining the concentration from a measured intensity value, the relationship between the unattenuated intensity measured by the instrument for various concentrations and the concentration has to be found. The unattenuated intensity (the maximum intensity at the very start of the cuvette which is not influenced by attenuation through absorption) has to be used since there are uncertainties in the concentration determination if attenuated intensities were used due to the fact that the attenuation curves for different concentrations cross after a certain depth, creating points were one intensity could refer to several concentrations. This means that to be able to calculate the concentration of a given sample at any depth, the intensity has to be "restored" to its unattenuated value before converting it into a concentration. For this restoration, one other parameter is needed: The rate at which each concentration decays with the measurement depth in the solution. To find an equation for this concentration-dependent decay parameter the set of recorded calibration curves has to be analysed. After all the necessary

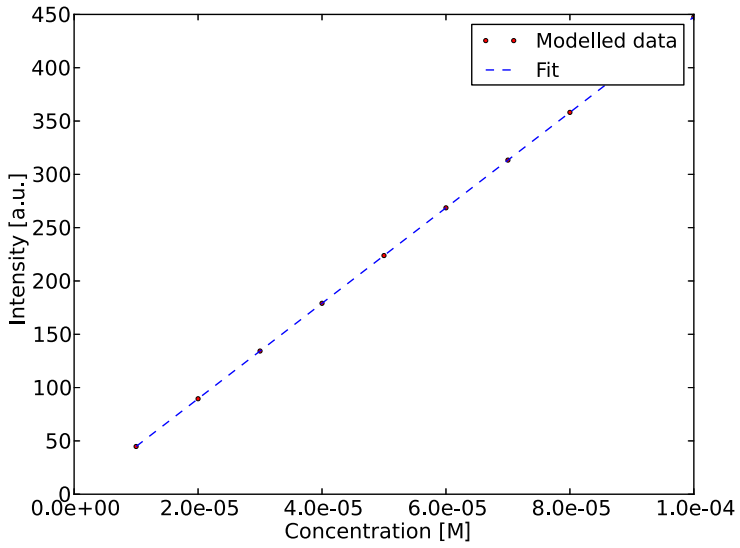

Figure 5.1: The intensity modelled at position 0 (i.e. no depth-attenuation) as a function of the concentration of the sample solution with no noise. The correlation coefficient R^2 is 1.0.

parameters have been found from the calibration curves, the concentration at any depth of a given sample can be calculated using an iterative approach that is explained below.

5.1.1 The model

To determine its suitability, the calibration routine was first carried out using the modelled Fluorescein decay curves from section 3.3. Ten modelled curves of the concentrations 100, 90, 80, 70, 60, 50, 40, 30, 20 and 10 µM were used, the same ones as depicted in figure 3.10. First of all, the relationship between the unattenuated intensity and the concentration was determined by finding the maximum intensity value for each concentration and fitting a linear regression to the maximum intensity as a function of the concentration. Obviously, since the calibration data in this case comes from a model, the correlation coefficient R^2 is 1.0! Both the unattenuated intensity and its linear regression as a function of the concentration are shown in figure 5.1. As expected, the measured (or in this case, the modelled) intensity behaves linear with concentration. Therefore the fit is of

the form

$$I(C) = m_C \cdot C, \tag{5.1}$$

where $I(C)$ is the unattenuated intensity and C is the molar concentration, with the gradient m_C being 4.476588×10^{06}. Using this calibration equation, the concentration can accurately be calculated for any given unattenuated intensity. Therefore, in a second step, the intensity measured at a specific location within the sample has to be restored to its unattenuated value. This restoration is carried out to remove the influence of depth on the signal as predicted by the Beer-Lambert law and to thus make it easier to identify changes in intensity that are caused by real changes in concentration. To be able to remove the depth dependent attenuation of the fluorescence intensity, the relationship between the extinction coefficient and the concentration of the fluorophore has to be found. For that purpose, the decay rates for the set of measurement curves the calibration is based on have to be known. The measurement curves follow an exponential decay of the form $I(x, C) = I_0(C) \cdot \exp(-\epsilon(C)x)$ as described in section 3.3, where $I(x, C)$ is the intensity of the fluorescence for the concentration C at position x, $I_0(C)$ is the concentration-dependent offset (i.e. the unattenuated intensity value), $\epsilon(C)$ is the concentration-dependent extinction coefficient (i.e. the decay rate) and x is the position of the focus in the sample. The parameter $I_0(C)$ does not have to be found because it is equal to the unattenuated intensity for the respective concentration, and the actual intensity rather than the parameter is used in the calculation of the concentration to account for small differences in the fitting procedures and to thus make sure that the calculated concentration matches the measurement data. To find how the extinction coefficient ϵ relates to the concentration C, the exponential data was first linearised to

$$\ln(I(x, C)) = \epsilon(C)x + \ln(I_0(C)),$$

where $\epsilon(C)$ and $I_0(C)$ are the decay rate and the unattenuated intensity as above, and x is the measurement depth in the cuvette. The data is linearised since a fitting routine might find more suitable fitting parameters for a linear regression fit rather than for an exponential decay fit where a small change in the decay rate results in a big change in intensity. Furthermore this enables the

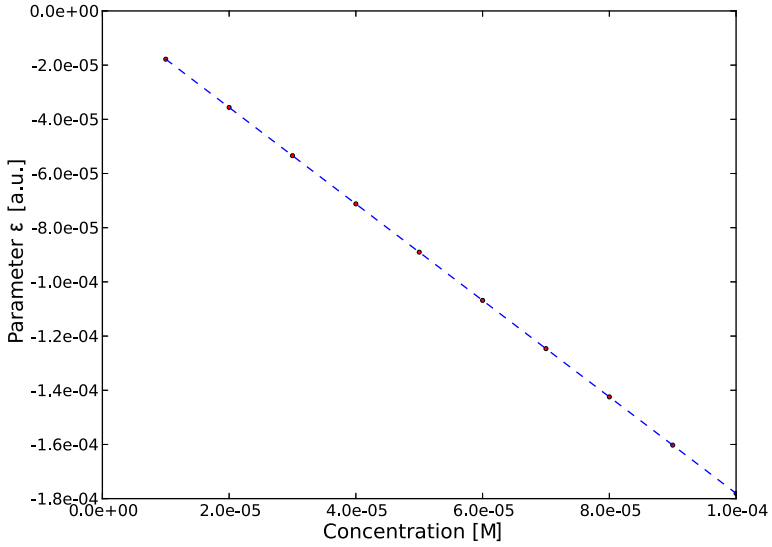

Figure 5.2: The parameter $\epsilon(C)$, the attenuation coefficient or decay rate, as a function of the concentration of the fluorophore in an ideal, noise-free measurement. The correlation coefficient of the fit is $R^2 = 1.0$.

researcher to spot any concentration that behaves in an unusual way more easily by eye. After the linearisation of the data, the parameter $\epsilon(C)$ is found for each concentration in the set of calibration curves. This gives the decay rates for the concentrations that were measured for the calibration. For the calculation of the concentration from any intensity, however, the decay rate for any possible concentration needs to be known. Therefore, the relationship between the extinction coefficient and the concentration has to be found. The coefficient is, in the case of the model, linearly dependent on the concentration of the fluorophore in the sample. Therefore, another linear regression of the format $\epsilon(C) = m_\epsilon \cdot C$ is calculated for the extinction coefficient. The extinction coefficient and the linear regression are shown in figure 5.2. The determined parameter for the gradient in this case was $m = -1.781 \times 10^{-06}$. Knowing the relationship between the unattenuated intensity and the concentration and the extinction coefficient and the concentration now makes it possible to calculate the concentration at any measurement position within the sample by following a five step approach for every measurement point:

In the first step, the concentration C at the current position x is found from the unattenuated intensity $I_{rec}(x, C)$ (either determined in the step before or taken from the measurement file if it is the first measurement point):

$$C(x) = \frac{I_{rec}(x, C)}{m_C}. \tag{5.2}$$

Then, the decay rate $\epsilon(C)$ for this concentration is found using the parameters determined from the calibration measurements:

$$\epsilon(C) = m_\epsilon \cdot C. \tag{5.3}$$

In the third step, the intensity expected at the next position for the determined concentration and decay rate $I_{th}(x + 1, C)$ is found by applying the Beer-Lambert law of absorption:

$$I_{th}(x + 1, C) = I_{meas}(x, C) \times \exp\left[-\epsilon(C)\Delta x\right], \tag{5.4}$$

where Δx is the step width between the current position x and the next position $x + 1$. After the expected intensity of the signal has been determined, the actual (i.e. measured) intensity at the next position $I_{meas}(x + 1, C)$ is compared to the expected intensity $I_{th}(x + 1, C)$ to find out if the signal has changed by more than just the expected value. The change in signal is calculated as a percentage of the expected intensity:

$$\%\Delta I = \frac{I_{th}(x + 1, C) - I_{meas}(x + 1, C)}{I_{th}(x + 1, C)}. \tag{5.5}$$

The difference between the actual and the expected intensity is measured in percent of the expected intensity because it can then be directly translated to the corrected intensity. This is due to the fact that the fluorescence intensity is linear with both the intensity of the excitation light and the concentration of the sample. Since the difference in expected and actual intensity, if above a certain error band, is assumed to be due to a change in concentration, the change in intensity of an unattenuated measurement point would be equal in percentage to the change detected in the attenuated measurement point if the same change in concentration was present. Thus, the

unattenuated (or recovered) intensity has to change by the same value to account for the detected change in concentration. Therefore, in the fifth step, the recovered intensity determined in the previous cycle for the current measurement point $I_{rec}(x, C)$ is changed by the determined percentage to set the recovered intensity for the next position (i.e. position $x + 1$):

$$I_{rec}(x + 1, C) = I_{rec}(x, C) - I_{rec}(x, C) \times \%\Delta I. \tag{5.6}$$

If the percentage change is within the error band, the recovered intensity from the measurement point before is set as the recovered intensity for the current measurement point without changing it:

$$I_{rec}(x + 1, C) = I_{rec}(x, C). \tag{5.7}$$

The whole process is then repeated until the last data point has been recovered. A flow chart of the procedure is shown in figure 5.3 for clarity. The abbreviations used in the equations are defined as follows:

Abbreviation	Definition
$\mathrm{I}_{meas}(x)$	Measured intensity at position x
$\mathrm{I}_{th}(x)$	Expected intensity at position x
$\mathrm{I}_{rec}(x)$	Intensity recovered for position x

To illustrate this process, a sample calculation was carried out in table 5.1. The first column shows the depth of the measurement position in the sample in micrometers. The second column holds the intensity measured (or in this case, modelled) at each depth in scaled units (all measurements were scaled to a gain of one on the photo-multiplier). The third column contains the expected intensity values, calculated for the next position using the measured intensity of the current position (column two) as described in step three above. The fourth column indicates the difference between the expected and the actual (measured) intensity at the next position in percent of the expected intensity. If the measured intensity is greater or smaller than the expected intensity, this change is registered here. The restored intensity is calculated in column five using the percentage

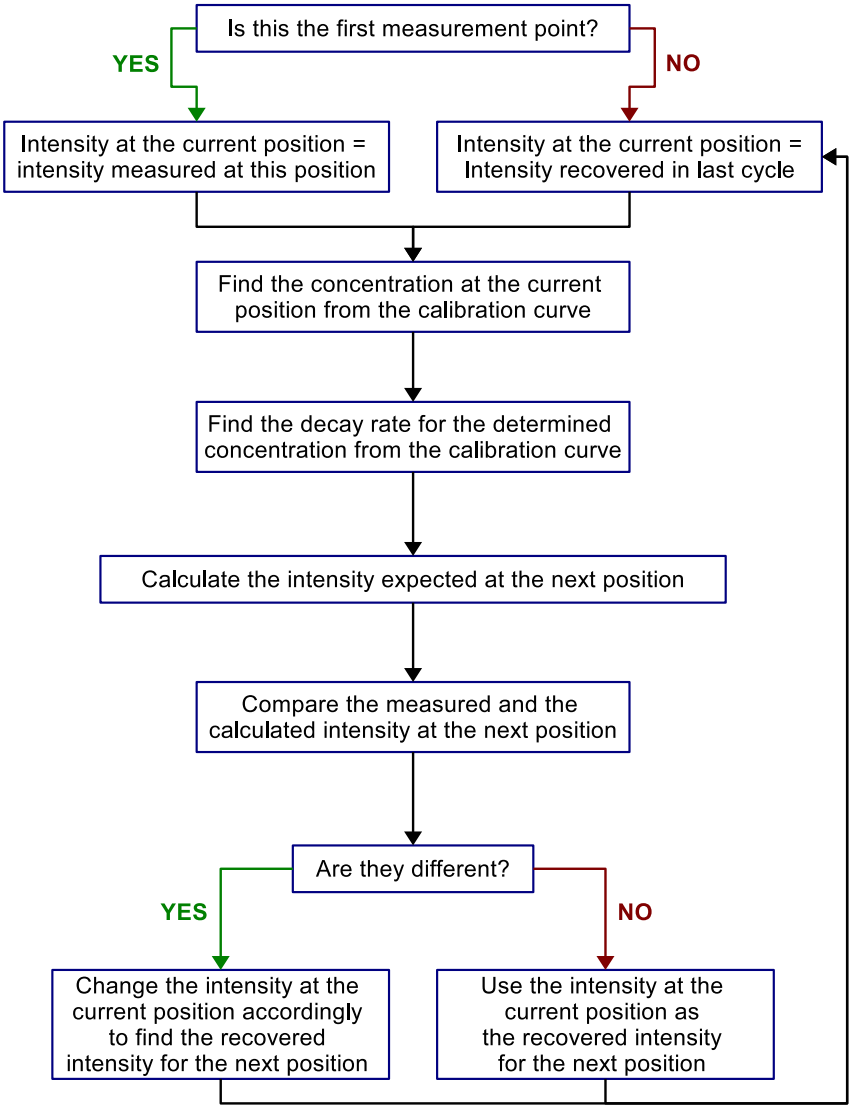

Figure 5.3: A flowchart showing the procedure of the recovery of concentration.

Depth [µm]	$I_{meas}(x, C)$ [s.u.]	$I_{th}(x+1, C)$ [s.u.]	ΔI [%]	$I_{rec}(x, C)$ [s.u.]	$C(x)$ [M]
0	357.60	–	0	357.60	$8 \cdot 10^{-5}$
1000	310.31	310.31	0	357.60	$8 \cdot 10^{-5}$
2000	269.28	269.28	0	357.60	$8 \cdot 10^{-5}$
3000	233.67	233.67	0	357.60	$8 \cdot 10^{-5}$
4000	202.77	202.77	0	357.60	$8 \cdot 10^{-5}$
5000	175.95	175.95	0	357.60	$8 \cdot 10^{-5}$
6000	152.69	152.69	0	357.60	$8 \cdot 10^{-5}$
7000	132.49	132.49	0	357.60	$8 \cdot 10^{-5}$
8000	114.97	114.97	0	357.60	$8 \cdot 10^{-5}$
9000	99.77	99.77	0	357.60	$8 \cdot 10^{-5}$
10000	86.58	86.58	0	357.60	$8 \cdot 10^{-5}$

Table 5.1: Exemplary calculation of the concentration of a homogenous solution of Fluorescein.

determined in column four. If there is no difference between the expected and the measured intensity, it is assumed that the measured loss in intensity is only due to the attenuation of the excitation light and not due to a change in concentration, leaving the unattenuated intensity unchanged. If there is a difference between the expected and the measured intensity, it is assumed to be due to a change in concentration and the recovered intensity is changed by the same value as explained above.

The result of the determination of the concentration for all modelled intensities is shown in figure 5.4. This graph clearly shows that for the model the concentration can be accurately determined for any depth within the cuvette. It also shows that the crossing over of intensities in the measurement curves after a specific depth in the sample as shown in figure 3.10 does not influence the calculation of the concentration since only the decay rate is used to restore the intensity. The decay rate follows a linear trend with concentration and thus has a unique value for each concentration, preventing any uncertainties in the process.

In a second step, the calibration routine was used on a modelled sample where the concentration changes by a known value throughout the data set. Again, the data set was created using the actual calibration data from Fluorescein calibration measurements to make it resemble an actual measurement. The intensities in the data set were set to change from the equivalent concentrations

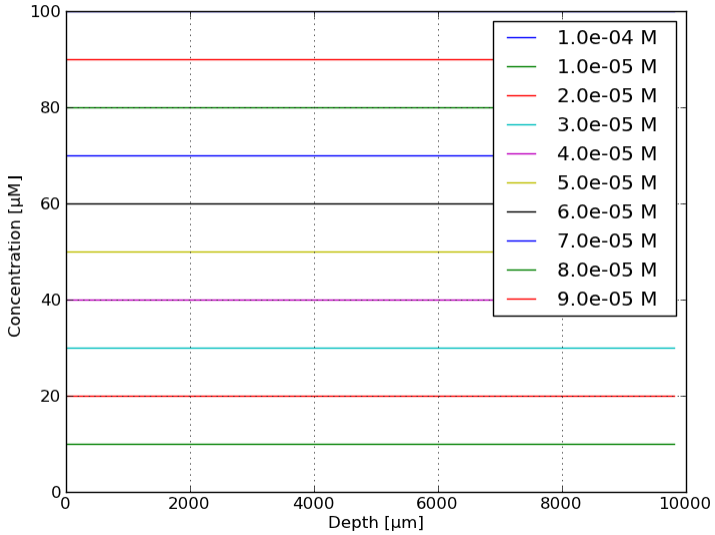

Figure 5.4: A plot of the determined concentration values from the calibration. The values given in the legend are the modelled concentrations, the values on the y-axis are the determined concentrations. They are an exact match.

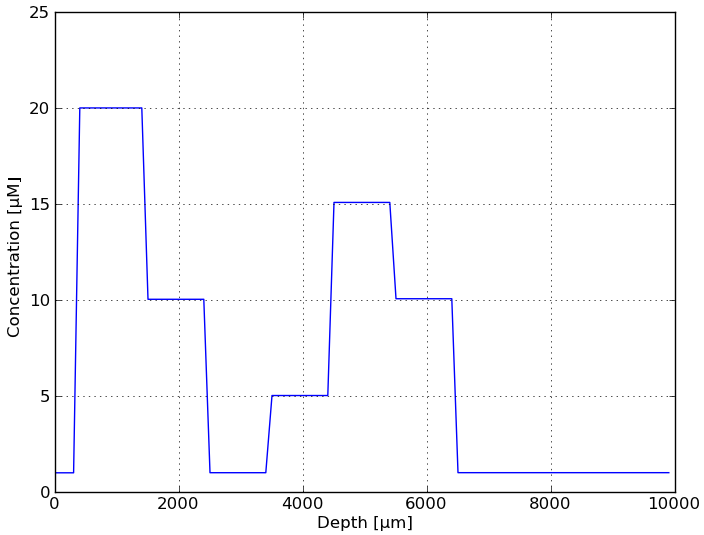

Figure 5.5: Restored concentrations of a modelled inhomogeneous sample. As above the determined concentrations are an exact match with the input concentrations.

of 1 to 20 μM at 400 μm, from 20 to 10 μM at 1500 μm, from 10 to 1 μM at 2500 μm, from 1 to 5 μM at 3500 μm, from 5 to 15 μM at 4500 μm, from 15 to 10 μM at 5500 μm and from 10 to 1 μM at 6500 μm depth. The appropriate attenuation introduced by each concentration was included in the calculation of the intensities. The resulting determined concentrations match the set concentrations perfectly as shown in figure 5.5. This second test of the calibration routine shows that unknown, changing concentrations can also be accurately recovered from the given intensity values using the calibration algorithm described in this chapter.

5.1.2 Fluorescein

High-power measurements

As a next step, homogeneous solutions of known concentrations of Fluorescein were measured in a cuvette of known path length to confirm that the calibration routine is valid for real measurements. The instrument was first configured such that an optical chopper (Thorlabs) was modulating the beam at a frequency of 1 kHz after the last lens of the system, and the modulated fluorescence signal was then locked to the reference signal from the chopper and amplified by a lock-in amplifier (LIA) (LIA MV 150S, Laser Components) to remove unwanted background signal from the measurement data. It was, however, found that the integration time of 3 ms on the LIA was too short for the frequency of the chopper to effectively reject noise from the system. In fact, noise was actually added due to aliasing effects between the chopping frequency, the integration time and the sampling frequency of the ADC. To run the chopper/lock-in system effectively, either the chopping speed or the integration time would have to be increased. Unfortunately, the chopper that was used in this set up was not capable of running at a higher frequency. A blade with thinner sections and thus a higher frequency could theoretically have been used, but since the blade was not in the focus of the beam this would have meant that not the whole beam would have been blocked by a dark section of the blade. This then would have lead to incomplete modulation of the signal and the introduction of more noise. The only options would therefore have been to

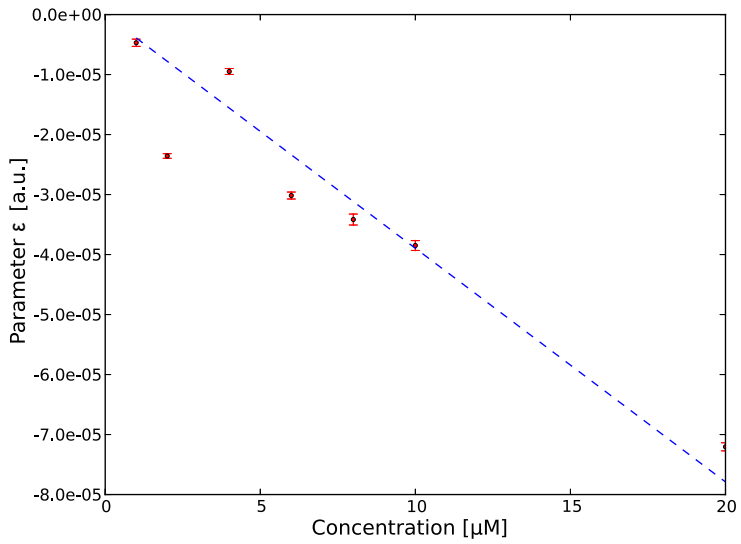

Figure 5.6: The relationship between the decay rate and the concentration as measured with the optical chopper.

either re-design the system such that an additional focal spot was provided where the chopper blade could be placed or to increase the integration time. Adding a second focal spot would mean adding more lenses and thus more aberration, reflection and auto-fluorescence to the system, and it was decided not to follow this route. A longer integration time, on the other hand, was also not feasible since this would influence the shape of the measurement curve so that only slow temporal changes in concentrations would be detectable and the amplitude of the fluorescence would thus be falsified and a wrong concentration detected. Nonetheless, calibration measurements were taken with the chopper and lock-in set up to gain a data set for comparison with the active low-pass filter described in section 4.2.4. Figure 5.6 shows the relationship between ϵ (the decay rate) and the concentration. The error bars for ϵ were calculated from the variance-covariance matrix provided by the fitting routine. The variance is found by calculating the square root of the main diagonal in the matrix, i.e. of the values at position 1,1.

The solutions of Fluorescein used for all calibration measurements discussed in this chapter were diluted in series from a stock solution of Fluorescein. The stock solution was made by weighing

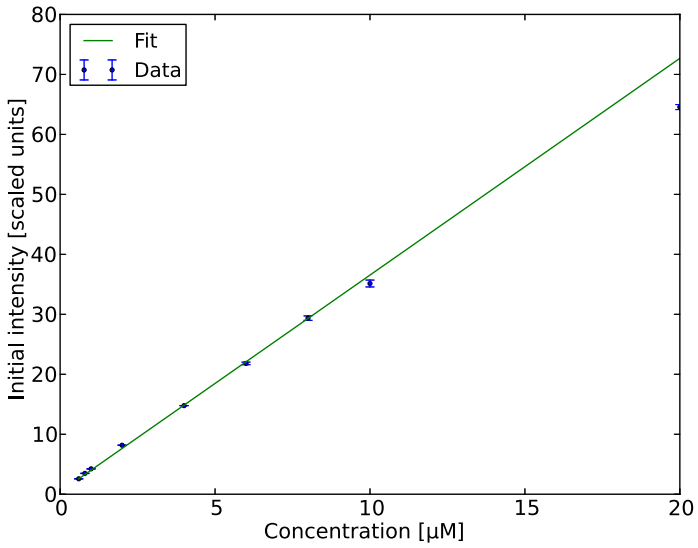

Figure 5.7: Linear fit to the unattenuated intensity of samples of different concentrations as measured with the optical chopper in place.

the needed amount of Fluorescein into an Eppendorf-tube using chemical scales and then adding the appropriate volume of water. Theoretically, to avoid cumulative errors from the dilution of the solution, each desired concentration should be weighed and mixed individually. However the available scales did not have high enough measurement resolution to measure the low weights of Fluorescein required which is why the serial dilution technique was chosen. The concentrations therefore have an error attached to them which was estimated by error propagation from the standard error of the pipetting volume and the standard error of the scales as given by the manufacturers. The estimated error in the mixed solutions is however at least two orders of magnitude smaller than the target concentration which is why it is not shown in the graphs. The measurement of each individual concentration was averaged over 20 consecutively taken scans to obtain the standard deviation of the measured intensity. All solutions were measured consecutively using the same reference voltage on the PMT to ensure minimal influence from external parameters. The measurements were repeated several times to confirm that the calibration parameters did not change from day to day. The most successful measurement (i.e. the one creating

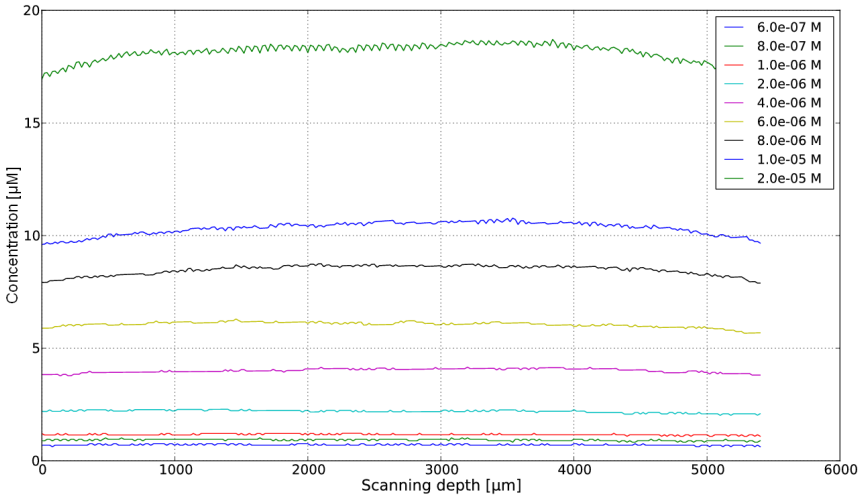

Figure 5.8: Concentrations calculated from the measurements taken with the optical chopper. The original concentrations are shown in the legend.

the most linear calibration curves) was used for the determination of the final set of calibration parameters.

Due to the non-linear behaviour of Fluorescein with concentration through mechanisms of self-quenching [92][93] only the linear part (up to a concentration of 20 µM) of the measurement data was used for the determination of the calibration parameters as shown in the graphs. The fit to the offset of the exponential decay fit is not used for the calibration and was thus omitted here. In the calibration, the fit to the unattenuated intensities as shown in figure 5.7 is used as described in section 5.1.1. The error bars on the data points in figure 5.7 show the standard deviation of the average maximum value for each concentration. The concentration can then be recovered from the measured intensities using these calibration parameters by removing the depth-dependency of the signal. The result of the recovery of the concentration from the measurement data is presented in figure 5.8. The graph clearly shows the aliasing effect introduced by the lock-in amplifier in the higher concentrations. This effect always occurs if the input signal is high enough, so that even though the lower concentrations seem fine in this graph, the effect would be visible there as well if

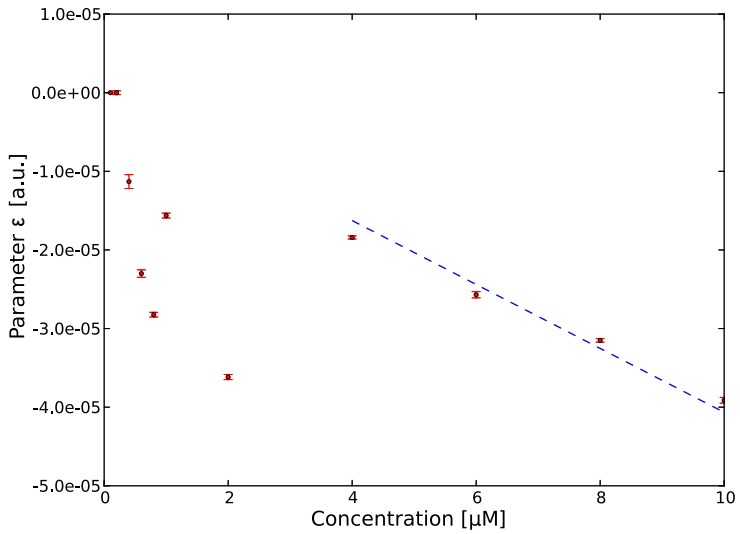

Figure 5.9: Linear regression fit to the decay rate versus concentration as measured by the low pass filter.

a higher gain on the PMT was used. It is, however, also visible that the concentrations calculated from the signal intensity are a very close match to the concentrations as they were mixed (given in the legend).

Due to the aliasing effect it was decided to remove the chopper from the system and use an active low pass filter instead as described in section 4.2.4. The resulting fit to the decay rate $\epsilon(C)$ is shown in figure 5.9, and the fit to the initial intensities in figure 5.10. For the fit to the decay rate the lower concentrations were omitted as is shown in the figure since they were clearly wrong whereas the higher concentrations show a good linearity with an intercept at zero as expected. The reason why the lower concentrations do not fit the linear trend is unknown. It is possible that due to the lower signal to noise ratio of the low concentrations the decay is not measured correctly by the instrument. Another reason might be that the absorption is so small that its effects are hidden by the random fluctuations in signal caused by the photon count on the detector. With the arrangement of using only the higher concentrations for the determination of the calibration curve the correlation coefficient as measured in R^2 is 0.96. It can of course be disputed if the

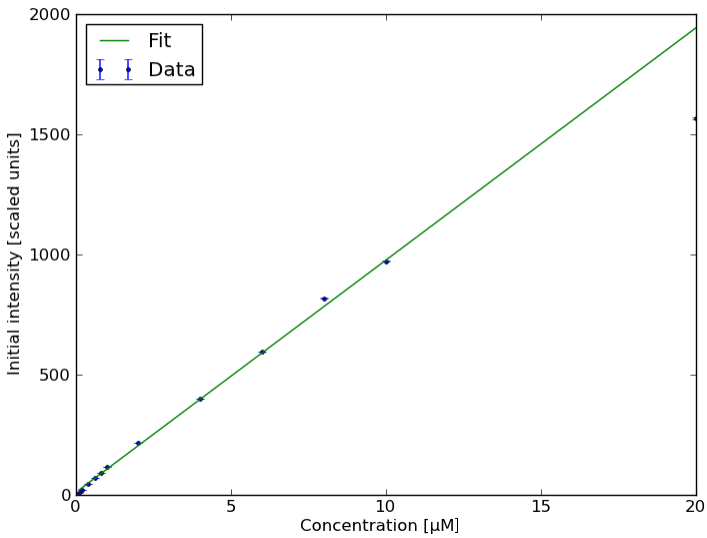

Figure 5.10: Fit to the unattenuated intensity of the measurement samples versus concentration as measured using the active low pass filter.

approach of not using the lower concentrations to find the relationship between the decay rate and the concentration is valid. Since this method showed good results for the recovery of the concentration from the measured intensities and no other data set recorded showed a better or rather more clear linear relationship between the decay rate and the concentration it was assumed that this measurement was valid. In addition all other measurements show a similar gradient for the decay rate. If only the higher concentrations are considered, the correlation is better for the set up with the low-pass filter than for the lock-in amplifier. Furthermore the error in the decay rate for the higher concentrations has been reduced compared with the measurements from the lock-in amplifier; however, the measurement points of the low concentrations do stray from the linear regression. The amplification provided by the electronic filter is much higher than with the lock-in amplifier and thus allows for better measurement resolution in terms of concentration. The most important point, however, is that no aliasing occurs and thus the signal is cleaner.

Figure 5.11 shows the recovered concentrations from the calibration with the low-pass filter. Again, the calculated concentration matches the mixed concentration as given in the legend very closely.

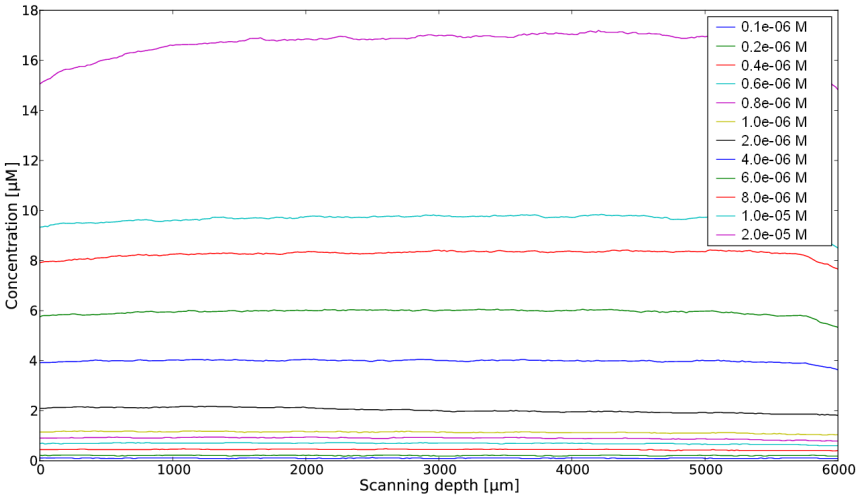

Figure 5.11: Concentrations recovered from the original measurement files. The input concentrations are shown in the legend.

It can be seen that the concentration of the 20 µM solution is estimated too low at approximately 16 µM. As the fit to the initial intensities of the samples shows this is due to the fact that Fluorescein starts self-quenching at this point and thus the emitted fluorescence is below the value which would be expected if the relationship between the unattenuated intensity and the concentration was completely linear for all concentrations. Apart from this quite high deviation from the true concentration value the error in the recovered concentrations lies below the 20% goal defined in the specifications for the instrument (see table 5.2). The four measurement points that show less good accuracy in terms of the average deviation from the true concentration value (i.e. 40 nM to 1 µM) are some of those points that do not match the fit of the decay rate in figure 5.9. However, even though the point for 2 µM also does not match the linear regression it is recovered quite well by the algorithm, so other factors seem to be influencing the calculation. It is for example possible that the correlation coefficient of the original exponential decay fit to the data set of the 2 µM was poor and thus the detected decay rate does not actually match the data set. The error on the determined decay rate for each concentration was calculated using the covariance matrix provided by the fitting routine and does therefore only show the standard deviation of the determined decay

Actual concentration (M)	Average recovered concentration (M)	Standard deviation of average recovered concentration (M)	Highest deviation from true value (% of actual value)	Average deviation from true value (% of actual value)
1e-07	1.02e-07	9.47e-09	27.8	2.1
2e-07	2.04e-07	1.17e-08	11.3	2.2
4e-07	4.45e-07	1.50e-08	20.5	11.2
6e-07	6.94e-07	2.00e-08	20.7	15.6
8e-07	9.05e-07	2.72e-08	18.4	13.1
1e-06	1.14e-06	2.59e-08	18.7	13.8
2e-06	2.02e-06	8.84e-08	8.1	0.8
4e-06	3.97e-06	2.57e-08	2.7	0.8
6e-06	5.91e-06	4.73e-08	4.2	1.6
8e-06	8.18e-06	5.38e-08	3.3	2.2
1e-05	9.51e-06	7.70e-08	7.5	4.9
2e-05	1.62e-05	1.90e-07	22.3	18.8

Table 5.2: Accuracy of the recovered concentration values for the high-power measurement.

rate from the final value but not the deviation from any true value which is obviously unknown.

The reason why the calculated concentration suddenly drops in the last few micrometers of the scan is that the focus of the beam is getting closer to the back wall of the cuvette and thus signal is lost. The scanning depth of the focus is 10 mm but the data shown in figure 5.11 is cropped such that position zero in the graph is at the point in the cuvette where the signal is highest (i.e. immediately behind the front wall of the cuvette plus a little bit of distance into the cuvette to account for the wall influencing the signal level). Furthermore the position as displayed in the graph has not been corrected for the refractive index of the water and does thus not reflect the true depth in the cuvette. Since the focal volume is rather large due to aberrations the back wall of the cuvette starts influencing the signal at the depth shown in the graph although it is in truth still a couple of micrometers away. Since this signal decrease is not due to expected attenuation of the laser light by absorption it is picked up by the programme as genuine change in concentration and thus depicted here. Since it would be very hard to judge where this signal decrease begins in a real measurement situation where the concentration might change towards the back wall of the cuvette no attempt has been made to remove it from the measurement files.

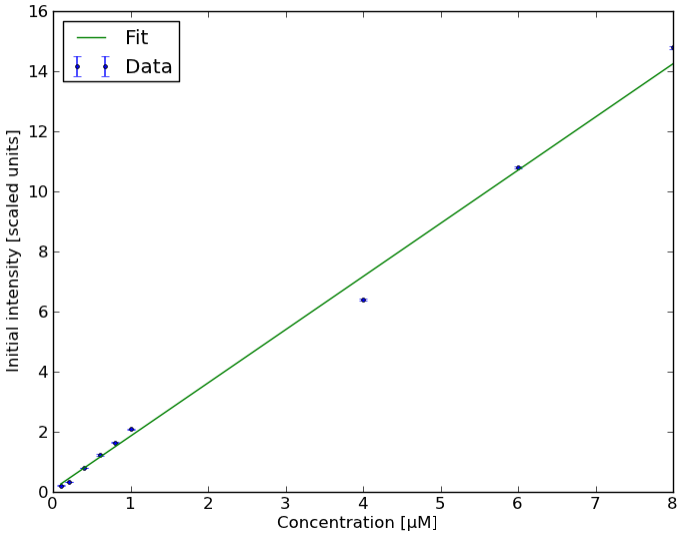

Figure 5.12: Fit to the unattenuated intensities as measured with low laser power.

Low-power measurements

As mentioned above data was also taken with the beam attenuated to a power of equal to or below 39 µW to assess the performance of the instrument at a power level that is safe for the human eye. It has to be kept in mind that the permitted exposure is dependent on the exposure duration and thus the results described in section 5.1.2 should not be considered to have been taken with a completely non eye safe laser power. In contrary, if the data acquisition speed would be increased (by e.g. increasing the scanning speed), the laser power used for the high-power measurements would become eye safe since the duration of exposure would be shorter. Therefore the results presented in this section are valid as an indicator to the sensitivity of the instrument only for the current measurement configuration where the exposure duration is comparatively long.

To obtain the low-power level measurements the same procedure as described above for the high-power measurements was followed. Several solutions of known concentrations of Fluorescein were measured and the decay rate and initial intensity found for each. The fit to the initial inten-

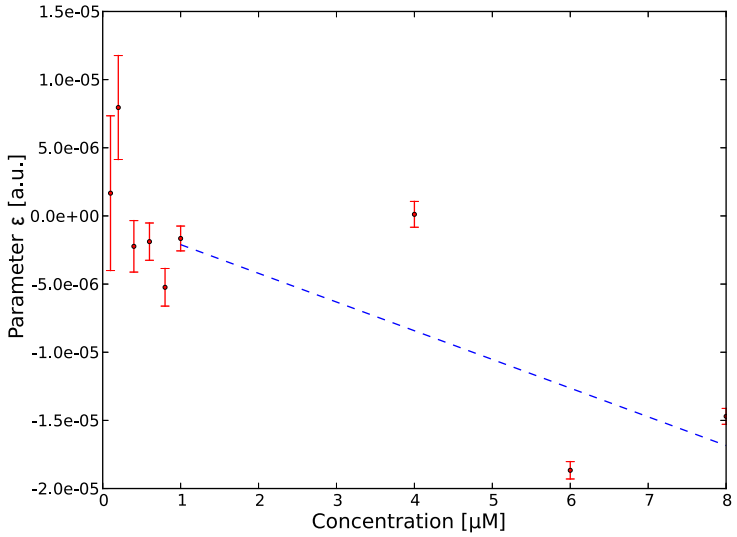

Figure 5.13: Fit to the decay rate of the exponential fit (parameter ϵ) with concentration. The data was measured with the low-power laser.

sity is shown in figure 5.12. As with the high-power measurements, the intensity shows a clear linear trend with concentration. It is, however, visible that the relationship between the decay rate (parameter ϵ) and the concentration is much less clear (figure 5.13) and the variance in the determined decay rate much larger. The returned fluorescent signal is very sensitive to the correct alignment of the cuvette which for the low-power measurements has to be done by eye since no reflection data is available due to the low power. Therefore some of the cuvettes might have been misaligned, thus leading to an incorrect calculation of the decay rate. The measurements which were clearly misaligned were omitted for the sake of the calibration but some residual error will have remained in the data set. Furthermore the signal to noise ratio is much lower for the low-power measurement and thus the exponential decay fits to the original measurement data have lower correlation coefficients which also leads to a falsification of the trend of the decay rate with concentration. This deficit of the instrument will be addressed in a future version, however for this dissertation the proof of the concept is what matters. The concentrations can still be recovered with an error of under 26% as shown in table 5.3 which is comparable to the high-power measure-

Actual concentration (M)	Average recovered concentration (M)	Standard deviation of average recovered concentration (M)	Highest deviation from true value (% of actual value)	Average deviation from true value (% of actual value)
1e-07	1.22e-07	3.28e-08	102.9	22.4
2e-07	2.51e-07	3.74e-08	78.7	25.7
4e-07	4.78e-07	3.45e-08	45.4	19.5
6e-07	7.16e-07	4.01e-08	43.7	19.3
8e-07	9.69e-07	5.50e-08	43.0	21.1
1e-06	1.20e-06	5.40e-08	33.1	20.4
2e-06	1.98e-06	2.25e-07	35.1	1.2
4e-06	4.03e-06	2.21e-07	15.1	0.7
6e-06	6.23e-06	1.32e-07	10.4	3.7
8e-06	8.71e-06	1.86e-07	14.2	8.9
1e-05	9.53e-06	6.01e-07	18.5	4.7
2e-05	1.75e-05	2.49e-07	15.9	12.7

Table 5.3: Accuracy of the calculated concentration values from the low-power measurement.

ments. The recovered concentrations are shown in figure 5.14. It is visible here that both 2 and 10 µM were misaligned when measured and thus the wrong concentration is recovered. Again, as with the high-power measurements, the lower concentrations are recovered with less accuracy than the higher concentrations due to the degradation of the signal to noise ratio with the low intensities.

It is clear from figure 5.14 that even with the very low power that can be used safely on the human eye the instrument is still capable of measuring Fluorescein solutions of low concentrations (the lowest concentration on this plot is 100 nM) with a reasonable accuracy. The reason why the accuracy is slightly less good than with the high-power measurement lies in the fact that the internal amplification of the PMT was higher due to the lower signal level, leading to a decrease in the signal to noise ratio.

The calibration with homogeneous solutions in a cuvette and the resulting recovered concentrations therefore show that the calibration routine is working correctly not only with the modelled intensities but with real measurement data. It is possible to accurately extract concentrations ranging from 2 nM to 10 µM using the current, calibrated instrument. Concentrations above 20 µM can

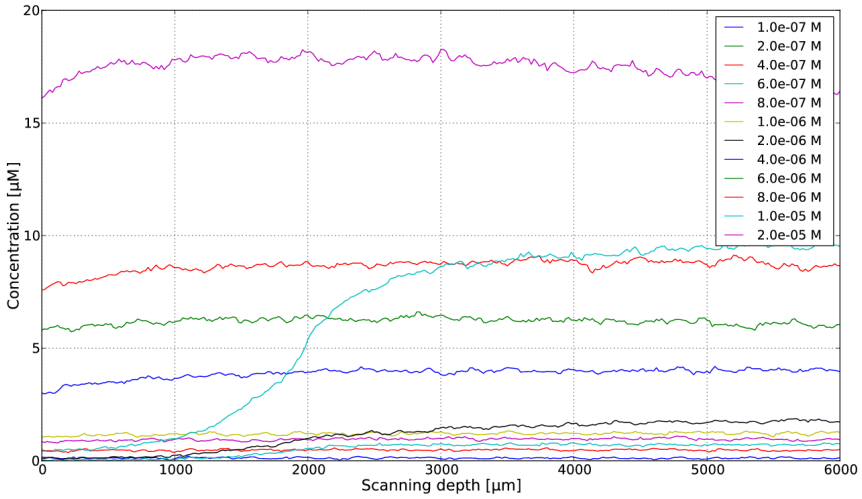

Figure 5.14: Concentrations recovered from the low-power measurement.

theoretically be extracted but will have an increasing error with higher concentrations due to the non-linearity of the initial intensity curve of which only the linear part for the low concentrations was used for the calibration of the instrument. The lowest measurable concentration that is within the 20% error band when using the higher laser power is 2 nM. For the lower power measurement, the lowest accurately detectable concentration is 100 nM. This is not necessarily due to the lower signal to noise ratio but might also be because the actual concentration of the measurement sample might not match the assumed concentration. The error propagation predicts that the errors for the nano-molar solutions are still very small (two orders of magnitude below the assumed concentration) but it cannot be ruled out that other errors in pipetting might have occurred which are not included in the error analysis. For a true calibration, the concentration of the samples therefore have to be confirmed with alternative methods before using them for the measurement. Unfortunately no alternative methods were available to accurately measure the concentration of the samples which is why they were used as is. Another approach would be to buy standard stock solutions for calibration purposes which are offered by some suppliers.

5.1.3 Brimonidine

High power measurements

After it was established that the calibration was working well with the reference standard Fluorescein, it was attempted to calibrate the instrument for Brimonidine. The calibration was at first carried out as for Fluorescein by fitting an exponential decay to the measured concentrations. However it then became clear that the determined decay rates for the individual concentrations had a big error associated with them due to the fact that the signal to noise ratio is poor for these low-intensity measurements. Furthermore the decay rate did not seem to follow an obvious trend with the concentration as expected; in fact the data showed very little decay at all. For the purpose of calibration comparatively high concentrations of 1 μM to 1 mM were used. Substantial decay rates were expected for these. Therefore, a model of the Brimonidine decay for these concentrations was created using the absorption coefficient that was measured as a by-product of the quantum yield measurements (see chapter 4). The modelled curves in figure 5.15 show that even at the highest concentration the decay is almost negligible. This is due to the fact that the excitation wavelength used in the instrument is at the very edge of the absorption spectrum of Brimonidine which absorbs mainly in the UV region and thus the extinction coefficient at a wavelength of 402 nm is low (0.00064 compared to 0.631 for Fluorescein). A shorter wavelength was not used for reasons of eye safety; As described in chapter 4 the risk to the cornea and lens increases dramatically for UV wavelengths. Once a similar level of noise as present in the measurement data had been added to the model (figure 5.16) it became clear that the data is too noisy to extract any information about the decay rate. It was therefore decided to assume that the signal did not attenuate with depth. Thus only the fit to the intensity of the unattenuated signal is needed for the calibration. Since the data is so noisy, this value was obtained by taking the mean value of the complete data set (i.e. the intensity averaged over the whole depth of the sample) for each concentration. The calibration curve is shown in figure 5.17. For a reason unknown, the calibration curve does not intercept the y-axis at zero. The intensity should obviously be zero if no concentration is present. However there

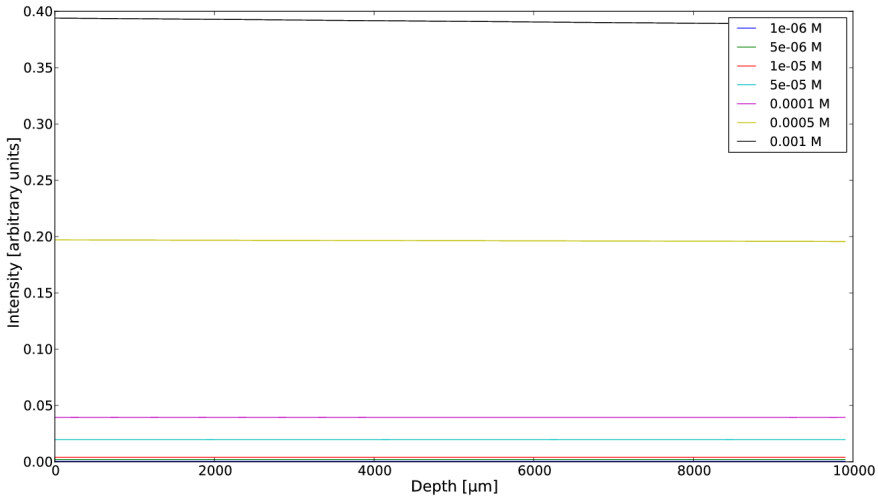

Figure 5.15: Modelled decay rates of different concentrations of Brimonidine. The concentrations are given in the legend.

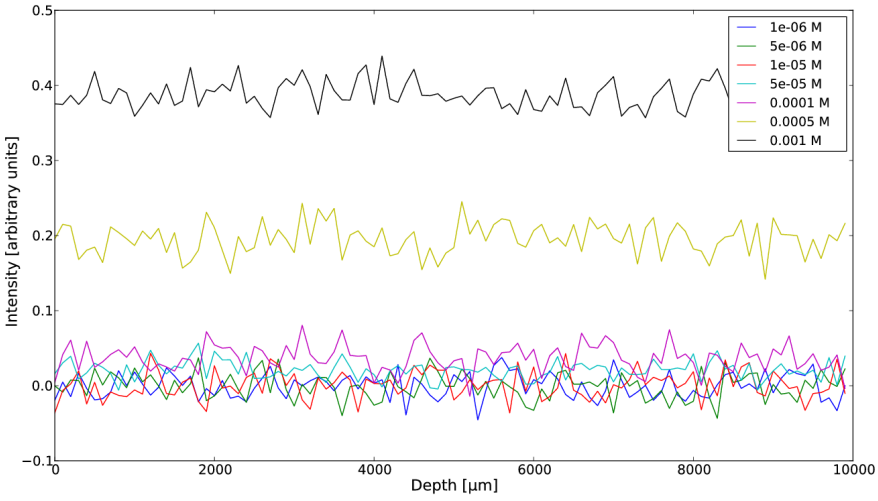

Figure 5.16: The same modelled decay rates with noise added similar to that encountered in the real measurement.

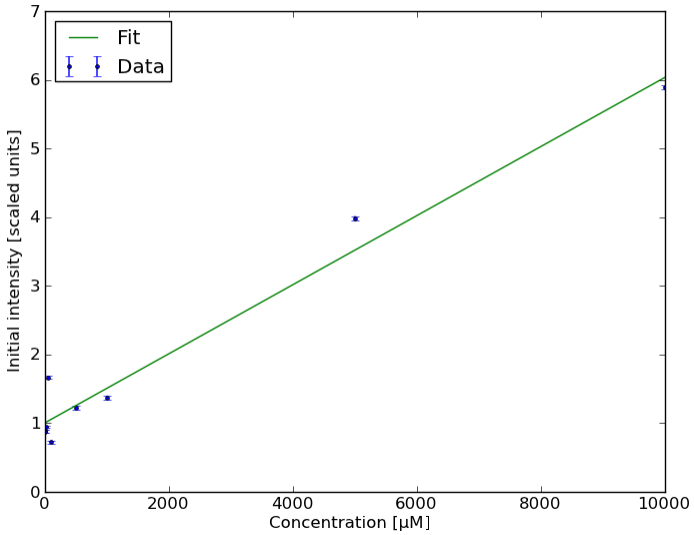

Figure 5.17: Unattenuated intensities extracted from the high-power Brimonidine measurement.

is an offset in the measurement which cannot be explained since the water background was subtracted from the measurement to remove the influence of any offset coming from either the cuvette or the instrument. It is interesting to note that a similar offset occurred when taking the measurements with the professional spectrophotometer to determine the quantum yield of Brimonidine, again after the background signal had been subtracted. This offset might be due to self-quenching of Brimonidine at high concentrations which would lead to the low concentrations fluorescing more than predicted by the high concentrations. However, no information on the spectroscopic and fluorescence properties of Brimonidine could be found in the literature.

Even though this recurring phenomenon cannot be explained, it was decided to use the calibration curve as it is to try and determine the concentrations of known solutions of Brimonidine. As expected from the noise in the measurement, the calculated concentration is also very noisy and has a standard deviation of approximately 500 μM as can be seen in figure 5.18. This is obviously not ideal since the poor signal to noise ratio prevents the software from recovering the concentration as accurately as it needs to be. Changes in concentration can however still be detected using

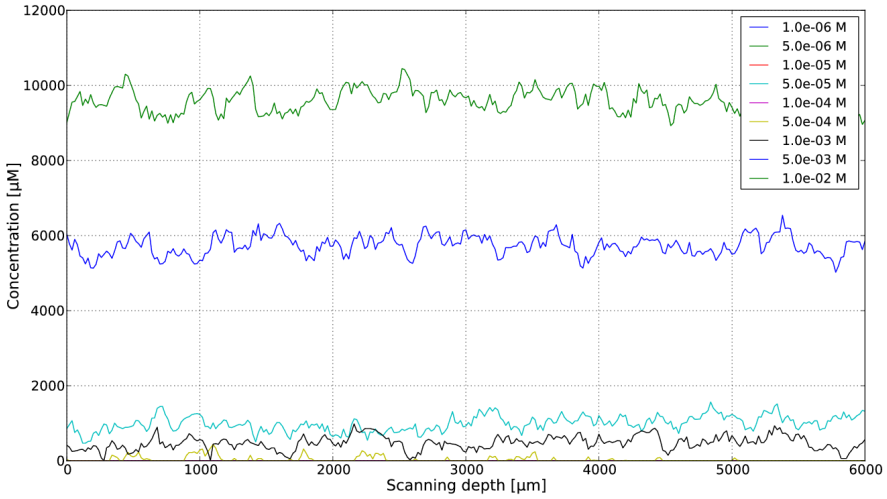

Figure 5.18: Concentrations recovered from the original Brimonidine data set.

the current set-up of the instrument as will be shown in chapter 6. To improve the signal to noise ratio of the measurements several steps could be taken as described in chapter 8. Although the results presented here are not ideal they show that the current version of the instrument is sensitive enough to detect comparatively high concentrations of Brimonidine and extract the concentration value from the average of the measurement. The lowest measurable concentration currently is 500 µM. This proves that the measurement concept is working well. The author of this thesis therefore believes that the instrument will be capable of measuring very weak fluorescent signals with a good signal to noise ratio with few improvements to the instrument.

Low power measurements

Since the signal to noise ratio and thus the accuracy of the recovered concentrations for the measurements of Brimonidine with the high laser power was poor, no measurements were taken for the low-power configuration of the instrument.

5.1.4 Repeatability of the measurement results

To determine the temporal stability of the instrument and its calibration the repeatability of the high-power Fluorescein measurements was assessed. The high power Fluorescein measurements were selected for this task because it was assumed that the repeatability for all measurements will be the same. This assumption is based on the fact that the samples will not change during one week (the same set of samples was used for every repeatability measurement) and that the spread in the detected concentration for a specific sample is due to instrument parameters. These parameters will change within the same range, no matter what compound or at what laser power is measured. The repeatability values presented here are therefore considered to be valid for all measurements taken in the cuvette.

The repeatability was assessed by measuring the same set of samples several times throughout one day and then once a day for a week. For each measured sample, the average of the detected concentration was taken. The mean and standard deviation of the averages for the respective concentration was then used to determine the repeatability. It was found that during one day, the standard deviation in the measurements was smaller than 11% of the average value. In the course of one week, however, the standard deviation increased to being below 23% for concentrations down to 400 nM and then increasing drastically. The specifications for the F410 state that a repeatability of not worse than 10% should be reached. Over the course of one day, this value is almost met by the current instrument. However, over one week, the repeatability is not sufficient to meet the requirements. The instrument therefore needs improvement in stability of the laser and the electronics to ensure a good repeatability of the measurement results.

5.2 Calibration in *in vitro* porcine eyes

Since the F410 is ultimately to be used on animal or even volunteer's eyes for pharmacokinetic studies of Brimonidine and other fluorescent ophthalmic compounds, the instrument was also cal-

ibrated for measurements in the eye. The measurements were performed on *in vitro* porcine eyes which were obtained from a wholesale meat supply in the area. Since that company only slaughters pigs on a Tuesday morning, eyes could only be obtained once a week. They were collected by car at 2pm in the afternoon, keeping them fresh in a Styrofoam box with a cooling pad. They were however not cooled in store and thus depending on when in the morning the eyes were removed from the pigs they were sometimes not very fresh when they were collected. Unfortunately, there was no way of determining the freshness of the eyes (the amount of aqueous humour left in them might have been an indication as described below), and it is likely that most of the time they were not fresh enough to use them as valid prediction to any *in vivo* eyes. Nonetheless measurements were carried out to better understand the background fluorescence levels that will occur in *in vivo* measurements and to show that the instrument is capable of measuring the concentration of Fluorescein as well as Brimonidine in a less-than-perfect measurement situation. It is assumed that if the instrument performs well with the *in vitro* eyes it will not be a problem to measure pharmaceuticals in *in vivo* eyes since the measurement conditions will be much better due to the fact that the cornea will be thinner and less attenuating than in the *in vitro* porcine eyes.

5.2.1 Calibration using Fluorescein

To measure the calibration curve for the *in vitro* eyes, a similar method as described for the measurements in the cuvette was used. First, the background fluorescence of the respective eye was measured after the eye had been aligned to the instrument by maximising the reflection from the cornea using the commercial control software of the ADC (Measurement Computing's "TracerDAQ"). In a second step, the eye was removed from its position in front of the instrument and as much of the aqueous humour as possible extracted using a BD Microfine insulin syringe (0.3 and 0.5 ml models were used). Due to the fact that the animals the eyes were from had been dead for a while and the corneal pump had thus stopped working, it was not uncommon that only very little or no aqueous humour could be extracted from the eye. The aqueous humour is primarily made out of water and when the corneal pump ceases to work with death, the cornea swells

up with the liquid from the aqueous [94][95][96]. This results in very thick corneas and very little aqueous left in the anterior chamber. The volume of extracted aqueous can thus be used as a measure for the decay state of the eye. Once the aqueous had been removed, a solution of Fluorescein of a known concentration was injected into the anterior chamber to replace the aqueous. The eye was then re-aligned to the instrument using the reflection from the cornea and the intensity of the Fluorescein solution was measured.

Since the signal that was returned from the Fluorescein was lower than expected, both the corneal thickness and the value by which the cornea attenuates the incoming excitation light were measured to assess the measurement parameters. According to the literature, the average porcine corneal thickness is approximately 666 µm in living eyes [97] and 0.83 to 1.12 mm in *in vitro* eyes [98][99]. It was however found that the corneal thickness of the eyes used in this experiment was at least five times as much as the thickness reported in *in vivo* eyes due to the breakdown of the corneal pump. The thickness was measured by slicing the cornea as thinly as possible, placing the slices sideways on a microscope slide and then measuring the length of a line that was drawn across the cross-section of the cornea using a microscope with inbuilt measuring function (SteREO Discovery.V12, Zeiss). A sample picture of the obtained measurements is given in figure 5.19. The average measured value of the corneal thickness was found to be (3570$\pm$340) µm.

The attenuation of the excitation light by the cornea was measured by removing the whole cornea from the eye and placing it onto a microscope slide. First, the transmission of the microscope slide without the sample present was measured using a photodiode. The transmission was then re-measured after the cornea had been placed on the slide. Four porcine corneas were measured this way and it was found that they attenuate the excitation light by a mean value of $(88 \pm 1)\%$. This means that the laser power inside the sample eye is significantly lower than the incident light and thus will influence the lowest measurable concentration. Furthermore the return light will also be scattered and attenuated by the cornea so that the total signal loss is significant. A cornea in a living eye will however never scatter or absorb the light as much as the measured *in vitro* corneas since otherwise vision would be very inefficient. It is of course of highest importance in

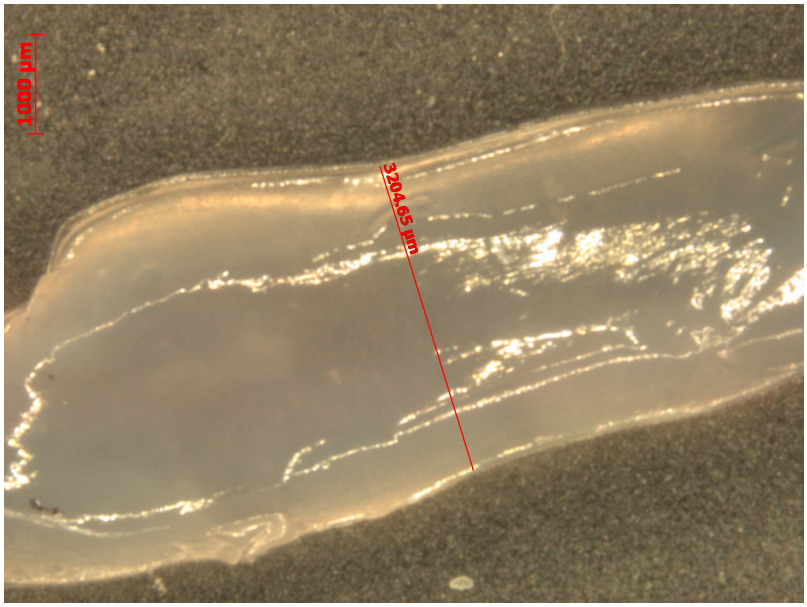

Figure 5.19: An image showing the measurement of the corneal thickness of *in vitro* porcine eyes.

a living eye that the cornea is very clear and does not attenuate the incoming visible radiation. As described in chapter 2, this is achieved by the very ordered structure of the cells in the cornea as well as the tearfilm which is covering its comparatively rough surface. Therefore the high attenuation of the light in the *in vitro* eyes is not only due to the absorption of light but mainly due to scattering on the surface and within the rough structure of the cornea, which is increased by the fact that without the tearfilm to protect it the corneal epithelium dries out and develops cracks. This creates a further problem for the F410 since the focus inside the *in vitro* porcine eye is much bigger than it should be due to scattering and thus less signal will reach the confocal detector. It is therefore clear that in a living, healthy eye the instrument will perform much better than the *in vitro* results presented in this thesis might imply.

Due to the varying freshness of the eyes and varying thicknesses of the cornea, the standard error of the measurement points is quite large. Figure 5.20 shows that the linear relationship between unattenuated fluorescence intensity and concentration can however still be detected. As a result of the problems mentioned above only a couple of eyes in every measurement session yielded us-

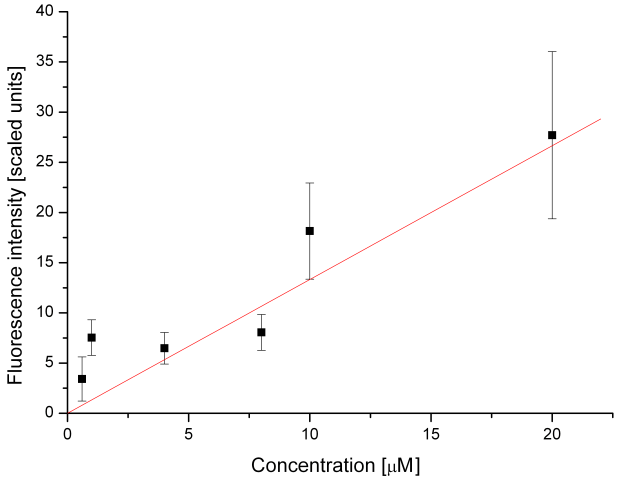

Figure 5.20: The unattenuated intensity of Fluorescein fluorescence versus concentration in *in vitro* porcine eyes. The correlation coefficient as measured in R^2 is 0.73

able data which is why only a limited number of eyes could be used for obtaining the calibration curve. It would have been desirable to measure more eyes to obtain smaller error bars and a more accurate calibration curve but the restriction of only being able to measure eyes once a week added a time limit to the measurements. Even so about 200 eyes were measured to obtain the results presented in this thesis, partly since the design of the instrument changed from the chopper/lock-in amplifier combination to using the active low pass filter which involved complete re-measurement of the calibration curve, and partly because only about 50% of the eyes actually yielded any useable results. The data points shown in figure 5.20 were obtained by first calculating the average of the maximum value measured in all scans of each eye after the background had been subtracted and then taking the mean of the averages of all eyes measured for that concentration. The error bars show the standard error of the mean of the maximum.

As described in section 5.1, two calibration parameters are necessary to enable the software to extract the concentration from the measured intensity: The relationship between the unattenuated intensity and the concentration and the relationship between the decay rate and the concentration.

For the eyes, however, no relationship between the decay rate and the Fluorescein concentration could be found. This is due to the fact that the fits found for the exponential decay of the intensity with depth in the eye were mostly rather poor. Several explanations can be found for this. First of all, the exchanging of the aqueous humour for Fluorescein solutions changed the shape of the cornea since the anterior chamber was filled completely rather than being empty or just half full, thus adding structural support to the cornea. This lead to the auto-fluorescence measured from the cornea having a different shape and/or amplitude in the Fluorescein measurement compared to the reference measurement, thus altering the shape of the fluorescence decay curve when the background was subtracted in the data analysis. Furhtermore the amplitude of the corneal auto-fluorescence was very dependent on the alignment of the eye to the instrument. A very small change in alignment would result in a major change in the fluorescence intensity. Thus removing the eye from its position in front of the instrument to exchange the aqueous humour, even when taking care to re-align the eye using the reflection measured off the cornea, lead to a change in alignment and thus a change in auto-fluorescence levels. This again influenced the shape of the fluorescence decay curve when the background was subtracted. Another reason might be that the measurement was influenced by other factors in the eye such as the Fluorescein binding to proteins in the eye [100]. Due to these reasons and the fact that the signal to noise ratio was poor for the low concentrations most of the exponential decays fitted to the measurement data had a rather low correlation coefficient and it is thus no surprise that the decay rates do not follow a clear trend with concentration.

The recovery of the measured concentrations was first attempted by assuming no decay of the intensity with depth as it was done with Brimonidine in the cuvette as described in section 5.1.3. It was however found that this was not sufficient since the signal does indeed decay, especially at the higher concentrations. Thus in a second attempt to recover the concentrations the best fit to the decay rate versus concentration was used to find the respective decay rate for each concentration. This approach improved the results marginally but shows very clearly that the decay rates extracted from the original measurement data are not very accurate since the high concentrations

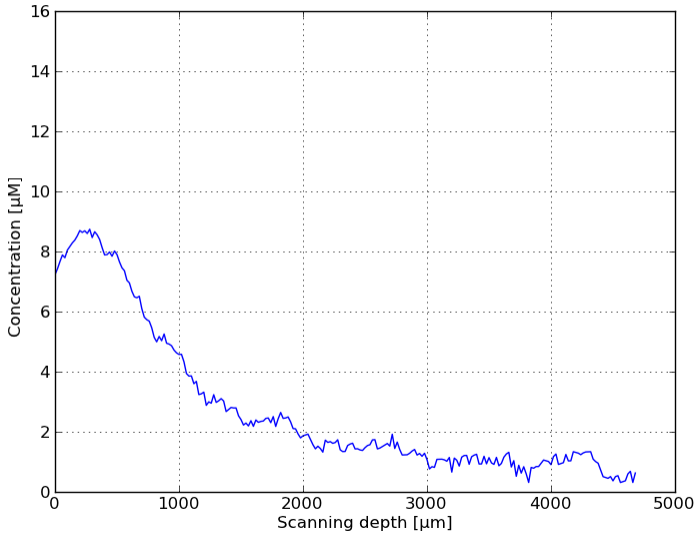

Figure 5.21: An exemplary graph showing the concentration determined from a scan through a 10 µM solution in an *in vitro* porcine eye.

(i.e. 10 and 20 µM start increasing when recovered, ultimately reaching infinity, whereas the lower concentrations still show the decay of the signal. An example of the concentration recovered from the measurement of an eye with 10 µM injected into the anterior chamber is shown in figure 5.21. This phenomenon does not only indicate that the extracted decay rates are incorrect, but also that some other mechanism than just the absorption of the excitation light is influencing the decay of the signal with depth.

The recovered data furthermore shows that even though the concentration at the front of the eye matches the actual injected concentration more closely than further into the eye, it is not estimated very accurately. This is due to the fact that the data points for the calibration curve are the average values from all eyes measured for that concentration and have large errors. Thus none of the measured eyes will fit the calibration curve exactly. It is therefore necessary to improve the method of calibration for future versions of the instrument by either using perfused eyes (i.e. eyes that are being kept "alive" artificially by pumping saline solution through them), by performing the calibration routine on *in vivo* animal eyes or by using an artificial eye.

5.2.2 Brimonidine

Since it was not possible to calibrate the F410 for measurements in *in vitro* eyes using Fluorescein due to too large divergences in signal level from the eyes for each concentration, no calibration for Brimonidine in *in vitro* eyes can be performed. This is because the Brimonidine calibration would have been achieved by using the relationship between the Brimonidine and Fluorescein signal levels known from the calibration in the cuvette and applying it to the Fluorescein calibration in *in vitro* eyes.

5.3 Discussion of calibration results

The results of the calibration presented in this chapter highlight some problems of the F410. The calibration works very well for measurements that have a high signal to noise ratio such as the high-power measurements of Fluorescein in the cuvette, and the accuracy of the results obtained for this measurement lies within the 20% error band defined in the specifications. Due to changes in laser power, sensitivity to the alignment of the cuvette and poor measurement resolution of the ADC, the repeatability is however not very good (23% error within one week). The poor repeatability is caused by the high amplification of the system which increases the sensitivity of the instrument to small fluctuations in signal levels. This shows more obviously in the low-power Fluorescein measurements in the cuvette where the internal amplification of the PMT is higher, thus leading to higher deviations in the number of photons detected by the PMT for the same concentration in different measurement sessions. Furthermore the internal amplification was set to different values for different measurements to assure that the full range of the ADC input (0 to +10 V) was used. The obtained values for the intensities therefore had to be scaled to a common amplification so that the measurements became comparable. This scaling was done using the PMT transfer function which was measured by the author and thus also had an error attached to it.

In addition to the fact that there were small fluctuations in the signal levels coming from the PMT,

the laser intensity was changing slightly in the course of a day due to unknown reasons. Since the laser intensity was monitored by the external photo diode it was attempted to remove this change of excitation intensity from the data but it was found that this actually decreased the accuracy and repeatability. It is not exactly known if the change in laser intensity between different measurements had any influence on the performance of the instrument. The largest recorded change within one day was 3.5% of the highest measured intensity. This measured change in intensity, however, could also have been due to the resolution of the ADC which is 11 bit. Therefore, the lowest resolvable voltage is 4.9 mV which means that if there was a smaller change in the measured intensity the ADC might have jumped up to a higher voltage value. Furthermore the accuracy of the used ADC is only 4 times the least siginificant bit which in this case means an average accuracy of 19.5 mV which decreases to 39.5 mV at the full scale of the measurement (i.e. -10 V or +10 V) due to non-linearity in the gain of the ADC. It is thus quite possible that the laser intensity was actually only fluctuating very little or not changing at all and the error was introduced by the ADC. This poor accuracy possibly also lead to comparatively high fluctuations in the measured signal levels of the fluorescence coming from the samples, thus decreasing the accuracy and the repeatability of the measurement since any small error in the intensity reading gets amplified significantly by the low pass filter.

Another factor that introduces error to the concentration value determined from the measured intensity is that the F410 is very sensitive to the correct alignment of the sample. A small misalignment leads to a comparatively large error in the measured intensity and the shape of the measurement curve and thus an error in the recovered concentration which in turn influences the accuracy of the measurement. This is especially visible in figure 5.14 in the data sets for 10 and 2 µM where the concentration at the front of the cuvette seems much lower than at the back. This is purely due to an error in alignment since the same samples measured at another time yielded correct results.

It is furthermore obvious that the signal to noise ratio of the measurement holds an important role in the determination of the correct decay rate for each concentration, which in turn is important for

the accurate recovery of the concentration. The decay rates are comparatively well recovered from the Fluorescein measurements taken with the higher laser intensity as shown in figure 5.9, but for the low power measurements and the low intensity fluorescence the determination of the decay rate is not very accurate as shown by the large error bars in figure 5.13. This leads to a decrease in accuracy to 26% compared with 20% for the higher power measurements. The signal to noise ratio does of course also influence the recovered concentration directly - if the noise level is too high the noise will be detected by the algorithm as genuine concentration change, thus directly translating the noise of the measured fluorescence intensity to the noise of the recovered concentration.

Despite all the problems discussed above the instrument could still be calibrated to measure the concentration of Fluorescein in a cuvette with an accuracy that is within the value set in the specification. The described problems influence the calibration extensively but since they are all instrumentation issues they will be easily reduced or removed with further improvement of the instrument. The calibration routine presented in this chapter therefore is considered to be working well enough to prove that the measurement concept presented in this thesis is working. It furthermore shows that with future versions of the instrument the error in the accuracy can be reduced significantly.

The reason why the calibration in *in vitro* porcine eyes does not work well is due to several factors that are sample-related rather than instrument-related. First of all the porcine cornea scatters the incoming excitation light quite badly so that the fluorescence from the volume of light measured by the confocal detector is very low. However, due to varying states of decomposition of the eyes the scattering coefficient varies quite extremely so that very different signal levels were measured for the same concentration of Fluorescein in different eyes. The state of decay of the eye also influenced the absorbance of the cornea; corneas that had decomposed more were generally more absorbent and showed higher autofluorescence. Another factor was that sometimes not all the remaining aqueous humour could be removed from the eye, thus diluting the concentration of the injected Fluorescein solution. It is possible that the accurate concentration could have been determined by re-sampling the solution from the anterior chamber of the eye. However since it has

been reported that Fluorescein molecules bind to compounds within the eye [100] the re-sampled concentration would not necessarily have been an indicator of the concentration measured by the instrument, especially since the instrument only measures in a very localised area. Furthermore the alignment of the sample to the instrument again played a very important role, especially because the autofluorescence of the cornea was very high. Small changes in alignment thus lead to large changes in background signal which then caused an error in the shape of the measurement curve once the background had been subtracted. All these things resulted in large error bars and thus a poor correlation coefficient both for the fit to the unattenuated intensity versus concentration and for the decay rate versus concentration. Another method has thus to be found in the future to calibrate the instrument for eyes. This could for example involve perfusing the *in vitro* eyes to keep them quasi-alive artificially and thus reducing the decay [101], or by using living animal eyes. Another approach might be to transfer the calibration from Fluorescein in a cuvette directly to the eye as has been done before [52]. It might also be possible to use the calibration obtained from an artificial eye for the measurements of real eyes.

Chapter 6

Experiments and results

In this chapter the results of the experiments carried out during this research project are presented. At the very beginning of the project, some interest in measuring the thickness of the human tear film and the influence of medication for treating dry eye syndrome on the cornea and tear film was expressed by Allergan. Therefore, measurements were carried out with a different version of the instrument, a prototype (called the V370) built by Lein AD, to compare the performance of the measurement principle presented in this thesis to a commercially available instrument (Haag-Streit's LenStar). It however became clear after a short while that Allergan was more interested in being able to measure the pharmacokinetics of Brimonidine, ideally both in the anterior and the posterior chamber of the eye. For this work, the measurement area was restricted to the anterior chamber of the eye since measuring behind the crystalline lens is an additional challenge. After the F410 was calibrated as described in the previous chapter, the diffusion of unknown concentrations of Fluorescein and Brimonidine was measured both in the cuvette and in *in vitro* porcine eyes. These measurements not only show that the instrument and its software are capable of tracking the distribution of the fluorescent compounds over time but also that the concentration can be recovered from rapidly changing samples. Last but not least, the background fluorescence of healthy volunteers was monitored both over the course of a day and over the course of a week to

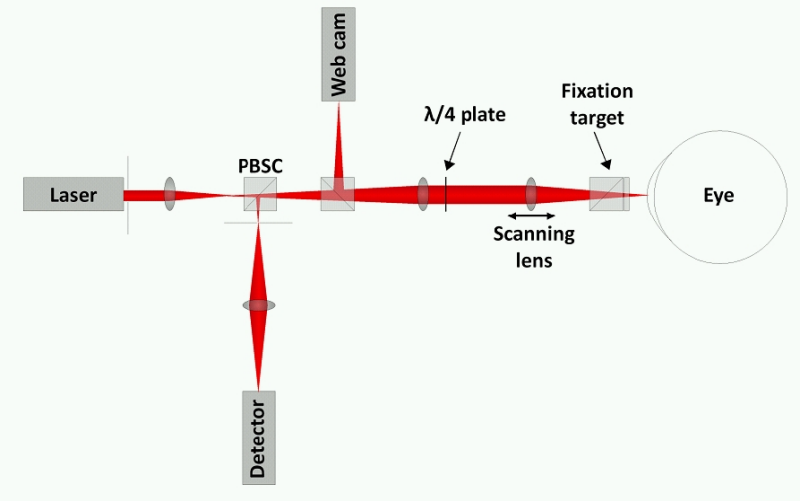

Figure 6.1: Schematic diagram of the V370.

assess the amplitude of the background signal that will occur in a real-life measurement situation.

6.1 Measurement of tear film thickness

As described in chapter 2, the tear film plays an important role in keeping the cornea healthy and nourished. If the production of the tear film is disturbed in any way it can lead to a condition called keratoconjunctivitis sicca, also known as dry eye syndrome. If the condition cannot be cured by removing the cause (for example long term wear of contact lenses) it is usually treated by giving artificial tear drops. Since Allergan produces such artificial tears, they were interested in measuring the influence of the eye drops on the tear film thickness and break up time at the beginning of this project. This is of interest because it is not fully understood how, and for how long, the artificial tear drops influence the tear film and thus gaining better understanding of the factors and timings involved would enable Allergan's pharmacologists to improve the eye drops.

For this purpose, the central corneal thickness (CCT) including the tear film of the author's left and right eye was measured over time with and without the application of the artificial tear drops

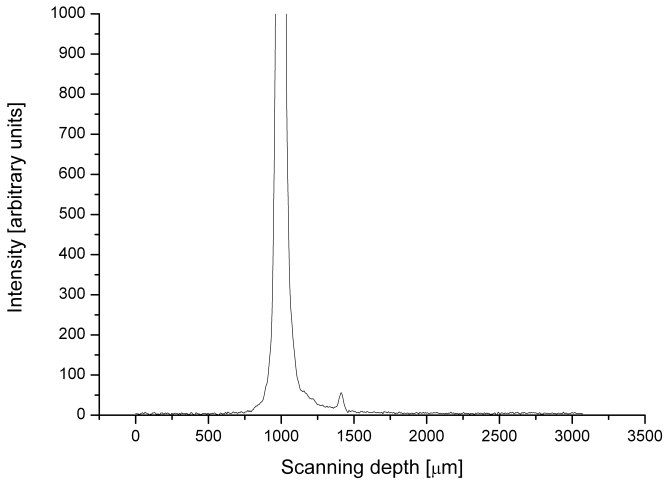

Figure 6.2: A typical scan through the cornea as produced by the V370.

to the right eye. Since these measurements were taken before the F410 was built, and since the measurement principle of the F410 is roughly based on the instruments built by Lein AD, one of their prototypes (the V370) was used to measure the CCT. A schematic diagram of the V370 is given in figure 6.1. The measurement principle is very similar to that of the reflection arm of the F410. The light leaving the laser (670 nm, Laser 2000, UK) is focussed by a lens to create a reference focal spot before expanding through a polarising beam splitting cube (PBSC) and a second beam splitting cube which diverts a small fraction of the light returned from the sample onto a web cam to enable the operator to monitor the alignment of the sample to the instrument. The light is then consequently collimated to a 12 mm diameter beam by an achromatic lens combination and passes through a quarter wave plate before being focussed onto the sample by a final lens that is mounted on a scanning stage (SMAC Europe Ltd., UK). As in the F410, this motorised scanning stage moves the focus of the beam along the optical axis of the eye, thus creating a one dimensional profile of reflection intensities on the detector. The light reflected by the sample is re-collimated and passes through the quarter wave plate again before being diverted by the PBSC and focussed through a pinhole and a relaying lens onto a photo diode. The double pass through the quarter wave plate

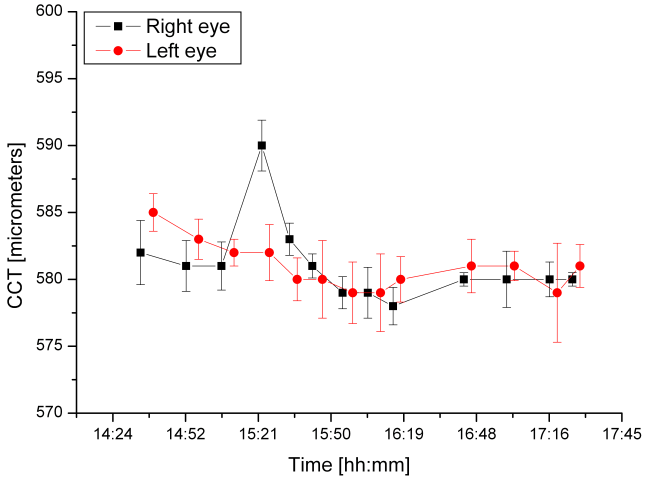

Figure 6.3: Measurement of central corneal thickness (CCT) in the right and left eye with the LenStar. Artificial tear drops were applied to the right eye at 15:20 hours.

in combination with the PBSC reduces unwanted reflections reaching the detector. After the light passes the last lens a fixation target is projected onto the beam, helping the patient to align their eye to the instrument. The full system has also been described by us in [102].

Figure 6.2 shows a typical scan produced by this instrument. The first peak at approximately 1000 µm scanning depth is the reflection from the anterior surface of the cornea, whereas the much lower intensity peak at approximately 1400 µm depth is the reflection from the posterior surface of the cornea. The graph has been cropped such that the posterior peak is clearly visible. The intensity from the anterior peak is much higher due to the fact that the change of refractive index is larger at the boundary between air and the anterior corneal surface than between the posterior corneal surface and the aqueous humour in the anterior chamber of the eye, leading to a higher Fresnel reflection. To compare the results with a commercially available instrument, measurements were carried out simultaneously with the LenStar produced by Haag Streit which is an interferometer based instrument and thus follows a different measurement principle than the V370. As mentioned above, the artifical eye drops (Optive^{TM}, Allergan Inc.) were applied to the

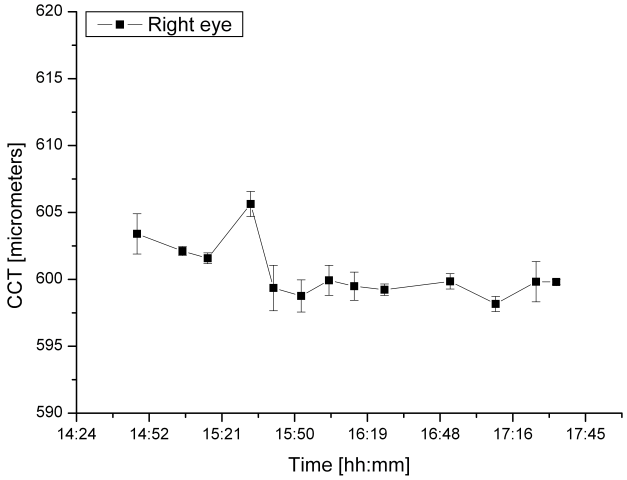

Figure 6.4: The corneal thickness (CCT) as measured with the V370 after the application of artificial tears.

author's right eye while the left eye was used as a reference. Measurements were taken quasi-simultaneously by first measuring the CCT of both the left and the right eye with the LenStar and then measuring the right eye using the V370 immediately afterwards. As shown in figure 6.3, the application of the artificial tear drops at 15:22 leads to an increase in the CCT of 9 µm, whereas no increase is visible in the left eye. The increase in corneal thickness is also visible in the measurements taken with the V370 (figure 6.4, however the measured change in thickness was only 4 µm.

This discrepancy in thickness is most likely due to the fact that it takes up to a couple of minutes to obtain one measurement with the LenStar and thus the measurement point taken with the V370 was collected 10 minutes after the application of the eye drops. During this time the CCT has decreased almost to its original value as the next data point taken by the LenStar shows. This point was taken 1 minute after taking the measurement with the V370 and the CCT had decreased to being only 2 µm thicker than the original value before the application of the eye drops. The reason why the corneal thickness as measured with the V370 is slightly higher lies in the fact that the

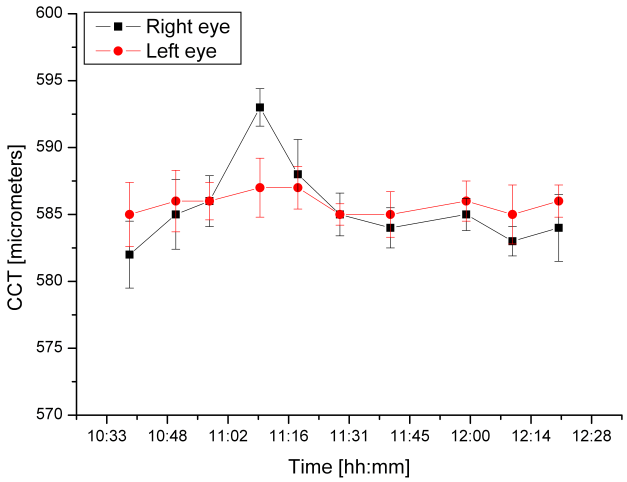

Figure 6.5: Repeat measurement of the increase in CCT after the application of eye drops.

instrument was not calibrated before use, and therefore the accuracy might have been compromised. For the measurement of the relative change of CCT the absolute thickness is however not of importance. Both instruments show a similar level of increase in thickness and thus it is clear that the V370 is capable of measuring the relative change of the CCT that is induced by the eye drops.

To show that the increase in corneal thickness was due to the eye drops and not some other undefined influence the measurements were repeated the next day using only the LenStar since this instrument was calibrated. Again an increase of the CCT of 7 µm was measured while the reference eye did not show any increase in thickness as shown in figure 6.5. As a second confirmation that the measurement was valid both eyes were measured in the afternoon without applying the eye drops, showing no increase in thickness whatsoever (figure 6.6).

Unfortunately, neither of the instruments were able to resolve the tear film from the cornea. It is thus impossible to say whether the application of the eye drops lead to an increase in the tear film thickness or to an effect called corneal plumping where the cornea swells slightly due to external

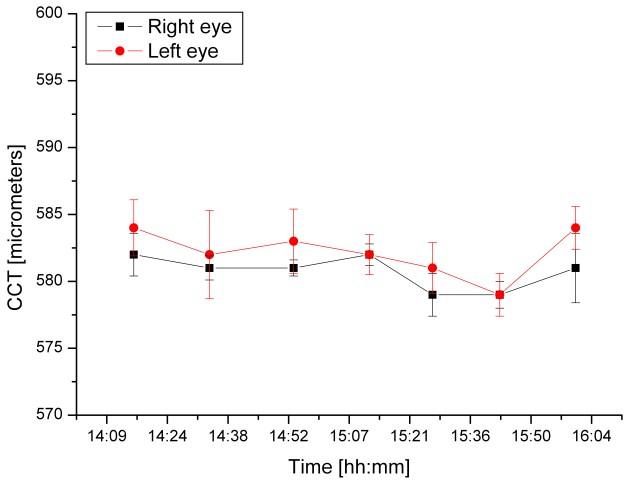

Figure 6.6: Measurement of the CCT with the LenStar. No eye drops were applied.

influences. The measurements presented here do however show that the combined effect can be detected as a relative change in thickness compared to the previously measured value. The initial plan for this PhD project was therefore to improve the prototype built by Lein AD so that the tear film would become resolvable and then monitor the influence of artificial tears on the corneal and tear film thickness and tear film break up time. The instrument would have been further improved by adding the capability to detect fluorescent light and the polarisation of the reflected light so that the instrument could provide information on the internal structure of the cornea.

It then became clear that Allergan was more interested in measuring the pharmacokinetics of Brimonidine which lead to a slightly different design of the instrument. Since the F410 was designed to measure the autofluorescence of weakly fluorescent compounds more attention was paid to collecting as much fluorescent signal as possible and increasing its signal to noise ratio than to having an axial resolution good enough to resolve the tear film. In principle the instrument for measuring the tear film thickness and break up time would however have been very similar to the F410, and there is no reason why the F410 cannot be developed into such an instrument in the

future. The beauty of the F410 lies within the fact that it is a very versatile instrument that can easily be adapted for different applications.

6.2 Determination of unknown concentrations in a cuvette

As described above the focus of the research changed quite soon after the start of the project from measuring the tear film thickness and break up time to measuring the pharmacokinetics of Brimonidine in the anterior chamber of the eye. The instrument was thus changed to the design described in chapter 4 and built and calibrated as described in chapter 5. After the instrument had been calibrated successfully to recover the concentrations from fluorescence intensities measured in a cuvette and it had been shown that the calibration routine theoretically also works on changing concentrations, the dispersion of a drop of both Fluorescein and Brimonidine in water was monitored over time. The results show that the F410 is not only capable of recovering the concentration from a static solution but also from solutions of concentrations that change rapidly with time. The temporal resolution of the instrument is currently approximately 0.6 s.

6.2.1 Fluorescein

High laser power

First of all, the diffusion measurement was carried out with a laser power that is slightly above the calculated safe level for human exposure to ensure a good signal to noise ratio. A drop of 20 µM Fluorescein (50 µl) was released into a cuvette filled with 2 ml of water. The diffusion of the Fluorescein into the water was consequently monitored for approximately 4.3 minutes. A three-dimensional representation of the diffusion of the drop with time is shown in figure 6.7. The scanning depth is shown along the x-axis, the recovered concentration along the y-axis and the measurement time in seconds along the z-axis. It has to be pointed out here that the figure does not show a three-dimensional representation of the cuvette but rather is a representation of

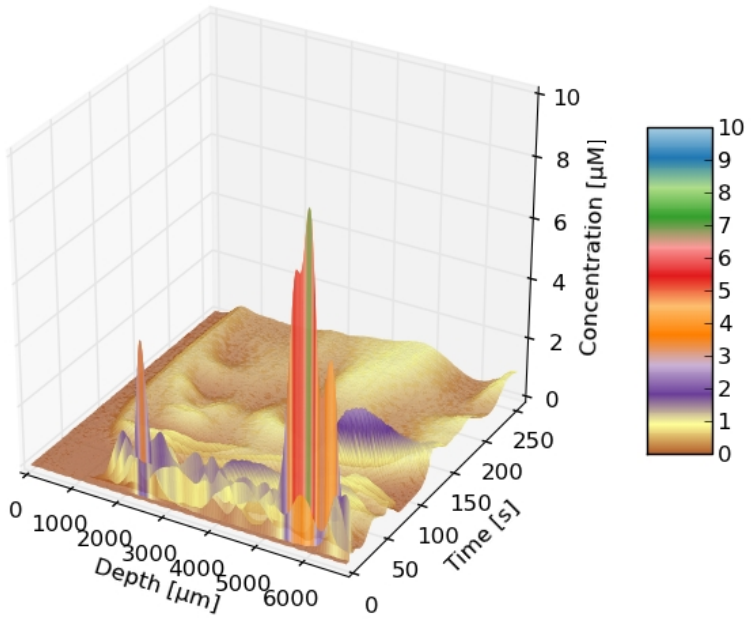

Figure 6.7: Three-dimensional represenation of a drop of Fluorescein diffusing in a cuvette.

how the two-dimensional scan changes over time. The concentration is colour-coded for ease of reading. At the beginning of the measurement the drop is released and falls through the focus of the beam while spreading in the water, leaving an interesting localised distribution of quite high concentration. It then diffuses through the cuvette over time and becomes less localised. At the end of the scan it is quite evenly distributed throughout the whole measurement volume. The average concentration of the last scan in the measurement is (495 ± 246) nM. The high standard deviation is due to the fact that diffusion was not completed by the time the measurement was stopped and thus localised small changes in concentration are still present. The expected concentration after complete diffusion for a 50 µl drop of 20 µM in 2 ml of water is 500 nM. These results therefore show that the concentration measured by the F410 is very close to the actual value, and it is assumed that if the diffusion had been monitored for longer the final measured concentration would have met the actual concentration even more accurately. The same measurement is shown in a different representation in figure 6.8 as temporal snapshots for clarity. Figure 6.8 (a) shows the

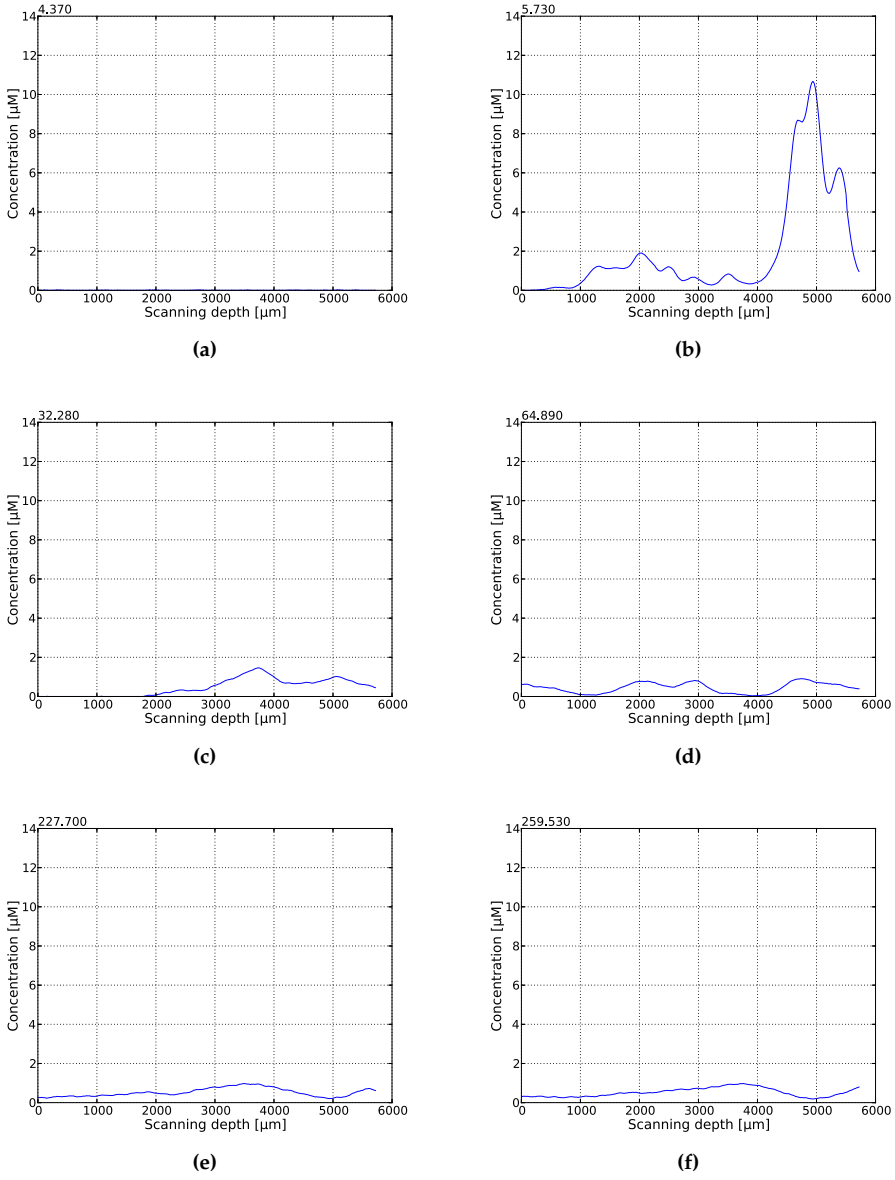

Figure 6.8: A drop of Fluorescein diffusing in a cuvette. (a) The background signal before the drop is released. (b) The drop has been released and is falling through the focus. (c) - (f) The Fluorescein is diffusing through the cuvette until a more equal distribution has been reached.

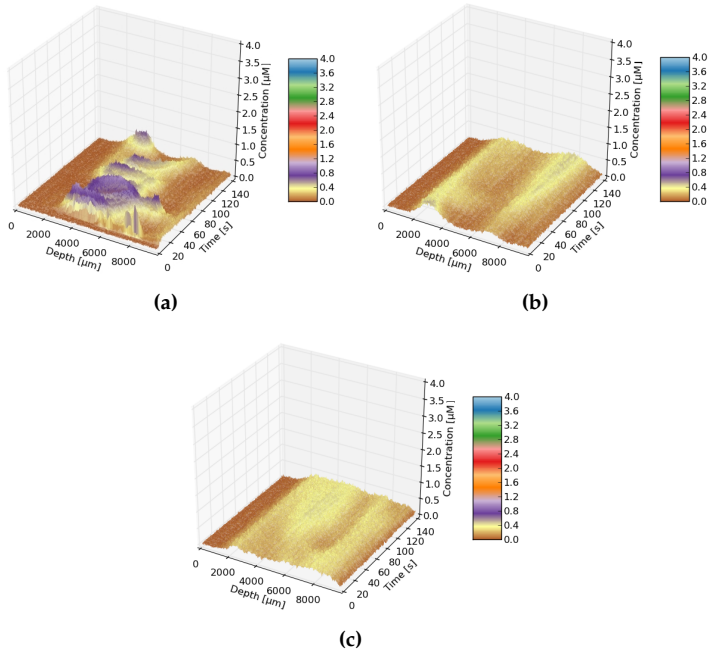

Figure 6.9: Measurement of a drop of Fluorescein diffusing in a cuvette filled with water. The measurement was taken at an eye safe laser power.

cuvette at time zero before the drop of Fluorescein is released. No concentration is present in the water. In (b), the drop has just been released and is falling through the focus of the beam into the cuvette while spreading sideways through the water. It then starts spreading more and more sideways while the concentration equalises throughout the length of the cuvette as is visible in scans (c) to (e). In scan (f) after which the measurement was stopped the Fluorescein has diffused almost completely and levelled at a concentration of approximately 500 nM. The time of measurement in seconds after the start of scanning is given in the top left hand of the respective graph.

Low laser power

The same measurement of a drop of Fluorescein diffusing in a cuvette of water was then carried out using the lower laser power that is safe for human exposure for this configuration of the instrument to show that even with such a low incident power the concentration of a rapidly changing

solution can be monitored with the F410. A three-dimensional representation of the diffusion of the drop of Fluorescein in the cuvette over time is given in figure 6.9. The three scans were taken consecutively in the order (a), (b), (c). As with the higher power measurement, the drop first falls through the focus of the instrument while starting to diffuse sideways. It then starts spreading more and more throughout the cuvette until a state close to final equilibrium is reached as can be seen in the last scan of figure 6.9(c). The same parameters as in the higher laser power measurement were used, i.e. a 50 µl drop of 20 µM Fluorescein in a cuvette filled with 2 ml water. The final concentration after complete diffusion will therefore be 500 nM as before. As can be seen in the snapshots taken from the measurement (figure 6.10) the final concentration measured is slightly below 500 nM, however this might be due to the fact that the Fluorescein had not diffused completely before the end of the measurement. The time of the measurement is shown in the top left hand corner of the graph. In figure 6.10(a), the drop has not yet been released. In (b) the drop falls through the focus while spreading slightly to the sides. The Fluorescein then diffuses throughout the cuvette through (c) to (e) until it is almost in equilibrium in scan (f).

It is obvious that the signal to noise ratio of the low power measurements is lower than for the higher power measurements. However it is also clear that even though the accuracy is slightly worse, the concentration is still measured correctly.

6.2.2 Brimonidine

Even though the calibration for recovering the concentration of Brimonidine from the measured signal does not work as well as with Fluorescein due to the lower intensity of the fluorescence and thus the lower signal to noise ratio, the same measurement as for Fluorescein was carried out. The diffusion of a drop of Brimonidine in a cuvette filled with water was monitored over time. When trying to recover the concentration from the measured data it however became clear that more research is needed to find why Brimonidine has an offset in the calibration curve and to generally better understand its fluorescent behaviour. The set of calibration solutions is recovered more or

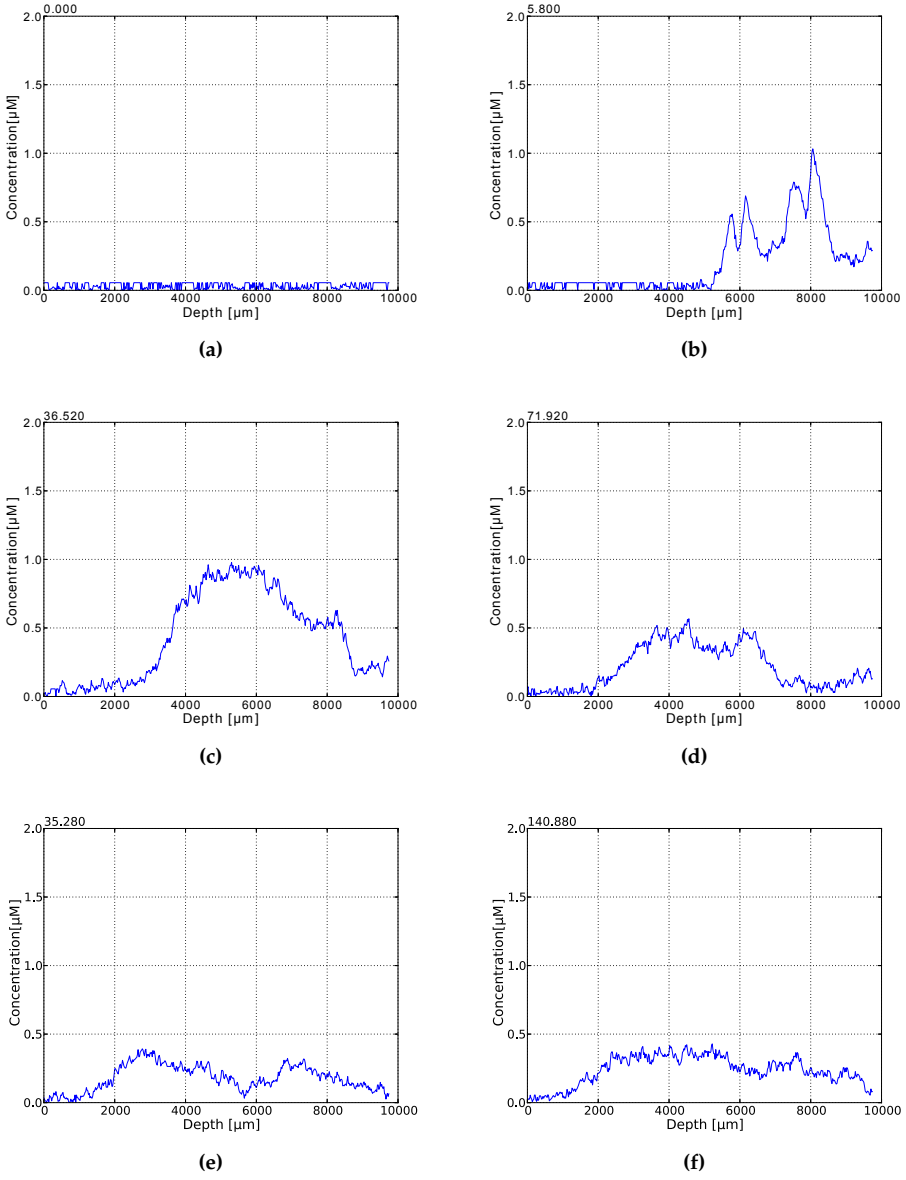

Figure 6.10: A drop of Fluorescein diffusing in a cuvette measured at eye safe laser power. (a) Before the drop has been released. (b) The drop has been released and falls through the focus. (c) to (f) The Fluorescein is diffusing through the cuvette.

less correctly as shown in figure 5.18, but the recovery of the measured diffusion does not work due to the fact that any signal that is below the offset is set to the offset by the algorithm so that no negative concentrations are measured. Since the offset found in the calibration is 1 V and most of the signal change measured during this experiment was below 1 V the concentration was thus set to zero. Therefore, the intensity of the measurement scaled to a gain of 1 on the PMT rather than the recovered concentration is shown in the graphs presented here.

Figure 6.11 shows temporal snapshots of a 50 µl drop of 10 mM Brimonidine diffusing in a cuvette filled with 2 ml of water. The time of measurement in seconds after the measurement start is shown in the top left hand corner of the graph. In (a), no Brimonidine is present and thus the average signal is zero. In (b), the drop of Brimonidine has been released and is falling through the focus of the instrument. The drop of Brimonidine then bounces of the bottom of the cuvette and starts diffusing sideways (scan (c) to (e)). After that the Brimonidine leaves the focus of the instrument until it has diffused throughout the whole cuvette (scan (f)). No three-dimensional representation of this measurement is included here since no interesting profiles are visible in the focus after the first 30 scans and the gradual increase in intensity is not visible in the three-dimensional image due to the poor signal to noise ratio.

These measurements show that although there is an issue with the calibration which needs further investigation the instrument is capable of measuring the change in intensity induced by the diffusion of a comparatively high concentration of Brimonidine in water. The final concentration after complete diffusion was calculated to be 250 µM which according to the calibration is below the resolvable limit due to the noise in the measurement. It is however clearly visible from graphs (a) and (f) that the average intensity has increased after the diffusion of the drop of Brimonidine. Therefore, even though the concentration cannot currently be extracted from the measurements, the change in intensity is measured and relative changes in concentration can thus be extracted. The instrument will therefore add valuable knowledge about the distribution properties of Brimonidine. Without doubt with the improvements suggested in chapter 8 a future version of the instrument will be capable of resolving and calculating the concentration of

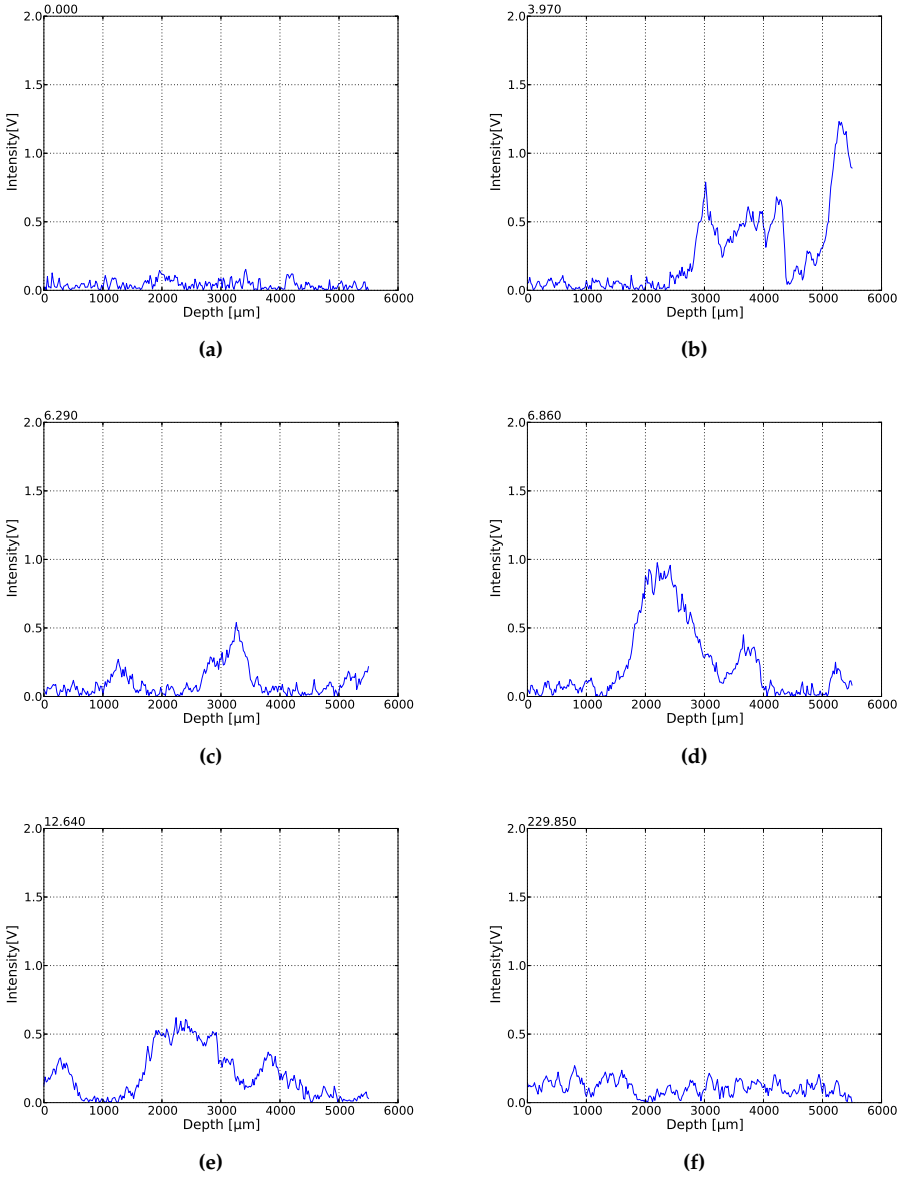

Figure 6.11: A drop of Brimonidine diffusing in a cuvette filled with water. (a) The background signal before the drop is released. (b) The drop has been released and falls through the focus. (c)-(e) The drop is starting to spread in the cuvette. (f) The Brimonidine has diffused almost completely.

Brimonidine with an accuracy similar to that already achieved for Fluorescein.

6.3 Determination of unknown concentrations in *in vitro* porcine eyes

6.3.1 Fluorescein

After it had been determined that the concentration of samples of unknown, rapidly changing concentrations can be recovered and monitored over time in the cuvette the same was attempted in *in vitro* porcine eyes. For this experiment, an arbitrary volume of Fluorescein was injected into the unknown volume of the aqueous humour of the porcine eye. The concentration injected was 20 µM but since the volume of the aqueous humour in the eye is unknown no predictions towards the final concentration after diffusion can be made. Figure 6.12 shows the very slow distribution of the injected drop of Fluorescein with time. The four measurements (a) to (d) were taken consecutively in that order. The eye was only monitored for approximately six minutes due to time restrictions - since the eyes were degrading very quickly it was of crucial importance to measure the next eye as soon as possible. Figure 6.12 (a) shows the eye at the point of injection. The high peak in fluorescence intensity at a depth of approximately 3750 µm comes from the degrading proteins in the cornea. The Fluorescein was injected at approximately 10 seconds into the first measurement, as can be seen by the peak of the cornal auto-fluorescence shifting about its position due to the deformation of the cornea by the needle of the syringe. The fluorescence from the Fluorescein is then very quickly visible at 12 seconds into the measurement and then starts becoming more and more intense with time.

Figure 6.13 again shows a selection of measurement scans at different time points in the same measurement. The time the scan was recorded at is indicated in the top left hand corner of the respective graph. Graph (a) shows the background fluorescence from the eye before the Fluorescein

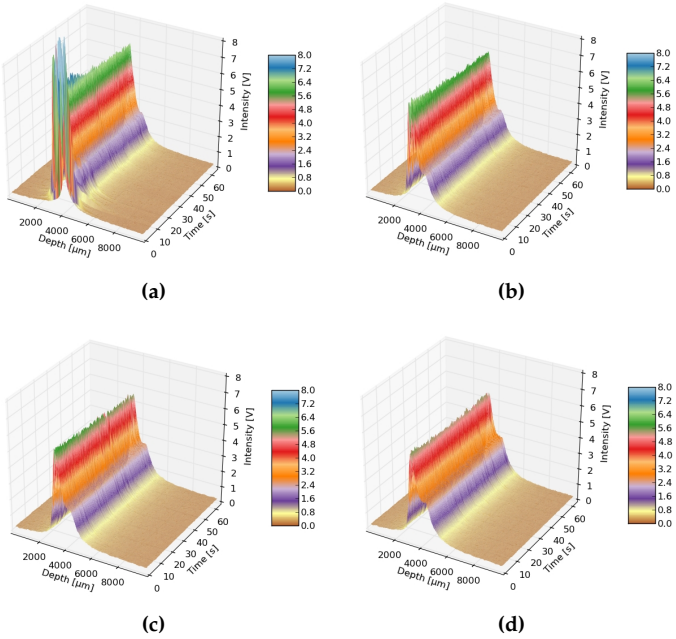

Figure 6.12: 3D representation of Fluorescein diffusing in an *in vitro* porcine eye.

was injected. Graphs (b) to (f) show the distribution of the Fluorescein over time. It is noticeable that unlike in the cuvette no distinctive profile of fluorescence intensity with depth is visible. This is most likely due to the fact that the aqueous humour has a different consistency to the water in the cuvette and thus the Fluorescein distributes more slowly. Furhtermore, since the eye is a closed system (in contrast to a cuvette), the slower and more even diffusion might also be due to smaller thermal and atmospheric influences that would mix the fluorescein with the solvent in unpredictable patterns. It might also be that due to the injection of the Fluorescein with a syringe it has more velocity than the drop released into the cuvette and thus distributes faster and more evenly throughout the measured volume than in the cuvette. That the properties of the diffusion are different in the eye from the cuvette can also be seen in the later scans where the intensity of the fluorescence rises very slowly and smoothly in the focus of the beam and does not seem to distribute further into the eye. Since no reflection from the lens is measured by the instrument due to the low signal level it is impossible to tell how deep the anterior chamber actually is. From the

author's experience of working with the eyes it seems however likely that the anterior chamber is not deeper than the 2 mm the depth of the Fluorescein distribution in scan (f) suggests. The anterior chamber of a human eye has an average depth of 3.5 mm [11] and since porcine eyes are similar in size it is likely that in their normal (i.e. living) state they have a similar depth. However as mentioned before the corneas of the eyes used for these experiments were swollen with the water from the aqueous and it is thus quite likely that the depth of the anterior chamber decreased with the increasing decomposition of the eyes.

Since the calibration for the measurement of the concentration of Fluorescein in *in vitro* porcine eyes did not yield satisfying results it was not attempted to calculate the concentration of the data presented here. It is however clearly visible that small changes in intensity are measured by the F410 and it is thus clear that once a better way of calibrating the instrument to the eyes has been found it will be possible to accurately recover the concentration from the measured intensity.

6.3.2 Brimonidine

The same measurements as described above for Fluorescein were carried out with a high concentration (1 mM) of Brimonidine to assess whether the change in intensity can be measured by the instrument at such low signal levels. Figure 6.14 again shows a three-dimensional representation of the whole data set split into four consecutive measurements. In graph (a) the Brimonidine is injected between 10 and 20 s after the measurement was started. This can be seen by the peak of the corneal auto-fluorescence shifting its position due to the deformation of the cornea by the needle. The Brimonidine concentration then starts increasing behind the cornea, but unlike the Fluorescein it does not seem to distribute throughout the length of the anterior chamber. This phenomenon has been observed in all measurements taken with Brimonidine and is confirmed by the literature [103][82]. Brimonidine binds to specific compounds and structures within the eye, one of which is the cornea. The measurements taken of Brimonidine diffusing in porcine eyes therefore show that the F410 is capable of accurately measuring the position of the drug in the eye.

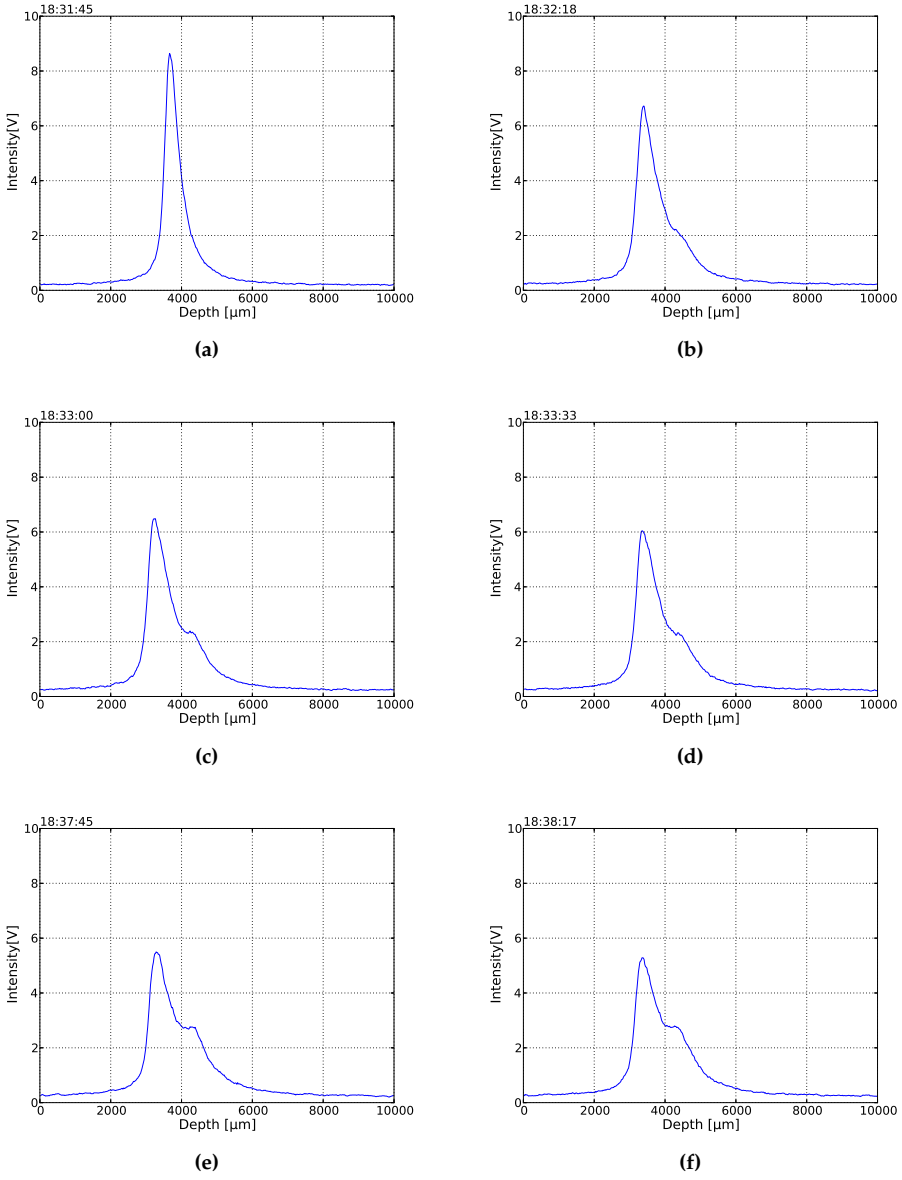

Figure 6.13: Snapshots of Fluorescein diffusing in a porcine eye. (a) Background fluorescence from the cornea before injection. (b) The Fluorescein has been injected into the anterior chamber. (c)-(f) The Fluorescein is diffusing through the anterior chamber.

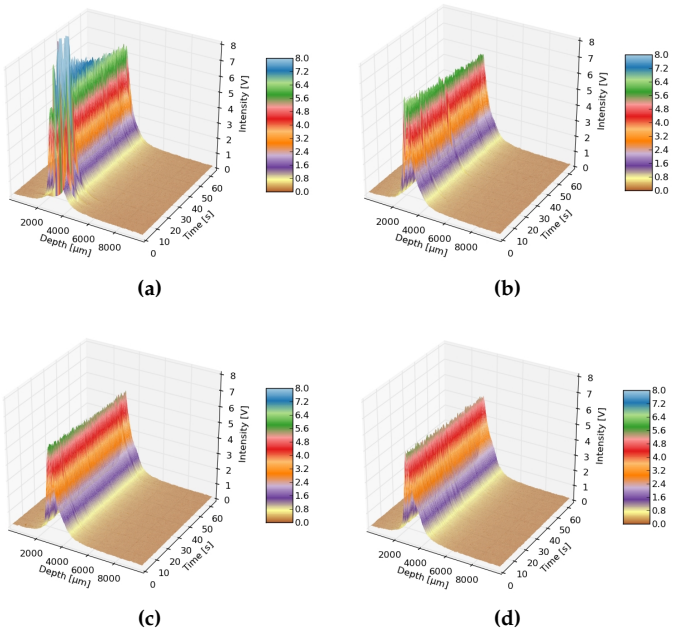

Figure 6.14: Brimonidine diffusing in the anterior chamber of an *in vitro* porcine eye.

Selected time points of the measurement are presented in figure 6.15. It is more clearly visible in these graphs than in the three-dimensional representation that Brimonidine does bind to the cornea. The depth of the distribution is only approximately 1 mm. It is again visible as in the measurements with Fluorescein that the diffusion in the eye takes place slower than in the measurements of a drop of Brimonidine diffusing in a cuvette. This is probably due to the fact that the components in the eye have started decomposing and the aqueous humour is thus more viscous than it would be in living eyes were it will have a viscosity close to that of water.

6.4 Fluorescent background in volunteers

After it had been confirmed that the F410 is capable of measuring rapid changes in concentration in cuvettes and *in vitro* porcine eyes the next logical step was to measure the background fluorescence in *in vivo* eyes. Ethics permission to measure the autofluorescence in healthy volunteers was

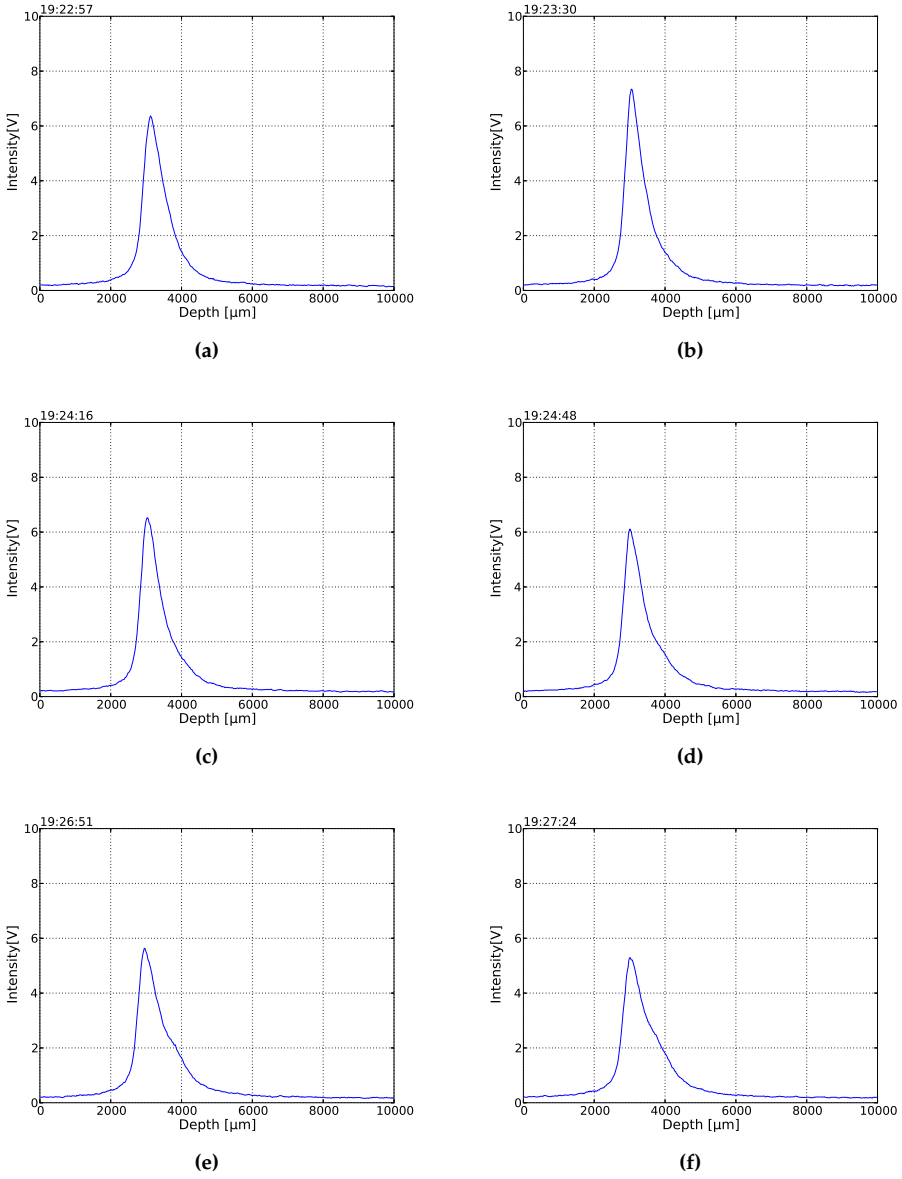

Figure 6.15: Temporal snapshots of Brimonidine diffusing in the anterior chamber of a porcine eye. (a) The background fluorescence from the cornea. (b) After the injection. (c)-(f) The Brimonidine is diffusing slowly through the anterior chamber.

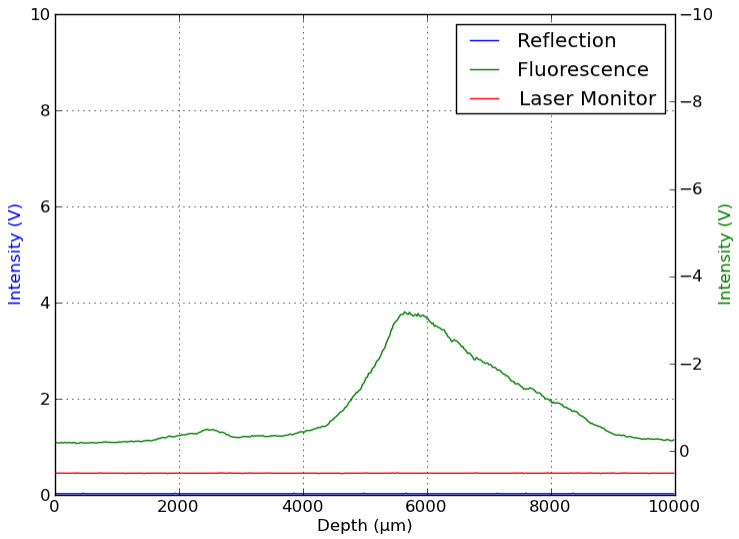

Figure 6.16: Typical scan of the F410 through a human eye.

subsequently granted by the departmental ethics committee. The ethics application and selection criteria for volunteers is given in appendix C. The autofluorescence of cornea and lens were thus monitored first over the course of one day and then twice a day over the course of one week. It seems to be the general convention in the literature to express the fluorescence intensity in terms of equivalent Fluorescein concentration; This has not been done here but will be added in the future prior to the publication of these results.

A typical scan through a human anterior chamber is shown in figure 6.16. The autofluorescence both from the cornea and the lens is clearly visible. The cornea fluoresces significantly less than the lens, with the fluorescence of the lens being age-dependent [49][104]. The fluorescence of the cornea does not seem to be age dependent and the intensity was within the same range for all measured volunteers. It is noticeable in the graph that no reflection from the eye is measured. This is due to the low power of the laser used in this experiment and its wavelength for which the detector is not optimised. The home-build electronics mentioned in chapter 4 include a detector with better sensitivity in the blue wavelengths to increase the signal from the reflection from the

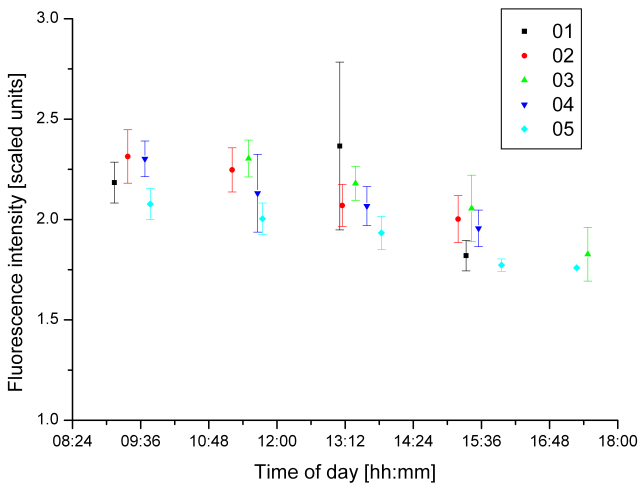

Figure 6.17: The level of human corneal autofluorescence measured over a day.

eye. The detection of correctly aligned scans could therefore not be done using the reflection. Instead, a combination of the amplitude of the corneal peak and the lens peak being above a threshold value was used to define a well aligned scan.

The autofluorescence of cornea and lens was then monitored in seven volunteers in total in two-hourly intervals on two consecutive days. It was found that the fluorescence of the cornea dropped within one day on both measurement days which contradicts other findings published in the literature [105][106]. These measurements were taken at slightly longer wavelengths than the one presented in this dissertation (430-490 nm excitation wavelength for both studies, and 530-630 nm detected emission). The excitation wavelength might thus have an influence on the autofluorescence of the cornea. Further investigation in this area would be very interesting to find if by choosing an appropriate excitation wavelength different corneal metabolic changes can be measured.

The peak fluorescence of the cornea versus the time of day is shown in figure 6.17 for the first measurement day and in figure 6.18 for the second measurement day. The drop in intensity was

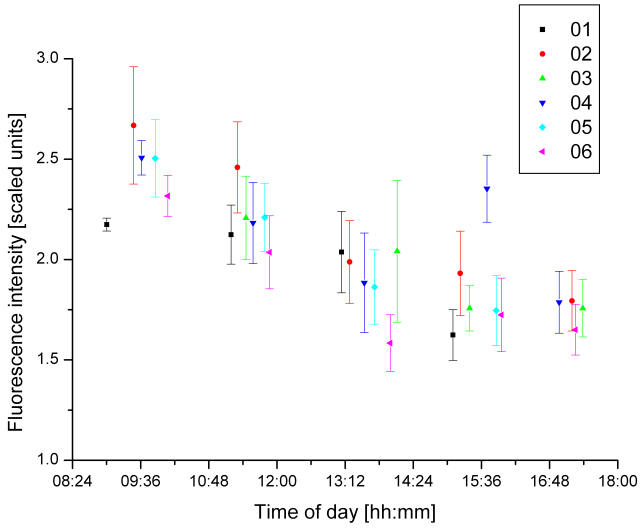

Figure 6.18: The human corneal autofluorescence changing over the course of a day.

found to be statistically significant on both days in all measured volunteers but one (paired t-test, $P < 0.0005$). No significant drop in intensity was found in the lens as can be seen in figures 6.19 and 6.20. It is however well known that the lens in patients with diabetes fluoresces more than in healthy subjects [107][108]. It was therefore no surprise to find that the lens of a volunteer with diabetes fluoresced significantly more than the lenses of other volunteers of the same age (unpaired t-test, $P < 0.005$). After it had been established that the fluorescence of the cornea seems to drop throughout the day it was decided to measure the autofluorescence of the anterior chamber over a week to find any cycles that might be present. The fluorescence intensity for the cornea is shown in figure 6.21 and the autofluorescence for the lens in figure 6.22. It can be seen that the corneal intensity seems to be decreasing on all days except Wedneday and except for volunteer H where in fact it seems to be increasing most of the days. In general there seems a lot of spread of decreasing and increasing so that no definite conclusions can be drawn. More volunteers and more repeats would be necessary to gain enough data for a meaningful analysis.

As with the corneal measurements the autofluorescence from the lens does also not seem to follow

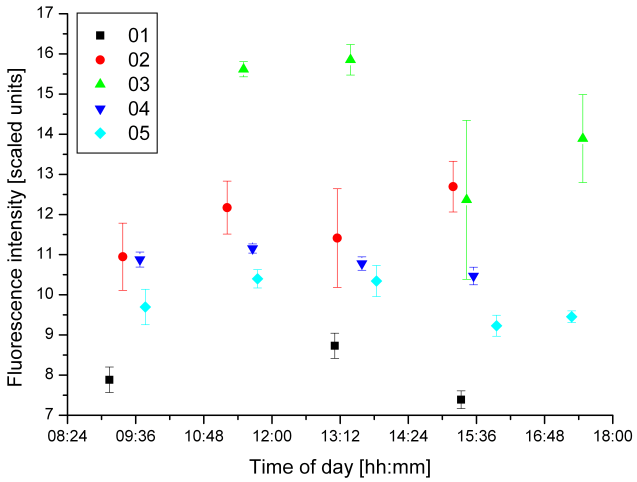

Figure 6.19: The autofluorescence of the human lens monitored over the course of one day.

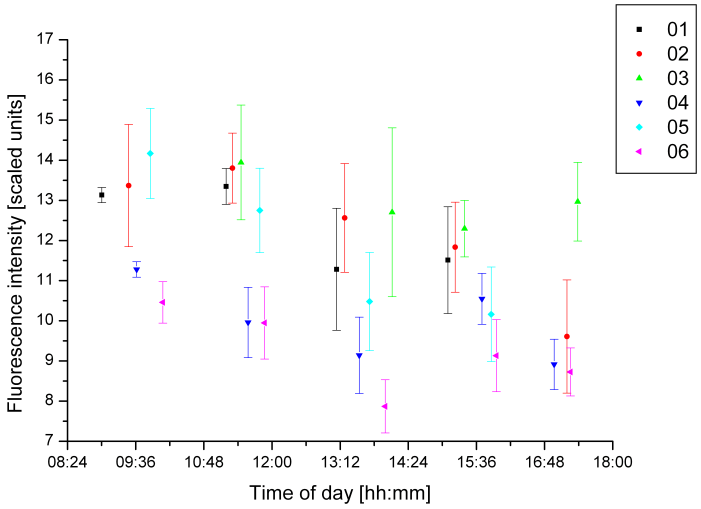

Figure 6.20: The diurnal change in autofluorescence of the lens of human volunteers.

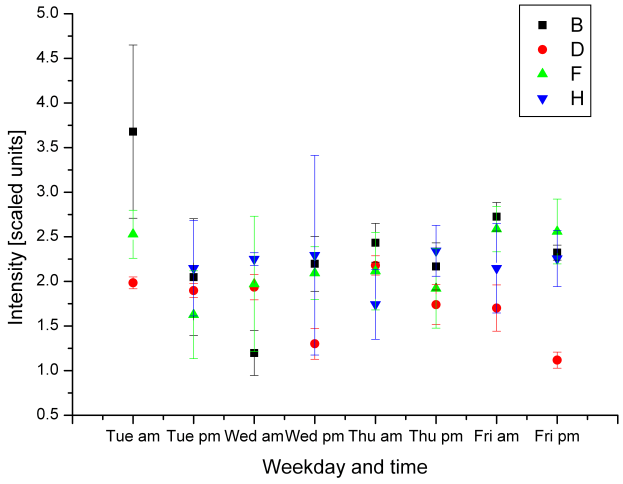

Figure 6.21: The autofluorescence of the human cornea monitored twice daily for a week.

a clear trend or cycle. It is however clearly visible that the lenses of older subjects (F and H, age: 30-35 years) fluoresce more than the lenses of younger volunteers (B and D, age: <30 years).

These results show that the F410 cannot only be used to monitor the diffusion of inherently fluorescent compounds within the anterior chamber of the eye but that a by-product of the design creates the ability to measure the autofluorescence of the cornea and lens. This feature can possibly be used to indicate the health status of either of these components. The fluorescence from the cornea, for example, can be used as an indicator for diabetic retinopathy and for the general evaluation of the corneal metabolism [50][105], whereas the fluorescence from the lens can be used to monitor for cataract and diabetes.

Once the detector in the reflection measurement arm has been changed the instrument will furthermore be capable of measuring the dimensions in the anterior chamber simultaneously which will provide valuable information on the exact location of the fluorescence source.

6.5 Discussion of measurement results

The measurements presented in this chapter show that the instrument is not only capable of measuring the concentration of static, homogeneous samples but also of rapidly changing concentrations of both Fluorescein and Brimonidine in a cuvette and in *in vitro* porcine eyes. Measurements were presented that show a drop of Fluorescein diffusing in a cuvette, both at a high and at a low laser power that is eye safe at the current configuration of the instrument. The final concentration measured in these experiments was close to 500 nM which is the expected concentration after complete diffusion of the drop. Although the concentration could not be recovered from a single drop of Brimonidine diffusing in a cuvette due to issues with the calibration, the measurements show that small changes in intensity are measured by the instrument. These changes in intensity can be used to determine a relative change in concentration even when the absolute concentration is not known. The measurements of Brimonidine diffusing in a cuvette also have poor signal to noise ratio. It is however not doubtable that once the improvements discussed in chapter 8 have been implemented the signal to noise ratio will be better and the instrument will thus be able to recover the concentrations from Brimonidine as accurately as it is currently working with Fluorescein.

In addition to having shown that the distribution of a drop of either Fluorescein or Brimonidine can be monitored in a cuvette, the results presented here also show that the distribution of both Fluorescein and Brimonidine can be monitored in *in vitro* porcine eyes. Unfortunately the concentration for these measurements cannot currently be recovered due to the problems with the samples as discussed in chapter 5. As with the measurements of the Brimonidine diffusion in the cuvette, however, the change in intensity caused by the diffusion of the fluorophore is measured by the instrument. Thus even though the absolute concentration is not known, relative changes in concentration can be recovered. It is thus clear that once a better calibration routine for the porcine eyes has been found the absolute concentration will also be recoverable.

As well as being able to measure small changes in intensity at such low laser power as is present in the porcine eyes, the F410 can also measure the position of the fluorescence accurately and

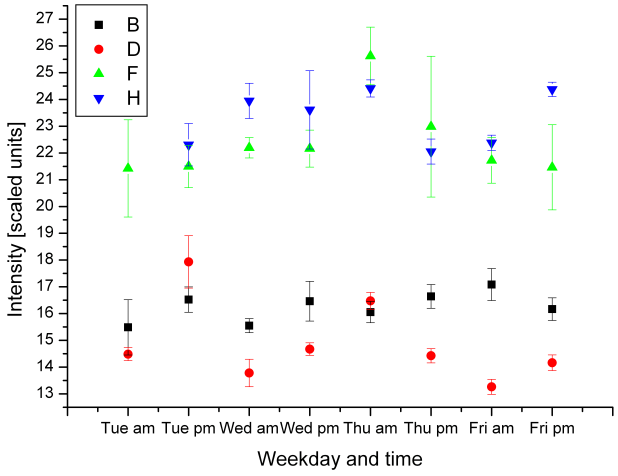

Figure 6.22: The change in autofluorescence of the human lens in a week.

confirms measurements that were published in the literature before of Brimonidine binding to the cornea of the eye. It is therefore clear that with the improvements suggested in chapter 8, the F410 will be able to measure the concentration and distribution of both Fluorescein and Brimonidine accurately both in cuvettes and *in vivo* eyes. The measurement conditions in *in vivo* eyes will be much better than in *in vitro* eyes since the autofluorescence of the cornea will be lower and the cornea much less absorbing and scattering than in the measurements presented in this chapter. It therefore has been proven that the measurement concept presented in thesis is working.

Further to being able to measure the diffusion of fluorescent compounds both in cuvettes and in *in vitro* porcine eyes the instrument is also capable of monitoring the autofluorescence of the human eye. This is an obvious side-effect of the measurement principle that opens doors into other areas of research such as cataract research. Furthermore a slightly modified version of the instrument that was briefly presented at the beginning of this chapter could be used to monitor the tear film and its break up properties. The tear film thickness and break up time are also commonly assessed by measuring the clearance time of Fluorescein eye drops. A potential application of an instrument that combines fluorescence and reflection is the monitoring of the health of the cornea, for

example in long-term contact lens wearers. Another potential application is using the instrument for monitoring the health of the lens which is related to monitoring the auto-fluorescence in diabetics because it is well known that patients with diabetes are more prone to getting early onset cataract [109][110][111].

The results presented in this chapter therefore show that the instrument is not only capable of measuring the pharmacokinetics of fluorescent ophthalmic compounds non-invasively in the eye with high temporal and spatial resolution but that it also has the potential to be used in other applications related to the measurement of fluorescence and reflection in the eye.

Chapter 7

Discussion and conclusion

The work presented in this dissertation deals with the design of a novel, non-invasive instrument to measure the fluorescence of inherently fluorescent drugs in the anterior chamber of the eye. Instruments that measure fluorescence in the eye are usually referred to as ocular fluorophotometers, and they have been in use since the late first half of the 20^{th} century [35][36]. The accepted gold standard instrument, the Fluorotron Master^{TM} (Coherent Inc., California, USA), has however been primarily designed for measuring the fluorescence in the vitreous humour (e.g. to assess the function of the blood-retinal barrier) and can only be used in the anterior chamber by adding a special adapter to the instrument. Its axial resolution using the anterior chamber adapter, measured as the distance from the peak of a signal to the point where the signal has fallen to 3%, is 0.2 mm [52], and without the adapter the resolution decreases to 2 mm [55]. The need for an instrument with higher axial resolution is thus obvious and has been expressed in the literature [32][52][56][57]. Furthermore, to the author's best knowledge none of the instruments that have been discussed in the literature have been used to measure the diffusion of an inherently fluorescent drug directly without the use of fluorescent markers or indirect measurement methods. The instrument presented in this thesis is capable of measuring the diffusion of Alphagan-P (Brimonidine), a drug that is used to lower the IOP in patients with open angle glaucoma, directly and without the use

of fluorescent markers. In addition the instrument discussed here does not only measure the fluorescence but also the reflection from the eye so that valuable information about the exact position of the fluorescence can be obtained.

The investigation was started by modelling the depth dependent decay of the fluorescent signal of Fluorescein solutions of different concentrations. This was done to predict the behaviour of a real sample and to be able to compare the obtained measurements of real samples with the mathematical model to confirm that the instrument is working correctly. For this purpose, the extinction coefficient for Fluorescein sodium salt in water of pH 7 and when excited with a wavelength of 402 nm was measured. It was found that the decay curves for different concentrations cross after a specific depth and thus cannot be used directly to remove the depth dependency of the signal since there is a point of uncertainty where a specific signal can be attributed to several concentrations. The intensity at the first position within the sample (i.e. where the laser beam and thus the fluorescence has not yet been attenuated by absorption) was found to increase linearly with increasing concentration. It was furthermore determined that the decay rate was also linearly dependent on the concentration, with larger concentration having higher decay rates as expected.

As a next step the quantum yield of the compound of interest, Brimonidine, was measured to assess its fluorescent properties. The quantum yield was measured against two standard fluorphores with known quantum yields, Rhodamine B and Fluorescein, and was found to be approximately 0.41% which is very low. In comparison, Fluorescein has a quantum yield that is 170 times higher. Knowing the quantum yield is important so that the instrument can be designed accordingly. A low quantum yield means that a very sensitive instrument with a good signal to noise ratio is needed to be able to measure the fluorescence of low concentrations of that compound. After the magnitude of the quantum yield had been established, a novel measurement concept for measuring the fluorescence and reflection from the anterior chamber of the eye was introduced. The performance of the instrument was assessed by measuring the axial resolutions of the two distinct detection arms which were found to be 285 μm for the reflection detection arm and 124 μm for the fluorescence detection arm. These values are larger than the values predicted by the theoretical

value due to aberrations in the beam produced by slight misalignment of optics and astigmatism introduced by the dichroic mirror, and due to the fact that comparatively large pinholes were chosen to collect more signal. To compare the instrument presented in this thesis with the gold standard ocular fluorophotometer, the Fluorotron Master^{TM}, the axial resolution was also measured as the width from the peak of a signal to the 3% point and was found to be 280 μm, which is below the axial resolution achieved by the competing instrument. It is however clear that once the prototype presented here has been developed further and issues with aberrations have been resolved the axial resolution will increase beyond the value achieved by the Fluorotron. The perfomance of the instrument was then futher analysed by measuring several types of noise that influence the measurement. It was found that the dark noise, although increasing with the reference voltage, was small compared to the unwanted background signal that reaches the detector. The type of noise that creates the highest fluctuation in the measurement was found to be the shot noise created by the random arrival of photons from the sample. This random fluctuation increased both with the reference voltage and with the concentration of the measured solution.

After the discussion of the instrument and its performance and limitations the control software was briefly introduced. The instrument is currently controlled by four major programmes which control the data acquisition, the calibration, the analysis of the data and the presentation of the data. It would obviously be better if all code was combined into one master programme that also incorporates a graphical user interface. This is an addition that is planned for the future development of the instrument. The currently available programmes are however clear enough for a trained person to use them.

Since the instrument was to be used on healthy volunteers the laser safety for exposing the eye to laser radiation was then assessed. According to the British standard, the maximum permissible exposure for an exposure time as given by the instrument presented here is 39 μW. The British standard, however, has not been designed for intentional viewing of the beam and does not consider the focussing of the beam in the anterior chamber of the eye. Instead, it assumes that the beam will focus on the retina and thus no danger is posed to the cornea and lens. To be able to assess

the danger for cornea and lens the illumination of the F410 was therefore simulated using Zemax. It was found that the measurement beam used in the instrument will never focus on the retina unless the eye is more than 60 mm away from the last lens of the instrument, in which case the beam will be overfilling the pupil and the irradiance on the retina will thus be reduced significantly. The highest irradiance on the retina was found to be $14\,\mathrm{Wm}^{-2}$ which is below the safety limit. The highest irradiance on the cornea and in the lens will obviously occur when the beam is focussed on the respective component. The theoretical irradiance in the focal spot as determined from the theoretical spot size (1.69 $\mu\mathrm{m}^2$) and the incident laser power (39 μW) is $7.22 \times 10^6\,\mathrm{Wm}^{-2}$. It is however very unlikely that this irradiance will ever occur due to the aberration of the beam and the resulting blur of the focus. Furthermore, according to guidelines published by the International Commission on Non-Ionizing Radiation Protection, the power of the beam can be averaged over an area as big as 1 mm to account for involuntary eye movements that occur even when head movements are restricted. Therefore, the irradiance can be said to be $49.7\,\mathrm{Wm}^{-1}$, although an averaging over a smaller area is possibly more accurate. Averaging over an area of 50 μm diameter yields an irradiance of $2 \times 10^4\,\mathrm{Wm}^{-2}$. This value is at half the safe limit as given by ANSI 2000. It was found that for the lens the instrument is only just within the safe limit as long as a 1 mm area is used for averaging. Since the actual exposure time is shorter than assumed for the calculation the instrument was however still considered to be safe for human exposure.

After it had been established that the instrument was safe for human use it was calibrated for the use of Fluorescein and Brimonidine in both cuvettes and *in vitro* porcine eyes. The calibration was first carried out using a set of modelled decay curves to show the validity of the calibration routine. As a second step, the instrument was then calibrates for the use of Fluorescein and Brimonidine in cuvettes at both a laser power too high for human viewing (to guarantee a good signal to noise ratio) and a laser power safe for human viewing. It was found that the calibration works very well for measurements that have a high signal to noise ratio, but that for measurements with low signals the accuracy of the recovered concentrations is not very good. The accuracy of measurements of high concentrations of Fluorescein is within a 20% error band as set by the specifications. The

repeatability was however found to be rather poor with an error of 23% within one week. This is most likely due to the high amplification in the system which increases the sensitivity of the instruments to fluctuations in the signal. Unfortunately, the calibration in *in vitro* porcine eyes was found not to work due to the different states of decomposition of the eyes. Another method to calibrate the instrument to *in vitro* eyes therefore has to be found in the future.

As a last step, measurements of diffusing drops of Fluorescein and Brimonidine were taken both in cuvettes and in *in vitro* porcine eyes. It was shown that the instrument can track the diffusion of the compound of interest with a temporal resolution of 0.6 s which is much faster than the Fluorotron, which needs 20 s for one complete scan through the anterior chamber. Due to issues with the calibration, the concentration of a single drop of Brimonidine diffusing in a cuvette could not be recovered, but it is shown that the change in intensity and thus the relative change in concentration can still be measured by the instrument. Results were also presented that show a drop of Fluorescein and Brimonidine diffusing in porcine eyes. Again, the concentration for these measurements cannot be recovered due to the fact that the calibration for *in vitro* eyes failed. However, as with the Brimonidine diffusing in a cuvette, the change in signal and thus the relative change in concentration is tracked by the instrument. It was found that the Brimonidine concentration is higher in areas close to the cornea than deeper in the aqueous humour which confirms findings discussed in the literature [103][82]. Further results that show the diurnal change in the autofluorescence of the eyes of healthy volunteers were presented. It was found that the peak fluorescence intensity of the cornea decreased over the course of one day which contradicts findings from slightly longer excitation wavelengths published in the literature [105][106]. No clear pattern was found in the change of autofluorescence in the lens. Furthermore, no clear change in fluorescence was found over the course of a week.

Concluding it can thus be said that a novel, non-invasive instrument has been presented in this dissertation which has the potential to become the new gold standard fluorophotometer. Its axial resolution is currently not quite as good as that of the current gold standard instrument but it is without doubt that once the improvements suggested in the last chapter of this thesis have been

implemented the instrument presented here will perform at least as good as the Fluorotron Master. The advantage of the novel instrument is the use of pinholes rather than confocal slits which allows for an increase in the resolution of the system. Furthermore a laser rather than a filtered lamp is used as the excitation source which increases the irradiance and thus the signal to noise ratio. In addition, the instrument described here records the reflection from the eye simultaneously with the fluorescence which increases the accuracy of the determination of the source of the fluorescent signal. A measurement point is taken every 20 μm in comparison to every 250 μm in the commercially available instrument. A better positional resolution is thus achieved. Another advantage of the F410 is that it only takes 0.6 s to acquire a complete scan through the anterior chamber of the eye whereas the Fluorotron takes 20 s for one scan. The diffusion of fluorescent compounds can thus be tracked with much higher temporal resolution than before. Other instrument that are faster than the Fluorotron Master exist [44], but to the best of the author's knowledge they have not been developed any further and have not extensively been used in research. As a last point it should be mentioned that the instrument presented here is comparatively low-cost and that it can easily be made smaller and lighter and thus find applications in home monitoring systems.

Chapter 8

Outlook

The F410 is only a prototype and therefore still harbours a number of problems that need improving. The most crucial limitation of the instrument currently is its signal to noise ratio which needs improvement before the concentrations of compounds with low signal levels or low quantum yields can be measured accurately. The author is convinced that with an improved design, the instrument will have the potential to become the new gold standard ocular fluorophotometer.

The first step to improve the instrument will be to use better optics (lenses that are anti-reflection coated in the specific wavelength region and achromatic) and to apply more sophisticated optical engineering to the existing instrument to decrease the optical aberrations currently present in the set-up. A decrease of the aberrations will lead to a tighter focal spot in the sample and thus an increased signal strength, which in turn will facilitate a higher signal to noise ratio. A tighter focal spot will also mean that the pinhole size can be reduced, thus improving the axial and lateral resolution of the system.

After these improvements have been made, the next important step will be to increase the speed of the data acquisition. A faster data acquisition will decrease the scanning time and thus the time the eye is exposed to the laser, which in turn means that the laser intensity can be increased

which leads to a direct increase in the signal to noise ratio. To make the data acquisition faster, the analogue to digital converter has to be exchanged for a model that can acquire more samples per second. The scanning speed of the motorised translation stage can then be increased as well to make the scanning time shorter. Eventually, a different translation stage that can scan at higher frequencies will have to be used. Increasing the data acquisition speed will also reduce the error introduced into the measurements by blinking and involuntary eye movements.

Then, it will be important to be able to further increase the laser power incident on the eye. This can be achieved by using a pulsed rather than a CW laser since the pulse durations are so short that the exposure time will decrease drastically. Again, this improvement will lead to a better signal to noise ratio which will in turn lead to a better measurement resolution of the instrument in terms of detected concentrations. Furthermore, if a pulsed laser source is used, it can become part of a lock-in amplification circuit which can replace the currently used active low-pass filter, further increasing the signal to noise ratio and probably reducing the size of the control electronics.

Another important improvement to make is the generation of a graphical user interface for ease of use of the software. Currently, all components of the software have to be run individually from the Python Shell so that it would be very hard for an untrained person to use them. Therefore a graphical user interface is needed to increase the usability of the system.

Lastly, reevaluation of the laser safety with the help of an expert would be required to ensure that the maximum possible laser power is used while staying within safe limits.

Less important for the immediate improvement of the instrument but also desirable for the future will be the decrease of the size of the instrument to make it less heavy and easier to transport. It can even be developed into a hand-held instrument for e.g. a home monitoring system. Another addition might be to use a different detection method like for example fluorescence life-time measurements which would allow for better distinction between the compound of interest and other fluorescent signals that might be detected, as well as adding the possibility to detect different ophthalmic compounds simultaneously. This might however be hard to combine with the current

spatial scanning technique and require more computing power, thus slowing down the acquisition speed.

With all the improvements suggested above it is expected that the instrument will perform better than currently available commercial instruments. It will thus not only fulfill the requirements set by Allergan but also has the potential to become the new gold standard of ocular fluorophotometers in specific areas of research.

Bibliography

[1] N. Worakul and J. R. Robinson. Ocular pharmacokinetics / pharmacodynamics. *European Journal of Pharmaceutics and Biopharmaceutics*, 44:71–83, 1997.

[2] R. Urso, P. Blardi, and G. Giorgi. A short introduction to pharmacokinetics. *European Review for Medical and Pharmacological Sciences*, 6:33–44, 2002.

[3] Soraya Dhillon and Kiren Gill. *Clinical Pharmacokinetics*, chapter 1, pages 1–44. Pharmaceutical Press, 1 edition, 2006.

[4] Uday B. Kompella, Rajendra S. Kadam, and Vincent H. L. Lee. Recent advances in ophthalmic drug delivery. *Therapeutic Delivery*, 1:435–456, 2010.

[5] Mark R. Prausnitz and Jeremy S. Noonan. Permeability of cornea, sclera, and conjunctiva: A literature analysis for drug delivery to the eye. *Journal of Pharmaceutical Sciences*, 87:1479–1488, 1998.

[6] Arto Urtti. Challenges and obstacles of ocular pharmacokinetics and drug delivery. *Advanced Drug Delivery Reviews*, 58:1131–1135, 2006.

[7] Jobin Yvon Horiba. A guide to recording fluorescence quantum yields.

[8] Serge Resnikoff. Global data on visual impairment in the year 2002. *Bulletin of the World Health Organization*, 82(11):844–851, November 2004.

[9] Wikipedia. Schematic diagram of the human eye, 2009. [Online; As of 5th July 2009, accessed on 21st July 2009].

[10] Wikipedia. Tear system, August 2008. [Online; As of 6th August 2008, accessed on 24th July 2009].

[11] Clyde W. Oyster. *The Human Eye - Structure and function*. Sinauer Associates, Inc., 1999.

[12] John I. Clark. Order and disorder in the transparent media of the eyes. *Experimental Eye Research*, 78:427–432, 2004.

[13] Chi ho To, Chi wing Kong, Chu yan Chan, Mohammad Shahidullah, and Chi wai Do. The mechanisms of aqueous humour formation. *Clinical and Experimental Optometry*, 85:335–349, 2002.

[14] National Institutes of Health (NEI/NIH) National Eye Institute. Facts about glaucoma, May 2009. [Online; Accessed on 30th September 2012].

[15] Daniel A. Goodenough. The crystalline lens. a system networked by gap junctional intercellular communication. *Seminars in Cell Biology*, 3:49–58, 1992.

[16] M. Dubbelman, G. L. Van der Heijde, H. A. Weeber, and G. F. J. M. Vrensen. Changes in the internal structure of the human crystalline lens with age and accommodation. *Vision Research*, 43:2363–2375, 2003.

[17] P. N. Bishop, M. Takanosu, M. le Goff, and R. Mayne. The role of the posterior ciliary body in the biosynthesis of vitreous humour. *Eye*, 16:454–460, 2002.

[18] M. M. le Goff and P. N. Bishop. Adult vitreous structure and postnatal changes. *Eye*, 22:1214–1222, 2008.

[19] Wikipedia. Retina, September 2012. [Online; As of 12th September 2012, accessed on 30th September 2012].

[20] G. A. Boutry and R. Auerbach. *Instrumental Optics*. Hilger & Watts, 1961.

[21] Nick Fogt. Interferometric measurement of tear film thickness by use of spectral oscillations. *Journal of the Optical Society of America A*, 15(1):268–275, January 1998.

[22] Jianhua Wang. Precorneal and pre- and postlens tear film thickness measured indirectly with optical coherence tomography. *Investigative ophthalmology & Visual Science*, 44(6):2524–2528, June 2003.

[23] J. M. Girkin. Private communication.

[24] Niels Ehlers. Applanation tonometry and central corneal thickness. *Acta Ophthalmologica*, 53:34–43, 1975.

[25] National Eye Institute. Facts about dry eye, July 2009. [Online; As of July 2009, accessed on 27th of July 2009].

[26] Berufsverband der Augenärzte Deutschlands e.V. Das trockene auge - eine ernstzunehmende krankheit. Leaflet, September 2007.

[27] Scot E. Moss. Prevalence of and risk factors for dry eye syndrom. *Archives of Ophthalmology*, 118:1264–1268, 2000.

[28] Janine A. Smith. The epidemiology of dry eye disease: Report of the epidemiology subcommitte of the international dry eye workshop (2007). *The Ocular Surface*, 5:93–107, 2007.

[29] Robert J. Noecker. The management of glaucoma and intraocular hypertension: current approaches and recent advances. *Therapeutics and clinical risk management*, 2(2):193–206, 2006.

[30] Royal National Institute of Blind People. Eye info - understanding glaucoma, 2009. [Online; As of 24th March 2009, accessed on 22nd July 2009].

[31] Clive W. Wilson. Private communication.

[32] Yoshiaki Kiuchi, Takeshi Yoshitomi, and Douglas S. Gregory. Do α-adrenergic receptors participate in control of the circadian rythm of iop? *Investigative Ophthalmology & Visual Science*, 33:3186–3194, 1992.

[33] Martin Göbbels and Manfred Spitznas. Influence of artificial tears on corneal epithelium in dry-eye syndrome. *Graefe's Archive for Clinical and Experimental Ophthalmology*, 227:139–141, 1989.

[34] Paul Ehrlich. über die färbung der tuberkelbazillen. *Deutsche Medizinische Wochenschrift*, 8:269, 1882.

[35] Marc Amsler and Alfred Huber. Methodik und erste klinische ergebnisse einer funktionsprüfung der blut-kammerwasser-schranke. *Opthalmologica*, 111:155–176, 1946.

[36] H. Goldman. Enthalten die kammerwassernerven kammerwasser? *Ophthalmologica*, 117:240–243, 1949.

[37] Maurice Langham and Kenneth C. Wybar. Fluorophotometric apparatus for the objective determination of fluorescence in the anterior chamber of the living eye. *British Journal of Ophthalmology*, 38:52–57, 1954.

[38] D. Maurice. A new objective fluorophotometer. *Experimental Eye Research*, 2:33–38, 1963.

[39] Stephen R. Waltman and Herbert E. Kaufman. A new objective slit lamp fluorophotometer. *Investigative Opthalmology*, 9:247–249, 1970.

[40] Reiji Aoshima, Keiji Iriyama, and Hiroshi Asai. High sensitivity fluorophotometer using photon counting. *Applied Optics*, 12:2748–2750, 1973.

[41] A. Trevor Smith, D. P. Jones, G. D. Sturrock, and Peter Wright. An improved objective slit-lamp fluorophotometer using tungsten-halogen lamp excitation and synchronous detection. *British Journal of Ophthalmology*, 61:722–725, 1977.

[42] D. P. Jones, A. T. Smith, G. D. Sturrock, and P. Wright. Ophthalmic fluorophotometry: an improved slit-lamp fluorophotometer. *Medical & Biological Engineering & Computing*, 17:365–370, 1979.

[43] D. P. Jones, W. R. S. Webber, A. T. Smith, D. Lloyd-Jones, and P. Wright. Ophthalmic fluorophotometry: a new solid state fluorophotometer. *Journal of Biomedical Engineering*, 4:113–117, 1982.

[44] Jay W. McLaren and Richard F. Brubaker. A two-dimensional scanning ocular fluorophotometer. *Investigative Ophthalmology & Visual Science*, 26:144–152, 1985.

[45] Ran C. Zeimer and Jose G. Cunha-Vaz. Evaluation and comparison of commercial vitreous fluorophotometers. *Investigative Ophthalmology & Visual Science*, 21:865–868, 1981.

[46] Charles R. Munnerlyn, John R. Gray, and David R. Hennings. Design considerations for a fluorophotometer for ocular research. *Graefe's Archive for Clinical and Experimental Ophthalmology*, 222:209–211, 1985.

[47] J. R. Gray, M. A. Mosier, and B. M. Ishimoto. Optimized protocol for fluorotron master. *Graefe's Archive for Clinical and Experimental Ophthalmology*, 222:225–229, 1985.

[48] R. C. Zeimer, N. P. Blair, M. M. Rusin, and J. G. Cunha-Vaz. The performance of a new commercial ocular fluorophotometer in the clinical environment. *Graefe's Archive for Clinical and Experimental Ophthalmology*, 222:223–224, 1985.

[49] Jaco C. Bleeker, Jaap A. van Best, Leo Vrij, Edo A. van der Velde, and Jendo A. Oosterhuis. Autofluorescence of the lens in diabetic and healthy subjects by fluorophotometry. *Investigative Ophthalmology & Visual Science*, 27:791–794, 1986.

[50] Thorsten R. Stolwijk, Jaap A. van Best, Johan P. Boot, and Jendo A. Oosterhuis. Corneal autofluorescence in diabetic and penetrating keratoplasty patients as measured by fluorophotomety. *Experimental Eye Research*, 51:403–409, 1990.

[51] Cris de Jong, Thorsten Stolwijk, Esmeralda Kuppens, Rob de Keizer, and Jaap van Best. Topical timolol with and without benzalkonium chloride: epithelial permeability and autofluorescence of the cornea in glaucoma. *Graefe's Archive for Clinical and Experimental Ophthalmology*, 232:221–224, 1994.

[52] N. Eter and M Göbbels. A new technique for tear film fluorophotometry. *British Journal of Ophthalmology*, 86:616–619, 2002.

[53] Pedro Beneyto and Teresa M. Perez. Study of lens autofluorescence by fluorophotometry in pregnancy. *Experimental Eye Research*, 82:583–587, 2006.

[54] D. J. Spalton. Mini review: Ocular fluorophotometry. *British Journal of Ophthalmology*, 74:431–432, 1990.

[55] www.ocumetrics.com. [Online; Accessed on 18th September 2012].

[56] Abhay Joshi, David Maurice, and Jerry R. Paugh. A new method for determining corneal epithelial barrier to fluorescein in humans. *Investigative Ophthalmology & Visual Science*, 37:1008–1016, 1996.

[57] E. Ian Pearce, B. Patrick Keenan, and Ciaran McRory. An improved fluorophotometric method for tear turnover assessment. *Optometry and Vision Science*, 78:30–36, 2001.

[58] Marvin Minsky. Microscopy apparatus, 1961.

[59] Marvin Minsky. Memoir on inventing the confocal scanning microscope. *Scanning*, 10:128–138, 1988.

[60] P. Davidovits and M. D. Egger. Scanning laser microscope for biological investigations. *Applied Optics*, 10(7):1615–1619, July 1971.

[61] W. B. Amos and J. G. White. How the confocal laser scanning microscope entered biological research. *Biology of the cell*, 95:335–342, 2003.

[62] J. G. White, W. B. Amos, and M. Fordham. An evaluation of confocal versus conventional imaging of biological structures by fluorescence light microscopy. *The Journal of Cell Biology*, 105:41–48, July 1987.

[63] James B. Pawley. *Handbook of Biological Confocal Microscopy - Preface*. Plenum Press, 1995.

[64] Thomas J. Fellers and Michael W. Davidson. Theory of confocal microscopy - introduction to confocal microscopy, 2009. [Online; As of 2009, accessed on 29th July 2009].

[65] Robert H Webb. Confocal optical microscopy. *Reported Progress in Physics*, 59:427–471, 1996.

[66] Michiel Müller. *Introduction to Confocal Fluorescence Microscopy*. Tutorial Texts. SPIE Press, 2 edition, 2006.

[67] T. Wilson and A. R. Carlini. Size of the detector in confocal imaging systems. *Optics Letters*, 12(4):227–229, April 1987.

[68] Lord Rayleigh. *Scientific Papers*, chapter On Pin-Hole Photography, pages 429–441. Cambridge University Press, 1902.

[69] Joseph R. Lakowicz. *Principles of Fluorescence Spectroscopy*. Plenum Press, 1983.

[70] M. C. Mota, P. Carvalho, J. Ramalho, and E. Leite. Spectrophotometric analysis of sodium fluorescein aqueous solutions. determination of molar absorption coefficient. *International Ophthalmology*, 15:321–326, 1991.

[71] Nathan S. Claxton, Thomas J. Fellers, and Michael W. Davidson. Laser scanning confocal microscopy. [Online; Accessed on 30th September 2012].

[72] Beer. Bestimmung der absorption des rothen lichts in farbigen flüssigkeiten. *Annalen der Physik und Chemie*, 86:78–88, 1852.

[73] D. M. Maurice. The use of fluorescein in ophthalmological research. *Investigative Opthalmology*, 6:464–477, 1967.

[74] Douglas Madge, ROger Wong, and Paul G. Seybold. Fluorescence quantum yields and their relation to lifetimes of rhodamine 6g and fluorescein in nine solvents: Improved absolute standards for quantum yields. *Photochemistry and Photobiology*, 75:327–334, 2002.

[75] James H. Brannon and Douglas Madge. Absolute quantum yield determination by thermal blooming. fluorescein. *The Journal of Physical Chemistry*, 82:705–709, 1978.

[76] Aimin Song, Jinhua Zhang, Manhua Zhang, Tao Shen, and Ji'an Tang. Spectral properties and structure of fluorescein and its alkyl derivatives in micelles. *Colloids and Surfaces A*, 167:253–262, 2000.

[77] Albert M. Brouwer. Standards for photoluminescence quantum yield measurements in solution (iupac thechnical report). *Pure and Applied Chemistry*, 83:2213–2228, 2011.

[78] ISS, 2012. [Online; As of 2012, accessed on 02.10.2012].

[79] Douglas Madge, James H. Brannon, Teresa L. Cremers, and John Olmsted III. Absolute luminescence yield of cresyl violet. a standard for the red. *The Journal of Physical Chemistry*, 83:696–699, 1979.

[80] Kelly G. Casey and Edward L. Quitevis. Effect of solvent polarity on nonradiative processes in xanthene dyes: Rhodamine b in normal alcohols. *The Journal of Physical Chemistry B*, 92:6590–6594, 1988.

[81] G. Weber and F. W. Teale. Determination of the absolute quantum yield of fluorescent solutions. *Transactions of the Faraday Society*, 53:646–655, 1957.

[82] Andrew A. Acheampong, Martha Shackleton, Brian John, James Burke, Larry Wheeler, and Diane Tang-Liu. Distribution of brimonidine into anterior and posterior tissues of monkey, rabbit and rat eyes. *Drug Metabolism and Disposition*, 30:421–429, 2002.

[83] Christopher T. Culbertson, Stephen C. Jacobson, and J. Michael Ramsey. Diffusion coefficient measurements in microfluidic devices. *Talanta*, 56:365–373, 2002.

[84] I. N. Bronstein and K. A. Semendjajew. *Taschenbuch der Mathematik*. Verlag Harri Deutsch, 5. edition, 2001.

[85] Safety of laser products - part 1: Equipment classification and requirements, 2007.

[86] Hwey-Lan Liou and Noel A. Brennan. Anatomically accurate, finite model eye for optical modelling. *Journal of the Optical Society of America A*, 14:1684–1695, 1997.

[87] David Sliney, Danielle Aron-Rosa, Francois DeLori, Franz Frankhauser, Robert Landry, Martin Mainster, John Marshall, Bernard Rassow, Bruce Stuck, Stephen Trokel, Teresa Motz West, and Michael Wolffe. Adjustments of guidelines for exposure of the eye to optical radiation from ocular instruments: Statement from a task group of the international commission on non-ionizing radiation protection (icnirp). *Applied Optics*, 44:2162–2176, 2005.

[88] Francois DeLori, Robert H. Webb, and David H. Sliney. Maximum permissible exposures for ocular safety (ansi 2000), with emphasis on ophthalmic devices. *Journal of the Optical Society of America A*, 24:1250–1265, 2007.

[89] Dwight Grotte, Vernon Mattox, and Richard Brubaker. Fluorescent, physiological and pharmacokinetic properties of fluorescein glucuronide. *Experimental Eye Research*, 40:23–33, 1985.

[90] C. Seto, M. Araie, and M. Takase. Study of fluorescein glucuronide ii. a comparative ocular kinetic study of fluorescein and fluorescein glucuronide. *Graefe's Archive for Clinical and Experimental Ophthalmology*, 224:113–117, 1986.

[91] Robert Sjöbak, Jan Nygren, and Mikael Kubista. Absorption and fluorescence properties of fluorescein. *Spectrochimica Acta Part A*, 51:7–21, 1995.

[92] I. Lopez Arbeola. Dimeric and trimeric states of the fluorescein dianion. *Journal of the Chemical Society, Faraday Transactions 2*, 77:1735–1742, 1981.

[93] I. Lopez Arbeola. Fluorescence self-quenching of halofluorescein dyes. *Journal of Photochemistry*, 18:161–168, 1982.

[94] Stuart Hodson. Evidence for a bicarbonate-dependent sodium pump in corneal epithelium. *Experimental Eye Research*, 11:20–29, 1971.

[95] S. Diekstein and D.M. Maurice. The metabolic basis to the fluid pump in the cornea. *Journal of Physiology*, 221:29–41, 1972.

[96] Stuart Hodson. The regulation of corneal hydration by a salt pump requiring the presence of sodium and bicarbonate ions. *Journal of Physiology*, 236:271–302, 1974.

[97] Casten Faber, Erik Scherfig, Jan Ulrik Prause, and Knud Erik Sorensen. Corneal thickness in pigs measured by ultrasound pachymetry in vivo. *Scandinavian Journal of Laboratory Animal Science*, 35:39–43, 2008.

[98] Timothy W. Olson, Scott Sanserson, Xiao Feng, and William C. Hubbart. Porcine sclera: Thickness and surface area. *Investigative Ophthalmology & Visual Science*, 43:2529–2532, 2002.

[99] J. Lay, A. Brocas, K. Singh, J.-C. Kieffer, I. Brunette, and T. Ozaki. Determination of porcine corneal layers with high spatial resolution by simultaneous second and third harmonic generation microscopy. *Optics Express*, 16:16284 – 16293, 2008.

[100] David C. Herman, Jay W. McLaren, and Richard F. Brubaker. A method of determining concentration of albumin in the living eye. *Investigative Ophthalmology & Visual Science*, 29:133–137, 1988.

[101] Martin J. Koeberle, Patrick M. Hughes, Graham G. Skellern, and Clive G. Wilson. Pharmacokinetics and disposition of memantine in the arterially perfused bovine eye. *Pharmaceutical research*, 23:2781–2798, 2006.

[102] K. K. Buttenschön, J. M. Girkin, and D. J. Daly. Development of a low-cost confocal instrument to measure the axial dimensions of components in the anterior section of the eye. *Clinical Optometry*, 2:67–72, 2010.

[103] Andrew A. Acheampong, Martha Shackleton, and Diane D-S. Tang-Liu. Comparative ocular pharmacokinetics of brimonidine after a single dose application to eyes of albino and pigmented rabbits. *Drug Metabolism and Disposition*, 23:708–712, 1995.

[104] Marjorie A. Mosier, Joseph R. Occhipinti, and Neal L. Burstein. Autofluorescence of the crystalline lens in diabetes. *Archives of Ophthalmology*, 104:1340–1343, 1986.

[105] Thorsten R. Stolwijk, Jaap A. van Best, Jendo A. Oosterhuis, and Wouter Swart. Corneal autofluorescence: An indicator of diabetic retinopathy. *Investigative Ophthalmology & Visual Science*, 33:92–97, 1992.

[106] Norihiko Kitaya, Satoshi Ishiko, Fumihiko Mori, Tohru Abiko, Hiroyuki Kagokawa, Masumi Takeda, Akira Takamiya, and Akitoshi Yoshida. Diurnal variation of corneal autofluorescence in normal and diabetic eyes. *Eye*, 12:934–937, 1998.

[107] J. M. Sparrow, A. J. Bron, N. A. Phelps Brown, and H. A. Neil. Autofluorescence of the crystalline lens in early and late onset diabetis. *British Journal of Ophthalmology*, 76:25–31, 1992.

[108] Tohru Abiko, Atsuko Abiko, Satoshi Ishiko, Masumi Takeda, Seiko Horiuchi, and Akitoshi Yoshida. Relationship between autofluorescence and advanced glycation end products in diabetic lenses. *Experimental Eye Research*, 68:361–366, 1999.

[109] E. Cotlier. Senile cataracts: Evidence for acceleration by diabetes and deceleration by salicylate. *Canadian Journal of Ophthalmology*, 16(3):113–118, 1981.

[110] Ronald E. Perry, M. S. Swarmy, and E. C. Abraham. Progressive changes in lens crystalline glycation and high-molecular-weight aggregate formation leading to cataract development in streptzotocin-diabetic rats. *Experimental Eye Research*, 44:269–282, 1987.

[111] Timothy J. Lyous, Giuliana Silvestri, John A. Dunn, Daniel G. Dyer, and John W. Baynes. Role of glycation in modification of lens crystallins in diabetic and nondiabetic senile cataracts. *Diabetes*, 49(8):1010–1015, 1991.

List of Acronyms

ADC: analogue to digital converter

A device that digitises an analogue input quantity. 53, 54, 62, 64, 96, 113, 119

AEL: accessible emission limit

The maximum accessible emission permitted within a particular laser class. 68–70, 73, 85

CCT: central corneal thickness

The thickness of the cornea at its apex. 124, 126–128

FWHM: full-width half-maximum

The full width of the point-spread function at half intensity. 29, 30, 36, 55, 57, 58, 82

IOP: intra-ocular pressure

The pressure within the anterior chamber of the eye. Normal IOP ranges from 8 to 21 mm Hg. 14–16, 152

MPE: maximum permissible exposure

The level of laser radiation to which persons may be exposed without causing damage to their eyes or skin. 68–71, 77, 80

NA: numerical aperture

A physical property of a lens related to the semi-angle of the aperture and the refractive index of the medium the light beam is travelling through. 25

PMT: photo-multiplier tube

A very sensitive detector in which the photo current is amplified over several internal stages. 53, 54, 57, 58, 64, 65, 97, 99, 106, 119, 134

PSF: point-spread function

A function describing the lateral or axial intensity distribution created by the focus of a lens. 25–30, 35, 36, 57, 58, 82

Appendix A

Specifications

Durham University
South Road
Durham DH1 3LE
UK

Specifications for the F410
-a fluorescence based system for the quantitative measurement of ophthalmic drugs in the eye-

Aim
The aim of this project is to determine the best technologies and solutions for a non-invasive optical instrument capable of quantitative concentration measurements of naturally fluorescing ophthalmic drugs in the eye. It will record one-dimensional depth concentration profiles along the optical axis of the eye through the aqueous chamber using confocal fluorescence microscopy.
This specification defines the targets for a device that is to be tested first on glass objects (*in vitro*), on perfused sheep's or pig's eyes (*in vitro*) and last on human eyes (*in vivo*).

Introduction
This specification defines target performance limits of the F410.

Detection and excitation wavelengths
This system is being designed to measure the fluorescence of Brimonidine which fluoresces in the region of 425 to 625nm when excited with 408nm. The excitation wavelength was chosen because the absorption curve of Brimonidine shows that a wavelength as short as possible while still being eye safe is needed to excite enough fluorescence for the detector to pick up in the lower concentration range. These factors define the detection and excitation wavelengths of the system as given below.

- Wavelength of detection: $\leq$470 nm to 700 nm
- Wavelength of excitation: 408 nm, Laser Class 1 as defined in IEC 60825-1
- Other wavelengths: White light source to illuminate the front of the eye for position detection with the web cam

Accuracy
Accuracy is defined as the proximity of the measurement result to the true value.

- Drug detection *in vivo*: As agreed with Allergan an error of 20% should be allowed.
- Axial position in the eye *in vitro*: 1 µm (acceptable: 10 µm)
- Axial position in the eye *in vivo*: 5 µm (acceptable: 20 µm)
- The measurement accuracy will be constant within 20% over the course of a day if the instrument is not being moved. The calibration will have to be checked on a day to day basis.

Repeatability
The capability of the measurement system to create repeatable results.

- Drug detection *in vitro*: Better than 5% standard deviation (acceptable: 10% standard deviation)
- Drug detection *in vivo*: Better than 20% standard deviation as agreed with Allergan
- Axial position in the eye *in vitro*: 1 μm (acceptable: 10 μm)
- Axial position in the eye *in vivo*: 5 μm (acceptable: 20 μm)
- The measurement repeatability will be constant within 20% over the course of a day if the instrument is not being moved. The calibration will have to be checked on a day to day basis.

Resolution
Resolution is defined as the smallest change in the underlying physical quantity that produces a response in the measurement.

- Axial resolution: Better than 50 μm (acceptable: Better than 100 μm)
- Lateral resolution: Better than 100 μm (acceptable: Better than 200 μm)
- Chemical resolution: Better than 100 nM Brimonidine (acceptable: Better than 500 nM Brimonidine)

Speed

- Data acquiring: All data has to be acquired in under 100 seconds including alignment time.
- Data analysis: Near real time analysis and display of collected data.

Detection limit
The detection limit is dependent on the power of the laser which has to be eye safe. Currently, the laser is operating at 660 μW. Therefore the target detection limit of the instrument is 100 nM Brimonidine currently, with better than 500 nM of Brimonidine being acceptable. The gain of the photo-multiplier will be switchable to detect different concentration ranges.

Safety

- Laser safety
  - The output of the instrument is that of a Class 1 laser device as defined by IEC 60825-1 under all conditions of operation, maintenance, service and failure.
  - The Class 4 laser used as a light source will be mounted within a protective box within the instrument.
  - The instrument cover will be connected to an interlock that switches off the laser if the cover is opened.
- Electrical safety
  - The device will be tested for electrical safety according to IEC 60601-1.
- Mechanical safety
  - No moving parts will be accessible from the outside of the instrument without removing the cover.

Mechanichal properties

- Dimensions and Weight: To be agreed, but suitable for easy handling and mounting on an ophthalmic stage.

Software
The software will perform the following functions:

- Turns on the light source and initialises the system for operation
- Checks that the light source power is within acceptable limits
- Runs the scanning function
- Collects acceptable data (discards poor data)
- Saves data in an appropriate format for post-processing in an electronic file
- Analyses data
- Saves the results of the analysis in a format appropriate for post-processing
- Stops the scanning function when the required quantity of data has been collected.

Appendix B

Software

```
from __future__ import division
from operator import itemgetter
import scipy.optimize
import fileopen, shift, average, norm, fit, conc_det, loadBack
import numpy, pylab, scipy, os

def lin_func(x, m, b):
    return m*x + b

def exp_func(x, a, b):
    return a*scipy.exp(b*x)

STEM = r'c:\Documents and Settings\kkb\Desktop\New Folder (2)\PhD\F410\PMT measurements\
         2012-08-24/'
files = [fname for fname in os.listdir(STEM) if fname[-5:] == 'M.txt']
C = []
backname = r'c:\Documents and Settings\kkb\Desktop\New Folder (2)\PhD\F410\
             PMT measurements\2012-08-24/water.txt'
p_back, m_back, r_back, f_back = loadBack.load_background(backname) #load background file
f_back = f_back

for fname in files:
    print fname
    pos, tim, mon, vref, ref, flu = fileopen.fopen(STEM+fname)  #read columns from file
    #shift arrays such that they are all aligned at the maximum reflection:
    shift_pos, shift_mon, shift_vref, shift_ref, shift_flu = shift.shift(r_back, pos, mon,
                                                                         vref, ref, flu)
    shift_pos_2 = shift_pos[::2]                    #cut arrays such that only every
                                                    #second entry is used-
    shift_ref_2 = shift_ref[::2]                    #only one direction is used due to too
                                                    #big position
    shift_flu_2 = shift_flu[::2]                    #discrepancies between the two scanning
                                                    #directions

    pos_av, pos_sd, pos_se = average.average(shift_pos_2)   #average position over all scans
    mon_av, mon_sd, mon_se = average.average((shift_mon)
    ref_av, ref_sd, ref_se = average.average(shift_ref_2)   #average reflection over all scans
    flu_av, flu_sd, flu_se = average.average(shift_flu_2)   #average fluorescence over all scans

    vref_conc = shift_vref[0]                       #create new array for concatenation
    for i in range(len(shift_vref)-1):
        #concatenate all reference voltage values to find the correct (most common) one:
        vref_conc = numpy.concatenate((vref_conc, shift_vref[i+1]))

    normed_flu_av = norm.norm(vref_conc, flu_av)    #norm the fluorescence signal to gain 1
    normed_flu_se = norm.norm(vref_conc, flu_se)    #norm the fluorescence error to gain 1
    normed_flu_cor = normed_flu_av                  #correct the data for fluctuations in laser
                                                    #intensity
    normed_se_av = normed_flu_se

    normed_flu_cor = normed_flu_cor - f_back        #subtract the background from the data
    normed_flu_cor = flu_av
    normed_se_av = flu_se

    max_idx = scipy.where(ref_av == max(ref_av))    #find the index of the maximum value
    max_idx = max_idx[0]                            #extract it from the variable
    max_idx = max_idx[0]
    thickness = int(1000/20)                        #thickness of the front wall
    max_idx = max_idx + thickness                   #set index to after the front wall
    newpos_av = pos_av[max_idx:]                    #cut datasets to only display data from
within
                                                    #the cuvette
```

```
    newpos_se = pos_se[max_idx:]
    newflu_av = normed_flu_cor[max_idx:]
    newflu_se = normed_se_av[max_idx:]
    ref_pos = newpos_av[0]                              #save reference position to re-set
                                                        #position values
    newpos_av = newpos_av-ref_pos                       #subtract the reference position from all
                                                        #values to make the position start at 0
    cut = -7

    lny = scipy.log(newflu_av)                          #linearise the data for a linear fit
    lnyerr = newflu_se/newflu_av                        #log the error too for the fitting function
                                                        #weighted fit

    p0 = [max(lny), -0.1]
##    p0 = [max(newflu_av),-0.5]
##    best_p, covar = scipy.optimize.curve_fit(exp_func, newpos_av[:cut],
##                                             newflu_av[:cut], p0, sigma=newflu_se[:cut])
    best_p, covar = scipy.optimize.curve_fit(lin_func, newpos_av[:cut],
                                             lny[:cut], p0, sigma = lnyerr[:cut])
    amp = scipy.exp(best_p[1])
    print amp
    exp = best_p[0]
    amp_err = numpy.sqrt(covar[1][1])
    exp_err = numpy.sqrt(covar[0][0])
    flu_fit = lin_func(newpos_av[:cut], exp, scipy.log(amp))
    SSerr, SStot = fit.SSq(lny[:cut], flu_fit)       #find sum of squared errors and total sum
of squares
##    flu_fit = lin_func(newpos_av[:cut], grad, offs)
##    SSerr, SStot = fit.SSq(newflu_av[:cut],flu_fit)
    Rsq = 1-SSerr/SStot                              #calculate R^2 as indicator for goodness
of fit
    print Rsq

    maxFluIdx = scipy.where(normed_flu_av == max(normed_flu_av))
    maxFlu = normed_flu_av[maxFluIdx]
    maxFluErr = normed_flu_se[maxFluIdx]

    conc = float(fname[1:-6])
    conc = conc*1e-6
    #write best parameters for each fit to a file:
    newFile = open(STEM + '\\_params_21-09-2012.txt', 'a')
    newFile.write('%.3e\t' %conc)
    newFile.write('%.6e\t' %amp)
    newFile.write('%.6e\t' %amp_err)
    newFile.write('%.6e\t' %exp)
    newFile.write('%.6e\t' %exp_err)
    newFile.write('%.6f\n' %Rsq)
    newFile.close()

    mon = numpy.average(mon_av)
    errMon = numpy.std(mon_av)
    maxFlu = newflu_av[0]
    errFlu = newflu_se[0]
    C.append((conc, maxFlu, errFlu, mon, errMon))
    print conc, maxFlu, errFlu

C_sorted = sorted(C, key = itemgetter(0))

X = []
Y = []
Yerr = []
for v in C_sorted:
```

```
    X.append(v[0])
    Y.append(v[1])
    Yerr.append(v[2])
X = numpy.array(X)
Y = numpy.array(Y)
Yerr = numpy.array(Yerr)
best_init_params, init_fit, merr, berr = fit.lin_fit(X, Y, Yerr)
SSerr_init, SStot_init = fit.SSq(Y, init_fit)
Rsq_init = 1-SSerr_init/SStot_init
print Rsq_init
grad_init = best_init_params[0]
offs_init = best_init_params[1]
#write best parameters for each fit to a file
newFile = open(STEM + '\\_params_init_fit_21-09-2012.txt', 'w')
newFile.write('%.6e\t' %grad_init)
newFile.write('%.6e\t' %merr)
newFile.write('%.6e\t' %offs_init)
newFile.write('%.6e\t' %berr)
newFile.write('%.6f\n' %Rsq_init)
newFile.close()
```

```
from __future__ import division
from operator import itemgetter
import numpy, scipy, pylab, os, fit
import scipy.optimize

def load_params():
    fname = r'c:\Documents and Settings\kkb\Desktop\New Folder (2)\PhD\F410\
              PMT measurements\2012-08-23\Brimo/_params.txt'
    fp = open(fname, 'r')
    data = fp.readlines()
    fp.close()
    params = []
    for line in data:
        line =[float(n) for n in line.split(None)]
        params.append((line[0], line[1], line[2], line[3], line[4]))
    p_sorted = sorted(params, key = itemgetter(0))
    return p_sorted

def go():
    params = load_params()
    C = []
    A = []
    A_err = []
    B = []
    B_err = []
    for val in params:
        c = val[0]
        C.append(c)
        A.append(val[3])
        A_err.append(val[4])
        B.append(val[1])
        B_err.append(val[2])
    C = numpy.array(C)
    A = numpy.array(A)
    A_err = numpy.array(A_err)
    B = numpy.array(B)
    B_err = numpy.array(B_err)
    init_m_A = 1e7
    init_m_B = -3
    x = -len(C)
##    best_params_B, fit_B, m_err_B, b_err_B = fit.lin_fit(C, B, B_err)
    best_params_B, fit_B = fit.lin_fit_0(C[x:], B[x:], B_err[x:], init_m_B) #fit: m1x+b1
##    best_params_A, fit_A = fit.lin_fit_0(C, A, A_err, init_m_A) #fit: m2x+b2
    best_params_A, fit_A, m_err_A, b_err_A = fit.lin_fit(C[x:], A[x:], A_err[x:])
    SSerr_B, SStotal_B = fit.SSq(B[x:], fit_B)
    SSerr_A, StotalE_A = fit.SSq(A, fit_A)
    Rsq_B = 1-SSerr_B/SStotal_B
    Rsq_A = 1-SSerr_A/StotalE_A
    print Rsq_A
    print Rsq_B
    m_A = best_params_A[0]
    m_B = best_params_B

    newF = open('_fit_to_params_21-09-2012.txt', 'w')
    newF.write('%.3e\t' %m_A)
    newF.write('%.3e\n' %Rsq_A)
    newF.write('%.3e\t' %m_B)
    newF.write('%.3e\n' %Rsq_B)
    newF.close()

    C = C*1e6
    pylab.figure()
```

```
    pylab.subplot(121)
    pylab.errorbar(C,A, A_err, fmt = '.b')
    pylab.plot(C, fit_A, '--r')
    pylab.xlabel(u'Concentration [\xb5M/l]')
    pylab.ylabel('Parameter A [a.u.]')
    pylab.subplot(122)
    pylab.errorbar(C,B, B_err, fmt='.r')
    pylab.plot(C[x:], fit_B, '--b')
    locs, labels = pylab.yticks()
    pylab.yticks(locs, map(lambda x: "%.1e" %x, locs))
    pylab.xlabel(u'Concentration [\xb5M/l]')
    pylab.ylabel('Parameter B [a.u.]')

    pylab.show()



if __name__ == "__main__":
    go()
```

```
from __future__ import division
import UniversalLibrary as UL
import ctypes as ct
import numpy
import time
import serial
import pylab
import csv, winsound

### --------------------------------Stage set up---------------------------###

### User dependent values: ###
START_POS = 0            # mm
STOP_POS = 10            # mm
SPEED = 40               # mm/s
ACC = 1000               # mm/s^2

### Internal constants stage: ###
COUNTS = 2000            # encoder counts per mm
K = 26214.4              # stage constant: k = 1*2000/5000*65536

### --------------------------------A/D set up-----------------------------###

# load DLL to memory:
cbw32 = ct.WinDLL('c:\\Program Files\\Measurement Computing\\DAQ\\cbw32.dll')

FuncType = 1

# set up for cbAInScan
BoardNum = 0
LowChan = 0
HighChan = 1
Count = 31*68          # collect 31*68 samples (integer multiple of packet size(31))
Rate = 3000            # will be ignored because set by trigger frequency
Range = UL.BIP10VOLTS  # +- 10V range
# convert AD data, run in background mode, re-arm the trigger automatically:
Options = UL.CONVERTDATA + UL.BACKGROUND + UL.RETRIGMODE
Values = numpy.zeros((Count*2,), dtype = numpy.int16)  # array for backward scan data
#scan = []

# additional set up for cbALoadQueue
NumChans = 4                                                # collect samples from 4 channels
ChanArray = numpy.zeros((NumChans,), dtype = numpy.int16)   # array of channel numbers
                                                            # to be sent to the ADC
GainArray = numpy.zeros((NumChans,), dtype = numpy.int16)   # array of gains to be sent to the ADC
ChanArray[0] = 1                                            # define channels
ChanArray[1] = 3
ChanArray[2] = 5
ChanArray[3] = 7
for x in range(NumChans):
    GainArray[x] = UL.BIP10VOLTS        # define gain for channels

### --------------------------------Sound set up---------------------------###

sound = r'c:\Documents and Settings\kkb\Desktop\New Folder (2)\PhD\F410\
          PMT measurements\2012-07-03\Click01.wav'

### -------------------------------Stage commands--------------------------###

class MyStage(object):
    def __init__(self, COM):
        # open COM port baudrate 19200, timeout .1s
```

```
        self.port = serial.Serial(COM, 19200, timeout = .1)
        self.flush()     # Echo on

    def home(self):
        # send stage home (gh - go home)
        self.port.write('GH\n\r')
##        self.flush()

    def sStart(self):
        # write starting position to register 56
        cmd = 'AL%i,AR56\n\r' %(START_POS*COUNTS)
        self.port.write(cmd)
        self.flush()

    def sStop(self):
        # write stopping position to register 89
        cmd = 'AL%i,AR89\n\r' %(STOP_POS*COUNTS)
        self.port.write(cmd)
        self.flush()

    def sVelocity(self):
        # write velocity (scanning speed) to register 23
        cmd = 'AL%i,AR23\n\r' %(SPEED*K)
        self.port.write(cmd)
        self.flush()

    def mForward(self):
        # Call Macro 100 (forward scan)
        self.port.write('MC100\n\r')
##        self.flush()

    def mBackward(self):
        # call macro 110 (backward scan)
        self.port.write('MC110\n\r')
##        self.flush()

    def mAbsolute(self):
        # move stage to position x
        cmd = 'MA%i,GO\n\r' %(STOP_POS*COUNTS)
        self.port.write(cmd)
        self.flush()

    def error(self):
        # display any errors
        self.port.write('TE\n\r')
        self.flush()

    def tPos(self):
        # read encoder count from controller
        self.port.write('TP\n\r')
        pos = self.port.read(100)    # save returned string in pos
##        print 'pos:',pos
        s = pos.split()              # split returned string
        p = int(s[2])                # use 1st entry of s, turn into integer
        return p

    def flush(self):
        # echo on (print command on screen)
        print self.port.read(100)

    def close(self):
        # close COM port
```

```
        self.port.close()

    def __del__(self):
        # automatically close port when program terminates
        print 'Auto-closing'
        self.close()
### ------------------------------------------------------------------------###
def read_status():              # read I/O status from ADC
    Status = ct.c_short(0)      # busy or idle
    CurIndex = ct.c_long(0)     # index of last data point in array
    CurCount = ct.c_long(0)     # sample count of last data point in array
    cbw32.cbGetIOStatus(ct.c_int(BoardNum), ct.byref(Status),
                        ct.byref(CurCount), ct.byref(CurIndex), ct.c_int(FuncType))
    return Status.value, CurCount.value

def go():
    time.clock()
    # acquire 4 samples per trigger:
    UL.cbSetConfig(UL.BOARDINFO, BoardNum, 0, UL.BIADTRIGCOUNT, 4)
    # load channels and gains into queue:
    UL.cbALoadQueue(BoardNum, ChanArray, GainArray, NumChans)

    stage = MyStage('COM6')     # open COM port
    stage.sVelocity()           # set stage velocity
    stage.sStart()              # set starting position
    stage.sStop()               # set stopping position
    stage.home()

    for x in range(20):         # set number of scans - remember: range(2)
                                #is one forward and one backward scan!
        print x+1
        scan = []
        p = stage.tPos()        # ask actual stage position to calculate
                                #trigger points (in encoder counts)
        p = p/2                 # divide encoder counts by 2 to get micrometers
        # start data acquisition (wait for trigger):
        UL.cbAInScan(BoardNum, LowChan, HighChan, Count, Rate, Range, Values, Options)
        time.sleep(0.1)         # wait to make sure trigger is armed
        if x%2 == 0:
            t = time.time()     # measurement date and time
            stage.mForward()    # if even loop count scan forward
        else:
            t = time.time()     # record measurement date and time
            stage.mBackward()   # if odd loop count scan backward
        while 1:
            Status, CurCount = read_status()    # read A/D status
            time.sleep(0.1)                     # don't have to read status all the time
                                                # (eats up cpu time)
            # if current data point index > 2000 stop the while loop:
            if CurCount == 2000 or CurCount > 2000: break
        # stop background data acquisition:
        cbw32.cbStopIOBackground(ct.c_int(BoardNum), ct.c_int(FuncType))
        Val = Values[:Count]    # clip array to size of samples
        for v in Val:
            EngUnits = -10 + v*(20/4096)        # convert a/d values to voltage
            scan.append(EngUnits)               # write voltage to list
        Scan = numpy.array(scan)                # turn list into array
        Scan = numpy.reshape(Scan, (Scan.shape[0]/4,4))  # reshape list to have 4 columns
        Scan = Scan[:499]       # crop list to only have 499 entries (delete overshooting)
##        ref = Scan[:,2]
##        if max(ref) > 0.16:
##            winsound.PlaySound(sound, winsound.SND_FILENAME)
```

```
        l = len(Scan)
        Sec = numpy.zeros(l)
        Sec.fill(t)
        Pos = numpy.zeros(l)                    # create empty array for position values
        if x%2 == 0:                            # calculate position values
            for c, v in enumerate(Pos):
                p = p + 20                      # position moves forward
                Pos[c] = p
        else:
            for c, v in enumerate(Pos):
                p = p - 20                      # position moves backward
                Pos[c] = p
        Pos = numpy.reshape(Pos, (Pos.shape[0], 1)) # reshape position values to have 1 column

        Sec = numpy.reshape(Sec, (Sec.shape[0],1))
        Pos = numpy.append(Pos, Sec, 1)             # append position values and data points
                                                    # into 5 column array
        Scan = numpy.append(Pos, Scan, 1)
        if x%2 != 0: Scan = numpy.flipud(Scan)      # flip data from backward scan
        try:                                        # if 'Data' exists do this:
            Data = numpy.append(Data, Scan, 1)      # append new scan to existing data
        except NameError:                           # if 'Data' doesn't exist:
            Data = Scan                             # Create new array named Data, write first
                                                    # scan into it
    print 'Data acquisition finished'
    time.sleep(1)
    stage.home()                                    # send stage home
    print time.clock()
    return Data

try:
    Data = go()
finally:
    cbw32.cbStopIOBackground(ct.c_int(BoardNum), ct.c_int(FuncType))

fid = open('Fluo resolution test.txt', 'w')
csvWriterObject = csv.writer(fid, delimiter='\t')
csvWriterObject.writerows(Data)
fid.close()
```

```
from __future__ import division
from operator import itemgetter
import scipy.optimize
import fileopen, shift, average, norm, fit, conc_det, loadBack
import numpy, pylab, scipy, os, csv, time

STEM = r'c:\Documents and Settings\kkb\Desktop\New Folder (2)\
         PhD\F410\PMT measurements\2012-07-05\non eye safe\Brimo calibration/'
files = [fname for fname in os.listdir(STEM) if fname[-5:] == 'M.txt']
backname = r'c:\Documents and Settings\kkb\Desktop\New Folder (2)\PhD\F410\
            PMT measurements\2012-07-05\non eye safe\Brimo calibration/Brimo background.txt'
p_back, m_back, r_back, f_back = loadBack.load_background(backname) #load background file
f_back = f_back

for fname in files:
    print fname
    #read columns from file:
    position, tim, monitor, reference, reflection, fluorescence = fileopen.fopen(STEM+fname)
    pos = numpy.array(position)          #turn position, monitoring PD, reference voltage,
    mon = numpy.array(monitor)           #reflection and fluorescence values into arrays
    vref = numpy.array(reference)
    ref = numpy.array(reflection)
    flu = numpy.array(fluorescence, dtype = numpy.float64)
    #shift arrays to be aligned at the maximum reflection:
    shift_pos, shift_mon, shift_vref, shift_ref, shift_flu = shift.shift(r_back, pos, mon,
                                                                         vref, ref, flu)

    vref_conc = shift_vref[0]            #create new array for concatenation
    for i in range(len(shift_vref)-1):
        vref_conc = numpy.concatenate((vref_conc, shift_vref[i+1]))

    C = []
    t0 = tim[0]
    t01 = t0[0]
    for counter, entry in enumerate(shift_pos):
        print 'Scan %i' %counter
        t1 = tim[counter]
        t11 = t1[0]
        tm = time.strftime("%H:%M:%S",time.localtime(t11))
        t = t1 - t0
        t2 = t11 -t01
        t2 = str(t2)
        mon_av, mon_sd, mon_se = average.average(mon)
        newpos = entry
        newvref = shift_vref[counter]
        newref = shift_ref[counter]
        newflu = shift_flu[counter]

        normed_flu = norm.norm(vref_conc, newflu)       #norm the fluorescence signal to gain 1
        normed_flu_cor = normed_flu
        normed_flu_cor = normed_flu_cor - f_back

        max_idx = scipy.where(newref == max(newref))    #find the index of the maximum value
        max_idx = max_idx[0]                            #extract it from the variable
        max_idx = max_idx[0]
        thickness = int(1000/20)                        #thickness of the front wall
        max_idx = max_idx+thickness                     #set index to after the front wall
        new_pos = newpos[max_idx:]                      #cut datasets to only display data from
                                                        #within the cuvette
        new_flu = normed_flu_cor[max_idx:]
        ref_pos = new_pos[0]                            #save reference position to re-set
                                                        #position values
```

```
        new_pos = new_pos-ref_pos                       #subtract the reference position from
                                                        #all values to make the position start
at 0

        conc = conc_det.calibrate_Brimo(new_pos, new_flu)
        C.append(conc)
        if counter < 10:
            n = '00' + str(counter)
        elif counter < 100:
            n = '0' + str(counter)
        else:
            n = str(counter)

        n_conc = numpy.array(conc[:-5])
        n_pos = numpy.array(new_pos[:-11])
        n_time = numpy.array(t[max_idx:-11])

        Pos = numpy.reshape(n_pos, (n_pos.shape[0],1))
        Tim = numpy.reshape(n_time, (n_time.shape[0],1))
        Con = numpy.reshape(n_conc, (n_conc.shape[0],1))
        Pos = numpy.append(Pos, Tim, 1)
        Pos = numpy.append(Pos, Con, 1)
        try:                                            #if 'Data' exists do this:
            Data = numpy.append(Data, Pos, 1)           #append new scan to existing data
        except NameError:                               #if 'Data' doesn't exist:
            Data = Pos


        n_conc = n_conc*1e6
##    lab = float(fname[11:-6])*1e-6
##    lab = '%.1e M/l' %lab
        pylab.clf()
        pylab.plot(n_pos[:-5], n_conc[:-5])#, label = lab)
        pylab.ylim(-0.2, 2)
        pylab.xlim(0,6000)
##    locs, labels = pylab.yticks()
##    pylab.yticks(locs, map(lambda x: "%.3f" % x, locs*1e6))
        pylab.text(0.0, 1.01, t2, fontsize=12, transform = pylab.gca().transAxes)

        pylab.grid()
        pylab.ylabel(u'Intensity [scaled units]')
        pylab.xlabel(u'Scanning depth [\xb5m]')

        pylab.savefig(STEM + 'Fig_%s' %fname + '_scan_%s' %n +'_recovered_22-09-2012.png',
                      dpi = 100)

    newF = open(STEM + '\\' + fname +'_recovered.txt', 'w')  #write each fit to a file (pos, fit)
    csvWriterObject = csv.writer(newF, delimiter = '\t')
    csvWriterObject.writerows(Data)
    newF.close()
```

```
from __future__ import division
import numpy, os, scipy, pylab, norm

def load_fit_params():
    '''Load the parameters for the fit to the exponential fitting parameters'''
    LUTname = r'c:\Documents and Settings\kkb\Desktop\New Folder (2)\PhD\F410\
                PMT measurements\2012-08-23\Brimo/_fit_to_params.txt'
    fp = open(LUTname, 'r')
    data = fp.readlines()
    fp.close()
##    params = []
    m = []
    for line in data:
        line = [float(n) for n in line.split(None)]
        m.append(line[0])                           #gradient is second column in file
##        b = line[2]                               #y axis intersection is fourth column in file
##        params.append((m,b))
##        params.append((m))
    return m

def load_Conc_Cal():
    '''Load the parameters for the determination of
    the concentration from the corrected intensity'''
    CalName = r'c:\Documents and Settings\kkb\Desktop\New Folder (2)\PhD\
                F410\PMT measurements\2012-08-23\Brimo/_params_init_fit.txt'
    fp = open(CalName, 'r')
    data = fp.readlines()
    fp.close()
    for line in data:
        line = [float(n) for n in line.split(None)]
        m = line[0]
        b = line[2]
    return m, b

def calibrate_Brimo(x,y):
    params_att = load_fit_params()
    params_det = load_Conc_Cal()
    gradI = params_det[0]
    offsI = params_det[1]
    gradB = params_att[1]
    print gradI, offsI, gradB
    dpos = 20
    C = []
    X = []

    for i in range(len(y)-1):
        pos = x[i]
        sig = y[i]
        if sig <= offsI: sig = offsI
        if i == 0:
            Int0 = sig
        else:
            Int0 = newInt
        c = (Int0-offsI)/gradI
        param_B = gradB * c
        I_1_th = sig + param_B * dpos
        sig_1 = y[i+1]
        if sig_1 <= offsI: sig_1 = offsI
        prcnt_change = (I_1_th-sig_1)/I_1_th
        if prcnt_change > 0.0001 or prcnt_change < -0.0001:
            newInt = Int0 - Int0*prcnt_change
        else:
```

```
            newInt = Int0
        C.append(c)
    return C

def calibrate(x,y):
    params_att = load_fit_params()
    params_det = load_Conc_Cal()

    gradB = params_att[1]
    gradI = params_det

    dpos = 20
    C = []
    X = []

    for i in range(len(y)-1):
        pos = x[i]
        sig = y[i]
        if sig <= 0.0: sig = 0.1
        if i == 0:                #for the first entry in the file (i.e. zero attenuation):
            Int_0 = sig           #final intensity is equal to measured intensity
        else:                     #for any other case:
            Int_0 = newInt        #final intensity is equal to intensity determined in
                                  #previous step
        c = Int_0/gradI           #calculate concentration from intensity (i=mc+b)
##        if c < 1e-9: c = 0
        param_B = gradB * c       #calculate parameter B for this concentration
        #calculate theoretical intensity at next position:
        I_1_th = sig * scipy.exp(param_B * dpos)
        if I_1_th == 0: I_1_th = 0.1
        sig_1 = y[i+1]
        if sig_1 <= 0: sig_1 = 0.1
        prcnt_change = (I_1_th-sig_1)/I_1_th      #calculate the change in intensity in percent
                                                  #of the theoretical intensity at that position
        #if the change is bigger than the error margin:
        if prcnt_change > 0.0001 or prcnt_change < -0.0001:
            newInt =  Int_0 - Int_0 * prcnt_change      #the detemined intensity is the final
                                                        #intensity from the step before minus
                                                        #the percent change
        else:
            newInt = Int_0
        C.append(c)                                     #append determined concentration to list

    return C
```

```
from __future__ import division            # make sure all divisions work properly
import _csv, numpy, os, time
import matplotlib.pyplot as plt
import sys
import fileopen

def FWHM(pos, ref):
    maxAmp = 0.0
    maxPos = 0.0
    # for the counter and all values in ref do the following:
    for c, v in enumerate(ref):
        if v > maxAmp:                     # if value is greater than the maximum amplitude:
            maxAmp = v                     # set value as new maximum amplitude
            maxPos = pos[c]                # save stage position of new maximum amplitude
            maxIndex = c                   # save index in arrayof new maximum amplitude
    halfM = maxAmp/2                       # find half maximum amplitude
    dOld = 100
    # initiate counter and for all values in ref up to maximum amplitude:
    for c, v in enumerate(ref[:maxIndex]):
        dNew = abs(v - halfM)              # find difference between value and half amplitude
        if dNew < dOld:                    # if new difference is smaller than old difference
            p1 = pos[c]                    # save stage position of closest value
            h1 = v                         # save value of closest value
            dOld = dNew                    # write new difference into old difference
    dOld = 100
    # do the same for values in ref after maximum amplitude:
    for c, v in enumerate(ref[maxIndex:]):
        dNew = abs(v - halfM)
        if dNew < dOld:
            p2 = pos[maxIndex+c]
            h2 = v
            dOld = dNew
    # the fwhm is the difference of stage position 2 minus stage position 1:
    #res = p2-p1
    return maxAmp, maxPos#, res

STEM = r'c:\Documents and Settings\kkb\Desktop\New Folder (2)\PhD\F410\
        PMT measurements\2012-09-18\Fluo es/'
files = [fname for fname in os.listdir(STEM) if fname[-4:] == '.txt']
for fname in files:
    print 'processing '+fname
    pos, tim, mon, vref, ref, fluo = fileopen.fopen(STEM + fname)
    n = len(pos)
    t0 = tim[0]
    for k in range(150,200,1):
        p = pos[k]
        t = tim[k]
        m = mon[k]
        r = ref[k]
        f = fluo[k]
        maxamp, maxpos = FWHM(p, r)

        print 'scan %i:'%k
        tm = time.localtime(t[0])
        tm = time.strftime('%H:%M:%S', tm)

        fig = plt.figure()
        ax = fig.add_subplot(111)
        lns1 = ax.plot(p, r, '-b', label = 'Reflection')
        ax2 = ax.twinx()
        lns2 = ax2.plot(p, f, '-g', label = 'Fluorescence')
        lns3 = ax2.plot(p, m, '-r', label = 'Laser Monitor')
```

```
        lns = lns1 + lns2 + lns3
        labs = [l.get_label() for l in lns]
        ax.legend(lns, labs, loc = 0)
        ax.grid()
        ax.set_xlabel(u'Depth (\xb5m)')
        ax.set_ylabel('Intensity (V)', color='b')
        ax2.set_ylabel('Intensity (V)', color ='g')
        ax.set_ylim(0,10)
        ax2.set_ylim(0,10)
        plt.text(0.0, 1.01, tm, fontsize=12, transform = plt.gca().transAxes)

        if k < 10:
            n = '00' + str(k)
        elif k < 100:
            n = '0' + str(k)
        else:
            n = str(k)

        plt.savefig(STEM + 'Fig_%s' %fname + ' scan_%s_100dpi.png' %n, dpi = 100)
```

Appendix C

Ethics application

DURHAM UNIVERSITY

ETHICS ADVISORY SUB-COMMITTEE in the DEPARTMENT of PHYSICS

Application form for ethical review and approval of work which involves human participants and/or gives rise to ethical issues

Note to applicants: information concerning the University's ethical procedures, the Human Tissues Act, data protection, freedom of information and links to research council ethics policies can be found at http://www.dur.ac.uk/research.office/local/research_governance/research_ethics/

Status (tick one)	Staff		Postgraduate project	✓	Undergraduate project	

Full scientific title of project:
Tracking ophthalmic drugs in the eye using confocal fluorescence microscopy

Short title of project (to appear on supporting documentation):
Tracking drugs in the eye

Name(s) of researcher(s): Kim K. Buttenschön
Email address(es): k.k.buttenschoen@durham.ac.uk

Name of supervisor (if applicable): Prof. John M. Girkin
Email address: j.m.girkin@durham.ac.uk

Proposed start date: 01/10/2011
Proposed end date: 31/10/2011

Check boxes for supervisor (if applicable):

The student has read the ethical guidance of the relevant research council	✓
The procedures for recruitment and obtaining informed consent are appropriate	✓

Comments from supervisor:

For the following questions, please delete the options (Yes/No/Not applicable) as appropriate.

1. Will you describe the main procedures to participants in advance, so that they are informed about what to expect? **Yes** / **No** / **Not applicable**

2. Will you tell participants that their involvement is voluntary, that they may withdraw from the research at any time (without their having to give any reason and without any repercussions) and that in such circumstances their data will be removed from the study? **Yes** / **No** / **Not applicable**

3. Will you obtain written informed consent for participation and for all intended uses of the data arising from this study? **Yes** / **No** / **Not applicable**

4. If the research is observational, will you ask participants for their consent to being observed? **Yes** / **No** / **Not applicable**

5. If recordings (video, audio etc.) are being made, will you explain how they will be kept and what will happen to them? **Yes** / **No** / **Not applicable**

6. With questionnaires or interviews, will you remind participants of their option of omitting questions they do not want to answer? **Yes** / **No** / **Not applicable**

7. Will you tell participants that their data will be treated with full confidentiality and that, if published, will not be identifiable as theirs? **Yes** / **No** / **Not applicable**

8. Will you debrief participants at the end of their participation (i.e. give them a brief explanation of the study)? **Yes** / **No** / **Not applicable**

9. If your project involves the use of archive data, has the appropriate approval previously been given? (Please attach details of the approval.)
Yes / **No** / **Not applicable**

10. Have you conducted a Risk Assessment ?
Yes / **No**

11. Do you declare that your participants will not be given financial or other inducements (other than reasonable expenses and compensation for time) to participate?
Yes / **No** / **Not applicable**

12. If the proposal involves an application for external funding, will it adhere to the ethical guidelines provided by the relevant funding body? **Yes** / **No** / **Not applicable**

13. Will your project involve deliberately misleading participants in any way? **Yes** / **No**

14. Is there any realistic risk of any participants experiencing either physical or psychological distress or discomfort? If Yes, give details in the space at the end of the form and state what you will tell participants to do if they should experience any problems (e.g. who they can contact for help). **Yes** / **No**

15. Have you consulted the University's Insurance Officer? (clare.robinson@durham.ac.uk) **Yes** / **No**

16. Does your project involve work with animals? **Yes** / **No**

17. Are drugs, placebos or other substances (e.g. food substances, vitamins) to be administered to the study participants or will the study involve invasive, intrusive or potentially harmful procedures of any kind? **Yes** / **No**

18. Will blood or tissue samples (including saliva and waste products) be obtained from participants (refer to the document on the Human Tissue Act, posted on Duo)? **Yes** / **No**

19. Will the study involve recruitment of patients or staff through the NHS? **Yes** / **No**

20. Do participants fall into any of the following special groups? Note that you may also need to obtain satisfactory CRB clearance (or equivalent for overseas students).

Children under 16 years of age	No
Children aged 16 or 17 years	No
The elderly (aged 75 or over)	No
People with learning or communication difficulties	No
People in custody	No
People engaged in illegal activity (e.g. drug-taking)	No

There is an obligation on the lead researcher (or Supervisor, in the case of undergraduate or postgraduate projects) to bring to the attention of the Departmental Ethics Sub-Committee any issues with ethical implications not clearly covered by the above checklist.

This form should be submitted to Clare Woodward by email (c.a.woodward@durham.ac.uk), in addition to a signed hard copy. Please also provide all the information listed below.

a). A brief description of your project including (where appropriate):

1. Title of project.
2. Purpose of project and its academic rationale.
3. Brief description of methods and measurements.
4. Participants: recruitment methods, number, age, gender, exclusion/inclusion criteria, incentives (financial or otherwise).
5. Consent and participant information arrangements, debriefing.
6. A clear but concise statement of the ethical considerations.

b). If applicable, any invitation letters, information sheets and consent forms.

c). A completed risk assessment form – see http://www.dur.ac.uk/physics/internal/safety/

If any of the above information is missing, your application will be returned to you.

DECLARATION:

The information provided on this form and in the attached documentation is, to the best of my knowledge, complete and accurate

Signed _____ Date _____

Print Name _____ (UG or PG Researcher(s), if applicable)

Signed _____ Date _____

Print Name _____ (Lead Researcher or Supervisor)

SECTION TO BE COMPLETED FOLLOWING REVIEW BY THE DEPARTMENTAL ETHICS ADVISORY COMMITTEE:

The Departmental Ethics Advisory Committee reviewed this application, and decided to:

- Give advisory approval*
- Give provisional advisory approval of the application subject to amendment*
- Defer*
- Reject*
- Refer this application*

[*please delete as appropriate]

Date: .....

The decision will be reported to the Faculty Ethics Committee on: ……..

Please note that this approval expires:

1. 12 months after the date of approval, if the project has not started by that date;
2. Where the project commences within 12 months of the date of approval and continues unchanged: three years after the date of approval;
3. Where there is any change to the project, from the date of that change unless the sub-committee's prior consent for that change is sought;
4. Where there is any change to the legislation/regulations affecting the ethical approval for this project, from the date of that change.

SUPPORTING INFORMATION: You are asked to provide all necessary information in the space below. Please ensure that any information given here is clearly cross-referenced to the relevant question in the form.

1. Title of project:
Tracking drugs in the eye using confocal fluorescence microscopy

2. Purpose of project and its academic rationale:
The purpose of this study is to measure the natural fluorescence of components in the anterior chamber of the eye of healthy volunteers using a novel, non-invasive instrument based on confocal fluorescence scanning microscopy. The aim of the main research project is to track Alphagan-P (Brimonidine, an ophthalmic drug for treating open angle glaucoma) in the eye using a non-invasive method to gain a better understanding of how the drug distributes and dilutes in the eye so that a) no further animals will have to be sacrificed during the development of the drug to measure the concentration in different parts of the eye and b) the measurement of concentrations in different parts of the eye will be easier and possible at much more discreet time intervals which could lead to a further development of the drug to better reach and have a greater effect on the relevant sections of the eye.
The present study aims to test the non-invasive instrument *in vivo* on healthy eyes to get a measure of the background signal we will have to expect. No drugs will be administered in this experiment. Participants will be asked to fixate on a fixation target within the instrument and measurements of the fluorescence levels of the components in the anterior chambers of their eye will be conducted by scanning a focal point along the axis of their eye several times. Preliminary data obtained from fresh dissected

sheep's eyes (cornea, aqueous humour and lens) suggests that the level of background fluorescence will be quite high. However to confirm that this is not a by-product of early decay and to investigate how the fluorescence levels might be changing during the course of a day or a week an *in vivo* study is necessary.
The results of this study will be used as part of Ms. Buttenschön's PhD thesis. They will also be reported in one or more articles to be submitted to peer-reviewed scientific journals.

3. Brief description of methods and measurements:

All participants will be healthy adults recruited from the University's student and staff bodies. Each participant will be involved in the study for repeated measurements lasting approximately 15 minutes or less 3 times a day for 5 days. The participants will first be briefed as to the purpose of the study and asked to provide signed and informed consent and to fill in a questionnaire (see Appendix A).
The participants will then be asked to find a comfortable position in the provided head rest and to look at a fixation target in the instrument. Once the instrument has been aligned to their eye by the operator it will be calibrated to the participant's eye in a first measurement phase (approximately lasting 10 minutes or less). The participant will also have the opportunity to practice the real scanning situation in this measurement phase. They will then be able to relax their eyes and head for a moment if necessary. In a second measurement phase lasting approximately 5 minutes or less, the fluorescence signal from components in the anterior chamber of the participant's eye will be recorded and saved. The total scanning time will be approximately 45 minutes on the first day with the time getting shorter throughout the week once the operator and participant are more experienced at aligning their eyes with the instrument.

4. Participants: recruitment methods, number, age, gender, exclusion/inclusion criteria, incentives (financial or otherwise):

A minimum of 10 and a maximum of 20 people, approximately half male and half female, will be recruited from the student and staff bodies of the University. All participants will be older than 18 years of age with a spread of participants aged 20 to 60. All participants will be white-Caucasian since any other population group is heavily under-represented within the bodies of the University we are recruiting from. The participants will be recruited by Ms. Buttenschön via an invitation letter send by email to the research group and via personal conversations. The only exclusion criteria are problems with sight or hearing. All participants will be recompensed for their time and effort with £5.

5. Consent and participant information arrangements, debriefing. Please attach intended invitation letters, information sheets and consent forms:

Signed, informed consent will be obtained from all participants prior to the start of the experiment. A copy of the combined participant information sheet, questionnaire and consent form is attached as Appendix A. Participation in the study is completely voluntarily and the participants will be made aware that they are free to withdraw at any point during the experiment without giving reason or having to fear adverse consequences. If they withdraw they will be given the option to have their data destroyed. However if they do not use this option and part of their data is useable for this study, we will keep it with their permission. At the end of their experiment session the participants will be debriefed and will have the opportunity to ask questions. Once the study is complete, a summary of the results will be sent to those participants who have chosen to have it sent to them.

6. A clear but concise statement of the ethical considerations (including issues around deception) raised by the project and how you intend to deal with them. Please refer back, as necessary, to the answers you have given to the questions above:

- Ms. Buttenschoen and Prof Girkin will adhere to the Physics Department's health and safety regulations and guidelines and have received complete laser safety training.
- The above mentioned personnel are trained and experienced in using the instrument.
- A risk assessment regarding the electrical and laser safety of the instrument has been carried out and is attached as Appendix B. The risk has been found to be low.
- The laser safety of the instrument has been evaluated using the British Standard BS EN 60825-1:2007 and the radiation leaving the instrument has been categorised as class 1 laser radiation and is safe for long exposure durations (see Appendix C). The instrument has been fitted with a laser power monitoring photo diode and a shutter so that the beam is cut off in case there is a power surge or a power loss.
- To help participants to keep their head and eyes as still as possible while still being comfortable a head rest and a fixation target are provided.
- Participants are able to take a break at any time during the experiment if they so desire.

-Appendix A-

Tracking ophthalmic drugs in the eye using confocal fluorescence microscopy

Principal Investigator: Kim Buttenschön
Supervisor: Prof. Girkin

PARTICIPANT INFORMATION SHEET

Background:
The aim of this research project is to build a non-invasive instrument to monitor the distribution and movement of Alphagan (a drug for treating open angle Glaucoma) in the eye. We are hoping to gain a better understanding of how the drug distributes and dilutes in the eye using a non-invasive method so that a) no further animal eyes will have to be sacrificed to measure the concentration in different parts of the eye and b) the drug can be developed further to have a greater effect in the relevant sections of the eye.
The present study aims to test the non-invasive instrument *in vivo* on healthy eyes to get a measure of the background signal we will have to expect. No drugs will be used in this experiment.
Our research is a CASE studentship award funded by the EPSRC (Engineering and Physical Sciences Research Council) and Lein Applied Diagnostics Ltd.

What is involved?
We will ask you to put your head in a head rest and keep it as still as possible during the measurement. We will also ask you to fixate on a target within the instrument (a green LED). We will monitor the position of your eye through a web cam.
We will then take 5 calibration measurements through the anterior part of your eye (cornea and aqueous humour). Both the thickness of your cornea and any fluorescent signal from within the anterior chamber of your eye will be recorded. This phase takes about 10 minutes or less. Once the instrument has been calibrated to your eye, we will take 30 measurements of your eye. There will be the opportunity to take a break between the calibration and the measurements. The measurements will take approximately 5 minutes. The total measurement time will therefore not be longer than about 15 minutes.
The instrument has been tested for eye safety and fulfils all requirements of the laser safety standard for a class 1 laser.
We will record your data by saving it on the computer. The stored data will be anonymous, so that no-one other than the research team can identify you with the results from your tests. Your data will remain confidential.

What are the benefits?
The benefits of this project lay mainly in the further development of the drug. The first direct benefit will be that no more animal eyes will have to be sacrificed in the future to learn the concentration of the drug in different parts of the eye. The second, less direct benefit is that we hope to increase the understanding of how the circulation of liquid works in the eye and from that how the drug can be altered such that it increases its effect on the relevant areas of the eye.

Your participation in the project is entirely voluntary, and you are free to withdraw from the research *at any time* and *without any adverse consequences.*

If you have any further questions, please ask a member of the research team.

Contacts

Miss Kim Buttenschön (Physics) k.k.buttenschon@durham.ac.uk
0191 33 43532

Prof. John Girkin (Physics) j.m.girkin@durham.ac.uk
0191 33 43589

-Appendix A-

Participant Details

Age group: <24 / 24-34 / 34-44 / >44

Sex: Male / Female

Will you be wearing contact lenses during the experiment? Yes / No

Do you have diabetes? Yes / No

Do you take any regular medication (including the pill)? Yes / No

Did you take any medication today? Yes / No

CONSENT FORM

TITLE OF PROJECT:

Tracking ophthalmic drugs in the eye using confocal fluorescence microscopy

(The participant should complete the whole of this sheet himself/herself)

	Please cross out as necessary
Have you read the Participant Information Sheet?	YES / NO
Have you had an opportunity to ask questions and to discuss the study?	YES / NO
Have you received satisfactory answers to all of your questions?	YES / NO
Have you received enough information about the study and the Intended uses of, and access arrangements to, any data which you supply ?	YES / NO
Were you given enough time to consider whether you want to participate?	YES/NO

Who have you spoken to? Dr/Mr/Mrs/Ms/Prof.....

Do you consent to participate in the study? YES/NO

Do you understand that you are free to withdraw from the study:

* at any time and
* without having to give a reason for withdrawing and
* without any adverse result of any kind? YES / NO

Signed ..... **Date** .....

(NAME IN BLOCK LETTERS) .....

Signature of experimenter..... **Date** .....

(NAME IN BLOCK LETTERS) .....

GENERAL RISK ASSESSMENT

Location:	**Activity:**
Physics Department Room 33 (Biophotonics Laboratory)	Measuring natural fluorescence in the anterior chamber of eyes of healthy volunteers

Hazards	**Those at risk**	**Description of risk**	**Risk Controls**	**Risk Rating**
Electrical equipment	Operator, Volunteers	Electric shock	All electrical and electronic equipment used has been PAT tested by trained safety personnel, no high voltage or high current equipment is being used	LOW
Class 4 laser radiation	Operator, Volunteers	Burns to eyes and skin	Any laser radiation not categorised as class 1 will be enclosed in a metal case fitted with a laser safety interlock and laser radiation warning labels. No class 4 radiation will be accessible unless the casing is opened and the interlock disabled. All radiation leaving the instrument is categorised as class 1. The instrument is fitted with a laser power monitoring photo diode which closes a shutter if the laser power exceeds a safe threshold. The shutter also closes if there is a power loss.	LOW

Risk Rating = Likelyhood x Severity = LOW, MEDIUM or HIGH

Assessor:

Name:_____ **Job Title:**_____

Signature:_____ **Date:**_____

Date Assessment to be reviewed:.....

UNIVERSITY OF DURHAM - Health and Safety Office

RISK ASSESSMENT FORM

FOR RESEARCH WORK
(include practical undergraduate projects)

Summary of Assessment - Tick Box	
CATEGORY A WORK	
CATEGORY B WORK	✓
REFER TO HEALTH & SAFETY OFFICE	

PART 1. PERSONAL DATA AND DETAIL OF PROJECT/EXPERIMENT

Department **Physics** Laboratory **33** Tel. Ext. **43630**

Name **Kim Buttenschön** Supervisor **Prof John Girkin**

Male/**Female** Staff/Technician/**Student** UG/**PG**

Degree/**Higher Degree Course** Starting Date **August 2011**

Proposed finishing date of Project/Experiment **Ongoing, reviewed annually**

Title of Project/Experiment **Tracking ophthalmic drugs in the eye using confocal fluorescence microscopy**

Description of Project/Experiment. Give a brief description of Project/Experiment, attaching copy of grant submission if appropriate.

A home built ophthalmic instrument based on confocal fluorescence laser scanning microscopy will be used to measure the natural fluorescence in the anterior chamber of perfused sheep's or bovine eyes and the eyes of healthy volunteers. The class 4 laser radiation (405nm) is guided into the measurement optics by an optical fibre. The beam power is then reduced to class 1 by using neutral density filters before it reaches the final optical element and leaves the instrument. A laser power monitoring photo diode is incorporated in the instrument which operates a shutter if the laser power exceeds a safe threshold. The shutter also closes if there is a power loss. The measurement optics and any laser radiation that is not class 1 are enclosed by a light tight metal case that has a laser radiation warning label and is fixed with an interlock so that the laser is switched off if the casing is opened during instrument operation.

.

Instructions

1. This form is to be completed by the Supervisor in consultation with (any) co-workers.
2. It encompasses postgraduate research and individual undergraduate project work, and individual research. (The summary assessment is, of course, not appropriate where the researcher works individually.)
3. It concerns practical work using materials or equipment, and field work but not theoretical or computing work.
4. It must be signed by the Supervisor or senior researcher and by the co-worker (or student) to indicate that HE or SHE has read it. After completion tick the summary box on the front.
5. One copy to Department records, one copy to co-worker/student, plus one to HEALTH & SAFETY OFFICE *only* if health surveillance, air monitoring or respiratory/ear protection required.
6. The aim of the Assessment is to satisfy Regulation 3 of "The Management of Health and Safety Regulations 1992" (Risk Assessment). Should the work depart from the aims, methods or materials envisaged, then a new assessment must be carried out.

PART 2. NATURE OF POSSIBLE HAZARDS

Chemical Hazards

Are chemicals, including proprietary materials, to be used? Yes/**No**

If **No** → Is Good Lab. Practice Sufficient (see COSHH Code of Practice)? Yes/No

If **Yes**

* Is there a cyanide/fluorine, 'very toxic' hazard? Yes/No/Possibly
* Is there a volatile material hazard? Yes/No/Possibly
* Is there an explosive or violent reaction hazard? Yes/No/Possibly
* Is there a carcinogenic, mutagenic or teratogenic hazard (see COSHH Code of Practice - Carcinogens)? Yes/No/Possibly
* Will hazardous dust or fume be created? Yes/No/Possibly

Ionising Radiation Hazards

Does project/experiment involve radioisotopes or ionising radiation sources (α, β, γ, X-ray or neutron emitter/sources)? Yes/**No**/Possibly

If **No** →

If **Yes** Submit written scheme of work to Departmental Radiation Protection Supervisor for approval before work starts

* Is the High-Activity Cell (Cobalt 60 source) to be used? Yes/No/Possibly

Laser Hazards

* Are class 3B or 4 lasers to be used? **Yes**/No/Possibly

Non-Ionising Radiation Hazards, Noise, Vibration

Is non-ionising radiation, noise or vibration used/generated in the project/experiment? Yes/**No**/Possibly

If **No** →

If **Yes**

* Ultra-violet YES/NO, infra-red YES/NO, Microwaves YES/NO, Radio-frequency YES/NO, intense magnetic or electric fields YES/NO, Noise > 85dBA YES/NO, Vibration which reaches the hands or body YES/NO.

Electrical Hazards

Is electrical equipment, other than tested 240V portable appliances connected to mains supply, to be used? Yes/No/**Possibly**

If **No** →

If **Yes**

* Will any electrical equipment using more than 50V a.c. or 100V d.c. be used out of doors or in wet conditions? Yes/**No**/Possibly
* Are voltages > 1000V to be used? Yes/**No**/Possibly
* Are there exposed circuits and terminals with voltages >50Va.c., 100V d.c. Yes/**No**/Possibly
* Are portable generators to be used? Yes/**No**/Possibly

Robotic Hazards

Is robotic equipment to be used? Yes/**No**/Possibly

If **No** →

If **Yes**

* Are restricted areas to be entered? Yes/No/Possibly
* Are mobile robots to be used? Yes/No/Possibly

Other Hazards

* Are there any other hazards which pose unusually high risks? Yes/**No**/Possibly
* Are explosives to be used? Yes/**No**/Possibly
* Does stored energy, e.g. machine rotation, present a hazard? Yes/**No**/Possibly
* Does the work entail entry to cold rooms or hot rooms, and/or sealed rooms which can be locked? Yes/**No**/Possibly
* Does the work entail work in the field? Yes/**No**/Possibly
* Are there pressure systems or closed systems in which over-pressure or under-pressure can occur? Yes/**No**/Possibly
* Is dangerous apparatus/equipment to be used, e.g. Chainsaw, Stihl Saw, Stunning Guns? Yes/**No**/Possibly

Biological Hazards

Are biological materials to be used (including exposure to animals or plant allergens)? Yes/**No**/Possibly

If **No** →

If **Yes** Complete BIO-COSHH form and if the answer to every other question is NO end this risk assessment. If other hazards are present, the Supervisor shall decide if this or the BIO-COSHH form, or both, is most appropriate.

If any starred (*) items are marked YES or POSSIBLY then include in assessment.

PART 3. DETAILS OF ASSESSMENT

The aim of the assessment is to identify preventative and protective measures which must be provided and used so that risks to the experiment and others are controlled. In most cases existing Departmental or University procedures will be sufficient but should be referred to.

If any question marked * in part 2 is answered YES then provide written details including safety procedure below.

A class 4 laser will be used inside the instrument. It will be reduced in power to class 1 before it leaves the instrument. All optics and unsafe laser radiation will be enclosed by a metal or plastic casing with a warning label and an interlock that switches the laser off if the casing is opened during operation. The instrument will be fitted with a laser power monitoring photo diode which will operate a shutter if the laser power exceeds a safe limit. The shutter will also close if there is a power loss. Maintenance will only be carried out in a room that is suitable for the use of class 4 lasers and when wearing adequate eye protection.
The instrument may operate using home built electronics in which case the instrument and all connected electronic devices will be tested for electrical safety by the in-house specialist.

GENERAL SAFETY INFORMATION RELATING TO PROJECT/EXPERIMENT

Means of containment (if applicable) to be used when appropriate		Fume Cupboard	Yes/**No**	…….. ……
		Biological Safety Cabinet	Yes/**No**	Grade
		Total Enclosure	Yes/**No**	
		Local Ventilation	Yes/**No**	
		Other	Yes/**No**	
Personal Protection to be worn when necessary		Lab Coat	Coveralls	Coveralls and Hood
		Hand Protection	Yes/**No**	Type ……..
	§	Respiratory Protection	Yes/**No**	Type ……...
	§	Ear Protection	Yes/**No**	Type … ……...
		Eye Protection	**Yes**/No	laser safety goggles for maintenance
		Foot Protection	Yes/**No**	
		Other	Yes/**No**	Specify ……..

§ refer to Health & Safety Office.

PART 4. WASTE DISPOSAL

Will Hazardous wastes arise? **No**

Waste Disposal (Departmental) practice …

……

……

PART 5. MONITORING

Is air monitoring required? (Materials ……) Yes/**No**

If YES, REFER TO Health & Safety Office.

Is health monitoring required? Yes/**No**

Compulsory, ionising radiations classified worker, exposure to animals/plant allergens, exposure to certain chemicals (see COSHH).

Voluntary, 3B/4 laser use, noise and vibration exposure, regular exposure to toxic chemical, field work.

Supervisor to submit names to Health & Safety Office (for referral to Occupational Health Adviser) with this form.

PART 6. EMERGENCIES

Special action to be taken after Accident. Indicate special measures needed for the work described in the assessment, e.g. first aid, major spillage, electricity/water failure, work in remote or hazardous environments.

The victim is to attend Sunderland Eye Infirmary for assessment in case of class 4 laser radiation eye encounter.

PART 7. SUMMARY

Supervisors should identify areas of work within the project in the categories below, which are not mutually exclusive. Category B is the expected initial assessment, as all practical work requires the supervisor's approval. Following demonstration and training, the supervisor may re-categorise some work to A. The Supervisor must give instructions and advice on safeguards, determine the extent and frequency of supervision, and state the name of any others used in supervision.

A - NOT to be undertaken without direct supervision.

B - NOT to be started without supervisor's approval.

WORK	**CATEGORY**	**SUPERVISOR**
…… …… ……	…… ……	…… ……
…… ……	…… ……	……
……	……	……
……	……	……
……	……	……

Signature of Supervisor …… Date ……

Signature of Co-worker/student
having read the assessment …… Date ……

Laser safety evaluation

To calculate how much power is allowed to be put into someone's eye within a given time frame to still keep the instrument eye safe the British Standard "Safety of Laser Products" (BS EN 60825-1:2007) was used. The value that has to be calculated is the Accessible Emission Limit (AEL. Since our beam is not collimated but depending on the position of the scanning lens with respect to the eye either divergent or convergent, the calculation for extended sources is used. The AEL for a class 1 laser (inherently eye safe) is calculated using table 5 (p. 44):

$AEL = 3.9 * 10^{-5}\, C_3\, W = 39\, \mu W$ (retinal photochemical hazard) and

$AEL = 7 * 10^{-4} C_6 T_2^{-0.25}\, W = 14.8\, mW$ (retinal thermal hazard)

With C_3 being 1 for λ = 400-450 nm , C_6 being 66.7 for sources with an angle of >100 mrad and T_2 being 100s again for sources >100 mrad. Since the value for the photochemical hazard is smaller it is the one to be used.

The laser power used will therefore be ≤39 µW.